CONTRACTOR REPORT ARLCD-CR-79005

ULTRASONICALLY ACTIVATED DIFFUSION BONDING FOR FLUIDIC CONTROL ASSEMBLY

SONOBOND CORPORATION
SUBSIDIARY OF CHRISTIAN METALS CORPORATION
WEST CHESTER, PENNSYLVANIA

HOWARD A. SCHEETZ
PAUL L. COPPA
JANET DEVINE

CONTRACT PROJECT ENGINEERS

DAVID SAMPAR
MICHAEL GOES

FEBRUARY 1979

US ARMY ARMAMENT RESEARCH AND DEVELOPMENT COMMAND
LARGE CALIBER
WEAPON SYSTEMS LABORATORY
DOVER, NEW JERSEY

The views, opinions, and/or findings contained in this report are those of the author(s) and should not be construed as an official Department of the Army position, policy or decision, unless so designated by other documentation.

Destroy this report when no longer needed. Do not return to the originator.

The citation in this report of the names of commercial firms or commercially available products or services does not constitute official endorsement or approval of such commercial firms, products, or services by the United States Government.

CONTRACTOR REPORT ARLCD-CR-79005

ULTRASONICALLY ACTIVATED DIFFUSION BONDING FOR FLUIDIC CONTROL ASSEMBLY

Howard A. Scheetz
Paul L. Coppa
Janet Devine

Sonobond Corporation
Subsidiary of Christiana Metals Corporation
West Chester, Pennsylvania 19380

February 1979

Final Report
Contract No. DAAA21-76-C-0186

Prepared for

DEPARTMENT OF THE ARMY
US ARMY ARMAMENT RESEARCH AND DEVELOPMENT COMMAND
DOVER, NEW JERSEY 17801

HARRY DIAMOND LABORATORIES
ADELPHI, MARYLAND 20783

UNCLASSIFIED

SECURITY CLASSIFICATION OF THIS PAGE (When Data Entered)

REPORT DOCUMENTATION PAGE		READ INSTRUCTIONS BEFORE COMPLETING FORM
1. REPORT NUMBER ARLCD-CR-79005	2. GOVT ACCESSION NO.	3. RECIPIENT'S CATALOG NUMBER
4. TITLE (and Subtitle) Ultrasonically Activated Diffusion Bonding for Fluidic Control Assembly		5. TYPE OF REPORT & PERIOD COVERED 6. PERFORMING ORG. REPORT NUMBER
7. AUTHOR(s) Howard A. Scheetz Paul L. Coppa Janet Devine		8. CONTRACT OR GRANT NUMBER(s) Contract No. DAAA21-76-C-0186
9. PERFORMING ORGANIZATION NAME AND ADDRESS Sonobond Corporation 200 East Rosedale Avenue West Chester, PA 19380		10. PROGRAM ELEMENT, PROJECT, TASK AREA & WORK UNIT NUMBERS
11. CONTROLLING OFFICE NAME AND ADDRESS US Army Armament Research and Development Command, DRDAR-LCN-C Dover, New Jersey 07801		12. REPORT DATE February 1979 13. NUMBER OF PAGES 145
14. MONITORING AGENCY NAME & ADDRESS(if different from Controlling Office) Harry Diamond Laboratories DELHD-R-CM-D Adelphi, Maryland 20783		15. SECURITY CLASS. (of this report) Unclassified 15a. DECLASSIFICATION/DOWNGRADING SCHEDULE

16. DISTRIBUTION STATEMENT (of this Report)

Approved for public release; distribution unlimited.

17. DISTRIBUTION STATEMENT (of the abstract entered in Block 20, if different from Report)

18. SUPPLEMENTARY NOTES

19. KEY WORDS (Continue on reverse side if necessary and identify by block number)

Diffusion welding
Ultrasonic radiation
Ultrasonic welding
Fluidic control devices

20. ABSTRACT (Continue on reverse side if necessary and identify by block number)

Modified ultrasonic metal bonding equipment was used to develop a new fluidic stack assembly process. Ultrasonically activated diffusion bonding was successfully applied to aluminum laminates of different sizes (up to 1 by 1 inches), different foil thicknesses (2, 3, and 5 mils), and different number of

DD FORM 1 JAN 73 1473 EDITION OF 1 NOV 65 IS OBSOLETE

UNCLASSIFIED

SECURITY CLASSIFICATION OF THIS PAGE (When Data Entered)

20. Abstract (Cont.)

layers (up to 18). Bonds were obtained without excessive deformation, within a few seconds of ultrasonic bonding time, on as-received surfaces, without special atmospheres, on commercially prepared etched foil fluidic laminate stacks. Bonds were judged good quality from visual examination of stack surfaces and edges, from electrical resistance measurements made face to face, and from photo-micrographic analysis of assembly cross sections.

Analysis of the bonding system led to establishment of fundamental bonding parameters and equipment requirements for assembly of larger and thicker stacks.

Investigation of the use of increased ultrasonic power for assisting the diffusion bonding of fluidic elements verified the fact that increased areas and/or thickness of laminates can be joined, but that dedicated tooling must be developed to assure the success of the process development.

SUMMARY

During this program, proprietary equipment and techniques for ultrasonic metal bonding were successfully extended from small spot welds to larger area diffusion bonds with multiple interfaces as associated with laminated-stack fluidic device assemblies. Photochemically etched aluminum laminates (up to 18 layers) with overlap areas up to 1.0 by 1.1 inches and stack thicknesses up to 0.060 inch were bonded.

Aluminum laminates consisting of manifold plates, fluid channel patterns, active elements, and combinations representative of active devices were assembled. Ultrasonic activation at low power permitted a high degree of interface consolidation with minimal channel distortion. Higher power activation provides strong bonds and greater leak resistance at the expense of fluid channel distortion.

This study exploited the use of newly developed microhmeters for monitoring the progress and status of interface contact development during bonding. In-situ measurements of stack resistance permit rapid determination of equivalent bond status under various combinations of bonding parameters. Simple static loading (to 2000 psi) reduces stack resistance tenfold. But ultrasonic activation reduces the stack resistance by an additional thousandfold. This technique has application in monitoring other diffusion bonding processes and the use of other laminate materials.

The ultrasonically activated diffusion bonding process develops very low contact resistance within one second at room temperature and ambient air conditions. Utilization of this short bonding cycle permitted assembly of over one hundred laminated stacks under controlled experimental conditions. These studies depleted the available supply of 1 by 3 inch photochemically etched laminates in thicknesses of 2, 3, and 5 mils.

The fundamentals of the diffusion bonding process and the ultrasonic equipment characteristics necessary for activation were examined and defined. Processing costs can be exceptionally low due to brief bonding time, low energy consumption, and freedom from special atmospheres or temperatures during bonding.

System requirements were established for the ultrasonic bonding of larger laminates (up to 3 inches diameter) and thicker stacks as envisioned for a variety of Army Ordnance applications. The design and construction of this larger fluidic device assembly system would provide a unique bonding capability and is strongly recommended.

The low power investigations showed the potential of the ultrasonic assist in assembling fluidic stacks. Investigation at increased power levels indicated promise in bonding laminates of larger area and greater thickness. However, unforeseen tooling problems compromised the success of the increased power effort. The laminate alignment pins used in the low power investigation were not applicable for the higher power work, and power levels in excess of 3500 RF watts were not effectively achieved.

Further investigation of tooling requirements will be necessary to assure a satisfactory process for diffusion bonding fluidic stacks with the ultrasonic assist.

FOREWORD

This final report on the development of ultrasonic diffusion bonding for the assembly of fluidic control devices was prepared by Sonobond Corporation, West Chester, Pennsylvania, under Army Contract DAAA21-76-C-0186. The basic contract, which covered the period from March 31, 1976 to April 1, 1977, was carried out under the sponsorship of the Department of the Army, US Army Armament Research and Development Command, Dover, New Jersey, with Dave Sampar, SARPA-NC-C-C, serving as project engineer. The work at Sonobond was performed by Howard C. Scheetz and Paul L. Coppa. Philip C. Krause served as administrative supervisor.

Subsequent modifications to the contract provided for additional evaluation of the ultrasonic diffusion bonding process for the period from October 1, 1977 to May 15, 1978. SSG Michael Goes was project engineer for the US Army Armament Research and Development Command during this period. The work at Sonobond was under the supervision of Janet Devine. This additional effort is described in Appendix A to this report.

The findings of this report are not to be construed as an official Department of the Army position.

TABLE OF CONTENTS

LIST OF ILLUSTRATIONS

LIST OF TABLES

I. INTRODUCTION

This report presents the results obtained on Army Contract No. DAAA21-76-C-0186, which was oriented to the development of ultrasonic equipment and techniques for facilitating the diffusion bonding of laminated aluminum fluidic circuit modules.

Under a previous contract (DAAA21-73-C-0234), an ultrasonic diffusion bonding apparatus was assembled. The ultrasonic system consisted of a Sonobond wedge-reed ultrasonic spot welding system appropriately modified for use under high vacuum conditions, with a shortened reed member for containment within a commercially available vacuum bell jar. Provisions for elevated temperature operation included an induction heating coil surrounding the welding and anvil tips with the workpiece interposed between. This entire assembly was installed within the bell jar, and appropriate driving, pumping, and indicating equipment was assembled to provide a complete functional unit.

The initial work on the present contract was oriented primarily to ultrasonically assisted diffusion bonding of small aluminum elements with the following objectives:

1. Reduced diffusion bonding time as compared with thermally activated bonding.

2. Reduced criticality in environmental control during bonding.

3. Bonding of laminate rectangular sections with overlap areas of 1/2 by 1/2 inches up to 1 by 1 inches.

4. Bonding of laminated stacks having 12 or more layers to simulate assembly of active devices.

5. Bonding of laminated stacks having thicknesses of 0.05 inch or more.

6. Definition of process variables for extension to thicker stack fluidic devices.

7. Definition of process variables for extension to larger area laminated assemblies.

8. Definition of process variables involved in a production-type ultrasonically activated bonding system.

Early efforts to assemble multi-layer aluminum foil specimens led to surprisingly good results without a vacuum or high-temperature environment. With the Project Engineer's approval, the approach was modified to place maximum emphasis upon ultrasonic activation and minimum emphasis upon thermal activation.

During the first few months, equipment and techniques were developed for ultrasonically activated diffusion bonding of aluminum laminates up to 1/2 inch square and up to 18 laminates thick. The resulting bond is rather unique, being different in mechanical properties from conventional ultrasonic metal bonding and different from thermally activated diffusion bonding. Ultrasonic bonding times of 2 to 4 seconds are orders of magnitude faster than thermally activated bonding and require no furnaces or high vacuum system. Potential cost savings for fabrication of multi-layer fluidic devices are great. Table 1 provides a comparison between two diffusion bonding processes as applied to aluminum laminates. Clearly, the ultrasonic approach has dramatic advantages.

With the assistance of the Army Project Engineer, realistic goals for bonding characteristics and fluidic device performance characteristics have been established. These practical goals have allowed engineering trade-offs between mechanical strength and fluid leak rates which permitted gross reductions in acoustic power density. Therefore the cost effectiveness of the selected ultrasonic system is substantially improved in comparison to thermally activated bonding or higher power ultrasonic systems.

A. WELDING VERSUS BONDING OF METALS

Welding is usually thought of as a fusion process. The process may be divided into three categories:

1. Liquid-phase welding occurs when the edges of two proximate members are melted and the members are joined by solidification of the molten material which exists between them at some stage of the process.

TABLE 1. DIFFUSION BONDING OF ALUMINUM FLUIDIC LAMINATES: A COMPARISON

Characteristic	Thermally Activated Diffusion Bonding	Ultrasonically Activated Diffusion Bonding
TEMPERATURE	1200°F	Ambient
Temperature Control	± 2°F	Not critical
Effects of Over Temp.	>1205°F = melting Device destroyed	Slightly more deformation
Effects of Under Temp.	No bonding	No effect
ATMOSPHERE	Oxygen-free	Dry air
Pressure	High vacuum	Ambient
TIME CYCLE		
Static Loading	¼ hour	1 second (pneumatic)
Vacuum Pumpdown	1 hour	0
Furnace Temp. Rise	2½ hours	0
Bonding	½ hour	1 to 4 seconds
Furnace Cooling	10 hours	0
Atmospheric Venting	½ hour	0
Fixture Removal	¼ hour	10 seconds
Total Time	15 hours	15 seconds

(Continued)

TABLE 1 (Concluded)

Characteristic	Thermally Activated Diffusion Bonding	Ultrasonically Activated Diffusion Bonding
SURFACE PREPARATION		
Oxidation	Minimal thickness	As is
Cleanliness	Chemically cleaned	As is, degreased is better
Roughness	Minimal	As is (~32 μin. rms)
INPUT ENERGY		
Line Power	~8 KW/batch	8 KW/square inch
Average Time Usage	4 hours	4 seconds
Input Energy	32 kilowatt-hours	0.009 kilowatt-hour
Energy Cost at 5¢/KWH	$1.60/batch	$0.0004/square inch

2. Liquid-solid phase welding occurs when only the added metal is liquid, the initial members to be joined remaining solid at all points.

3. Solid-phase welding is defined as a process of joining when none of the material is melted at any time. Solid-phase welding is the oldest of all types, being practiced in Egypt as early as 3000 B.C. (18). The bonding mechanism requires only interatomic interaction of nearest neighbors, i.e., at a distance of one lattice parameter within a metal crystal structure. This reduces the problem to one of mass transport wherein diffusion and more particularly self-diffusion plays the key role.

B. PHENOMENOLOGICAL REVIEW OF METAL BONDING

Early in this study, a brief review of the diffusion bonding literature was initiated. Very little has been written on diffusion bonding of aluminum or on ultrasonically activated diffusion bonding (14). Some of the literature uses the term "diffusion welding" (24) to describe nonfusion methods. Other authors (33) have used the phrase "solid state bonding."

The literature provides several general classes of diffusion bonding techniques based on the thermodynamic bonding parameters of time, temperature, pressure, and activation energy.

1. Yield stress controlled bonding relies primarily on mechanical disruption of the joint surfaces and

---

(18) Kinzel, A. B., "Solid Phase Welding," 25th Annual Meeting, American Welding Society, 1944.

(14) Joshi, K. C., "The Formation of Ultrasonic Bonds Between Metals." Welding J., Dec. 1971, p. 840-848.

(24) Miller, M. A., "Joining Aluminum to Other Metals." Welding J., Aug. 1953, 12 p.

(33) Storchheim, S.,"Some Studies of Al-Cu and Al-Zr Solid State Bonding." Trans. AIME J. Metals, Vol. 203, Aug. 1955, p. 891-894.

applied pressure across the bond interface to promote diffusion of metal atoms across the joint. This definition was provided years ago (3) specifically for a static loading condition. However, it is equally appropriate for the dynamic environment provided by ultrasonic metal bonding equipment, especially as applied to wedge-reed metal bonding systems.

2. Pressure welding is the formation of a solid-phase weld between metallic materials by the application of a deforming pressure at any temperature below the melting point of the components (24).

3. Diffusion welding is the joining of electroplated surfaces under rather low pressures and temperatures for a period of time sufficient to induce recrystallization of the plating alloys, e.g., 600°F for silver-plated aluminum (24).

4. Transient melt diffusion bonding uses a thin temporary liquid phase to transport metal atoms across the interface and thereby speed diffusion.

5. Thermally activated diffusion bonding relies primarily on elevated temperatures to induce diffusion across the joint. At any given temperature the process is controlled by the diffusion coefficient; hence it is also called diffusion-controlled bonding. Bonding pressure is applied to produce intimate surface contact in the joint.

6. Creep controlled bonding uses elevated temperatures to produce creep at the interface to establish a bond. Bonding temperatures are kept low enough so that the yield stress of the material remains higher than the bonding pressure.

7. Intergranular melt diffusion bonding uses a solute alloying element to help create a compositional gradient at grain boundaries. Carefully controlled temperatures lying between the liquidus and the solidus points or between the bulk and surface

---

(3) Blank, G. F., "A Practical Guide to Diffusion Bonding," Mater. Design Eng., Oct. 1966, p. 76-79.

eutectic points are used to produce a thin liquid phase to transport metal atoms across the interface (31).

8. Ultrasonically activated diffusion bonding provides the mechanism for simultaneously employing several of the above phenomena. With the proper selection of bonding parameters, yield stress, thermal activation, and creep controlled bonding can each contribute to the bonding process while avoiding the problems associated with transient melt diffusion and intergranular melt diffusion.

---

(31) Spurgeon, W. M., S. K. Rhee, and R. S. Kiwak, "Diffusion Bonding of Metals." Bendix Technical J., Spring 1969, p. 24-44.

II. CONVENTIONAL ULTRASONIC BONDING

Conventional ultrasonic metal bonding incorporates high ultrasonic energy density and moderate static clamping forces to induce plastic deformation of the contacting interface. Spot welding, seam welding, and ring welding concentrate the dynamic energy into a finite spot or weld track. The entire interface within this spot is diffusion bonded into nugget quality. When the dynamic shearing stress at the interface exceeds the local yield strength (in shear), plastic deformation begins and continues until intimate contact has been established across the full region (Figure 1). The tensile and shear strength properties of the resulting nugget are comparable to the parent material strengths. Tensile-shear tests on finite-size spot welds typically induce failure in the parent metal (not within the nugget) at the boundary of the nugget where the thinnest sections are found.

Table 2 lists ring weld characteristics for pertinent aluminum alloys. For a single ring weld in 3.5-mil-thick aluminum foil, with only two layers, an RF energy density of 1800 watt-seconds per square inch was used to obtain nugget quality. As the foil thickness increased to 8 mils, the energy density increased to 7000 watt-seconds per square inch. The 7000 watt-seconds per square inch energy density for an assembly thickness of 16 mils is directly comparable to the energy density used for 18-mil stacks of etched aluminum laminates, as described in Section IV.

Table 2 also shows a tenfold increase in static compressive stress for ring welds as compared with the clamping forces used with fluidic laminates.

A graphical presentation of the energy densities for ring weld data (circa 1972) listed in Table 2 and for spot weld data listed in Ref. (13) for 1100 series aluminum is shown in Figure 2. Both sets of data show an energy density (E/A) dependence upon thickness (t) raised to the 3/2 power (i.e., positive slope of 1.5 on a log-log plot of E/A

---

(13) Jones, J. B., N. Maropis, J. G. Thomas, and D. Bancroft, "Phenomenological Considerations in Ultrasonic Welding." Welding J., Vol. 40, July 1961, p. 289s-305s.

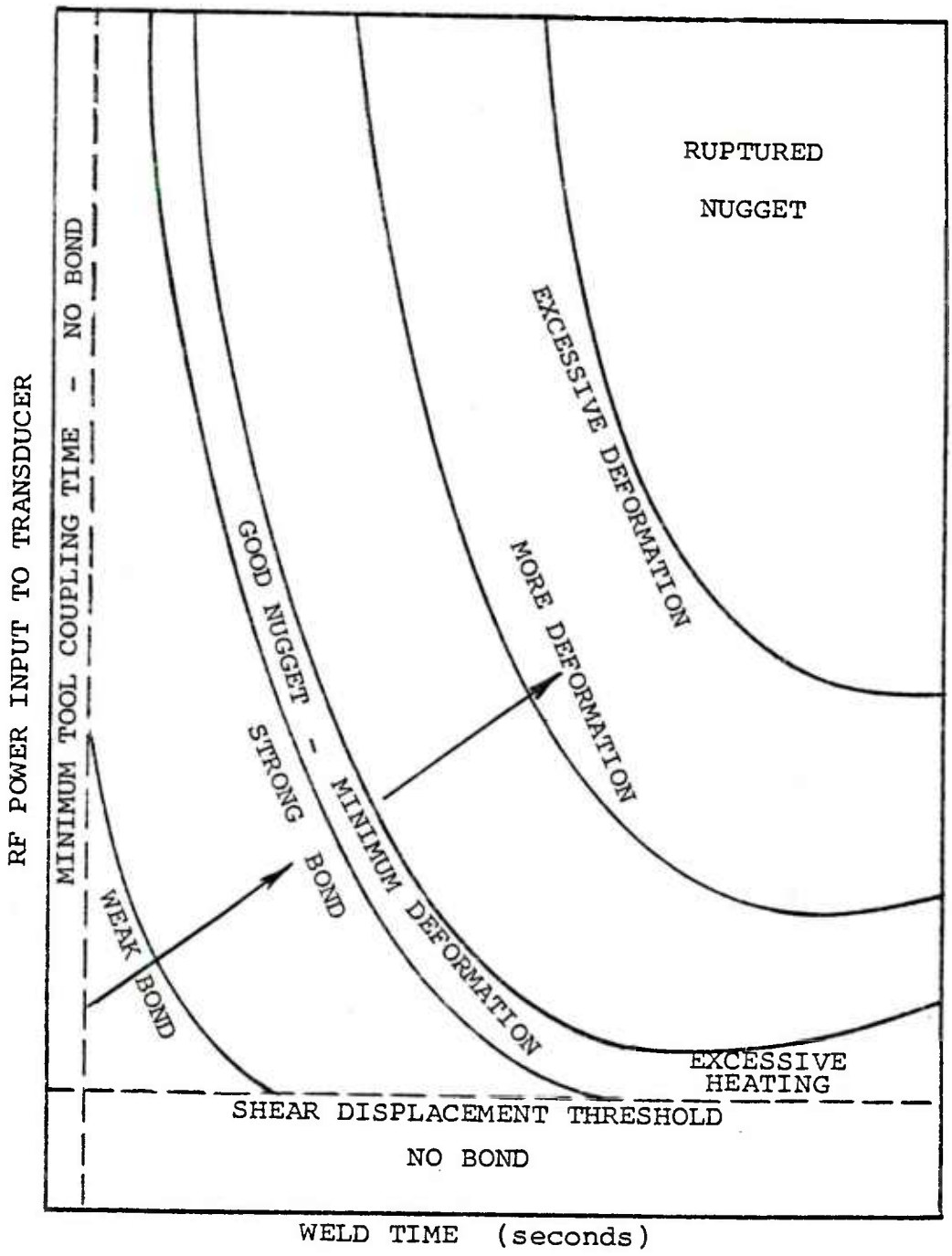

Figure 1. Ultrasonic bonding criteria in terms of bond energy.

TABLE 2. RING WELD CHARACTERISTICS IN ALUMINUM ALLOYS

Sonobond Model WR-3000RFW Welder with "Standard Horn"

Ring Spot Size: 1-inch mean diameter
0.05-inch-wide annulus

Weld Area: 0.0785 square inch

Material (1.5" x 3" Coupons)		Static Load		Weld Parameters		
Aluminum Alloy	Thickness (inch)	Clamp Force (lb)	Ring Compr. Stress (psi)	RF Power (watts)	Weld Time (sec)	Nugget* Weld Energy (watt-sec)
1145-H19	0.0035	1680	21,000	720	0.2	140
1100-0	0.008	1600	20,000	1800	0.3	540
1100-H14	0.020	1820	23,000	2400	1.0	2400

* Nugget quality indicates failure in parent metal outside bond area.

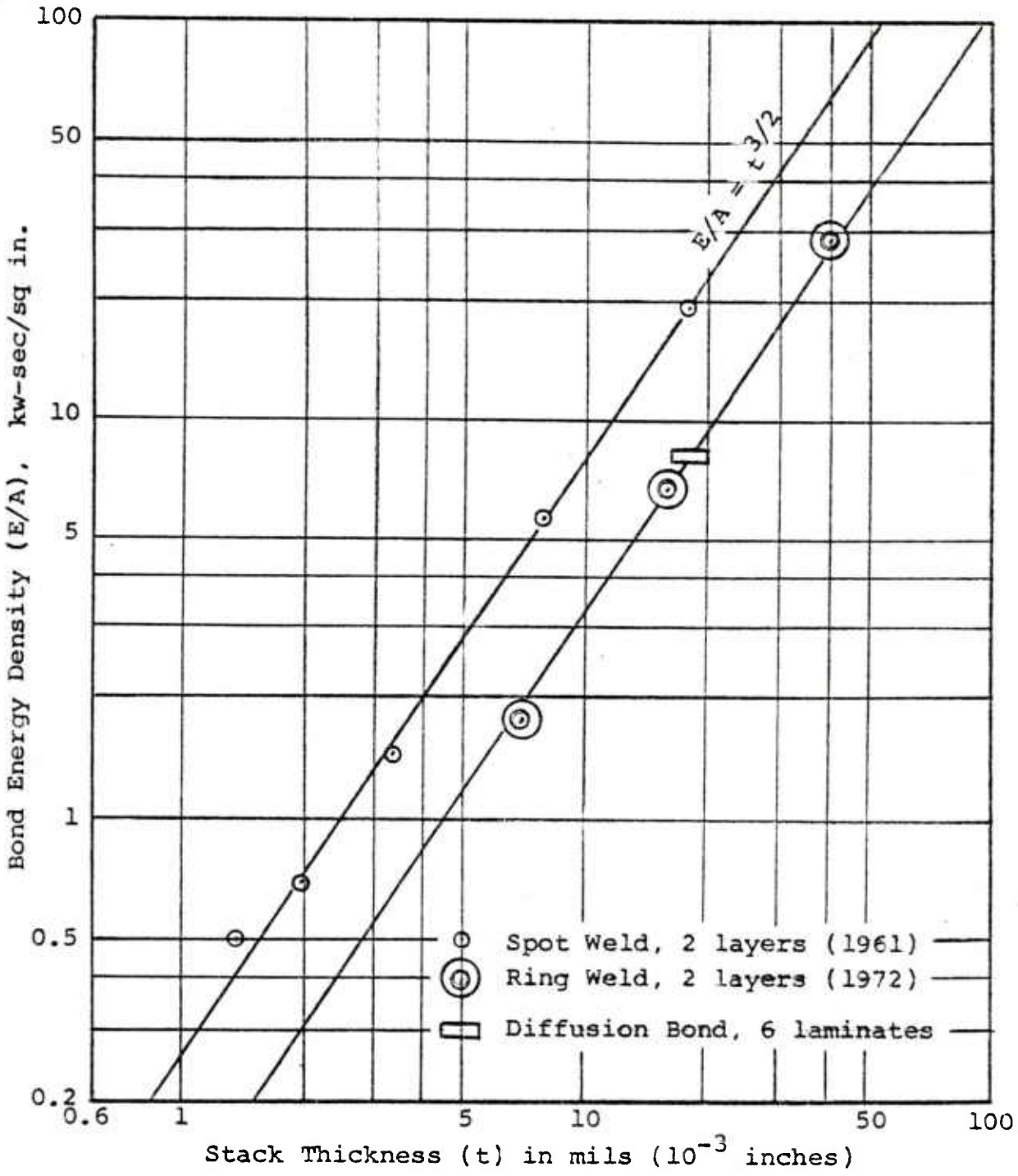

Figure 2. Ultrasonic bond energy density for aluminum foil.

versus t). Data for diffusion bonding of etched aluminum laminates as reported in Section V fall directly upon the ring weld data line. These diffusion bond data include sample sizes from 1/2 by 1/2 inch up to 1 by 1 inch.

The energy offset shown on Figure 2 between ring welds (1972) and spot welds (13) is largely due to differences in acoustical conversion efficiencies of the early magnetostrictive transducers and the higher efficiencies of piezoelectric tension-shell transducers.

A. RF POWER MONITOR

A wideband RF power meter has been incorporated into and is available for use with medium- or high-power ultrasonic equipment. The power monitoring module samples the frequency converter output power and detects the forward and load power based on the principle of directional coupling in a transmission line. This is processed electronically to provide true rms values and is displayed on the panel meter as either the forward or load power (as selected by a toggle switch). Load power refers to the true transducer drive power which has been acoustically absorbed. The difference between forward and load power represents the reflected power induced by impedance mismatches, either electrical or acoustical.

The functions of the RF power monitor are:

1. System Tuning

   Facilitates frequency tuning without the use of external instrumentation. At any given power step, the frequency is adjusted until maximum load power is indicated. This corresponds to the best operating frequency.

2. Electronic/Acoustic Impedance Matching

   Provides impedance matching information. With the power switch in the forward position, the meter indicates the power available from the frequency converter (P_F). In the load position, the power meter indicates the power being absorbed by the load (P_L). The difference between these readings is the reflected power (P_R).

Best ultrasonic efficiency is usually obtained with lowest reflected power. A large reflected power (when the unit is adjusted for best frequency) indicates an impedance mismatch. When a large mismatch is found during an initial machine setup, tap changes can be made in the RF transformer connections to remedy this situation and provide more efficient operation.

3. System Repeatability

Eases repeat setup for any application. Once it has been established that a certain application is successful at a given load power, the application can be set up again at any future time with the same load power.

4. Quality Control Monitoring of Laminates

Provides quality control monitoring. A malfunction in the ultrasonic unit or a substantial difference in the quality of the parts being processed will cause a change in the load power reading and alert the operator. If an increase in reflected power is discovered as a production application continues, this indicates a change in parts quality, or surface condition, or tooling wear as another quality control parameter.

$$P_L + P_R = P_F$$

Tuning goal: Maximize P_L.

Impedance matching goal: Minimize P_R.

The power monitor is standardly supplied with an analog panel meter. Response time is 1.5 seconds, which is suitable for any continuous-duty application, including ultrasonic tube drawing, seam welding, extrusion, machining, and deep drawing, or for welding applications requiring a 2-second or longer ultrasonic power pulse.

An optional light-emitting diode (LED) linear display with 50 point resolution and 15 millisecond response time is available for short pulse duty applications, including

ultrasonic spot welding, ring welding, plastics welding, insertion, staking, and upsetting. This LED display was used during this study.

B. IMPEDANCE MATCHING BETWEEN FREQUENCY CONVERTER AND ACOUSTIC LOAD

Well-designed and efficiently operated ultrasonic systems require an impedance matching network between the power amplifier and the ultrasonic transducer. As an ultrasonic bonding system is pushed toward its limits, impedance matching becomes increasingly more important.

Figure 3 shows the effects of impedance mismatch upon load power. The ability to deliver power to the load decreases rapidly as the impedance mismatch increases. For example, in order to deliver 3000 watts from the 4000-watt, 50-ohm frequency converter, the load impedance presented by the impedance matching network and the acoustic system must lie between 1/3 and 3/1 of 50 ohms (or between 17 and 150 ohms).

While not readily apparent, the effective electrical impedance of an ultrasonic transducer increases as the acoustic loading decreases. For example, if the bonding tip couples poorly to the workpiece, the effective load impedance appears high. Likewise, if the interface to be bonded is lubricated or has a low dynamic coefficient of friction, the effective load impedance appears high.

Contrarily, if the bonded interface area increases, the effective load impedance decreases. Consequently, the limitations of any given ultrasonic bonding system are strongly influenced by the acoustic response characteristics of the workpieces and the tip-to-sample coupling.

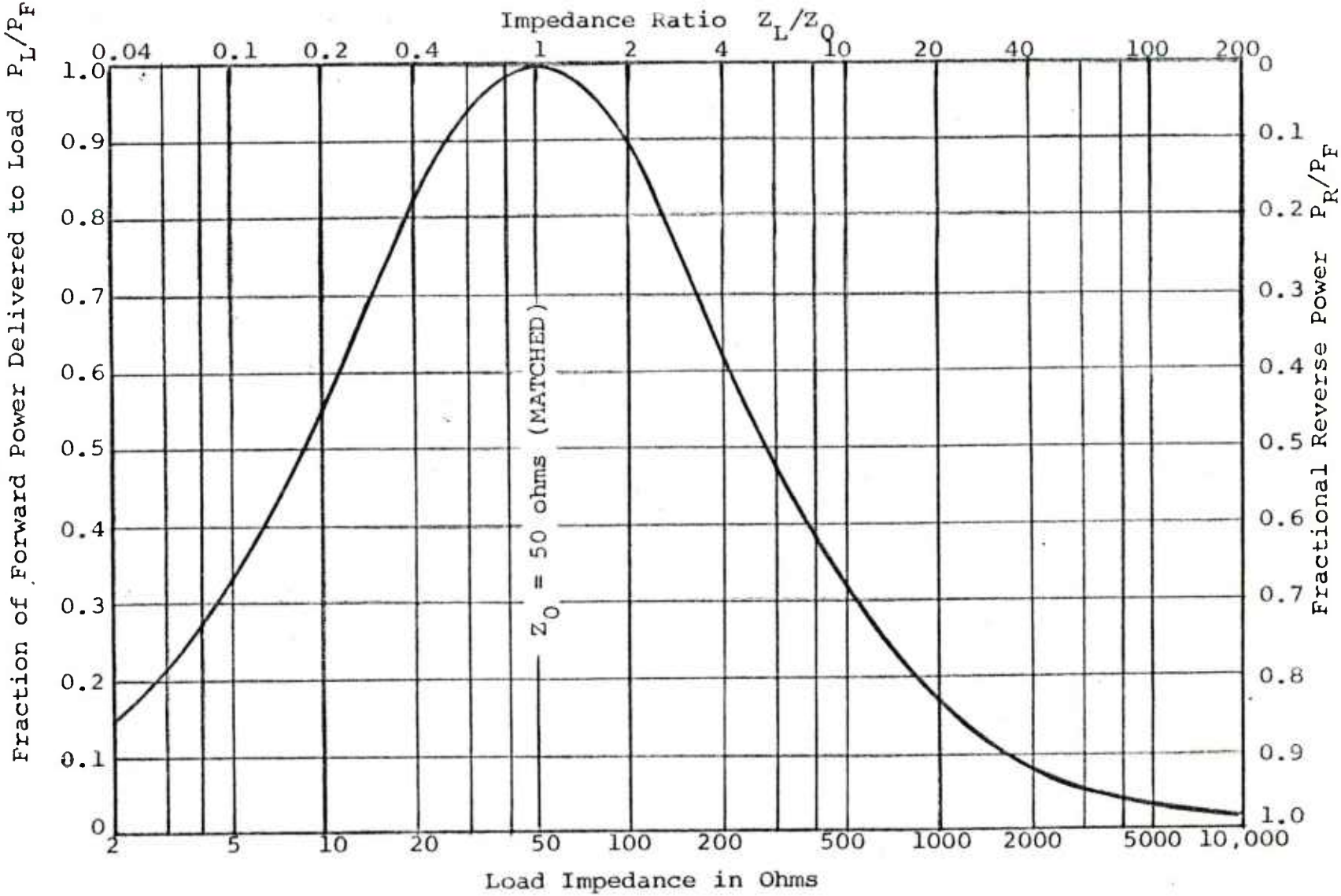

Figure 3. Load and reverse power ratios versus load impedance

III. ULTRASONICALLY ACTIVATED DIFFUSION BONDING SYSTEM

Sonobond pioneered the ultrasonic approach to metal "welding" over two decades ago. Considerable equipment development has occurred during that time span, leading to the apparatus used for this program. In recent years, it became apparent that ultrasonic "welding" is a misnomer and that metal bonding is a better term. Ultrasonically activated diffusion bonding is a more precise term, and it is appropriate to most of the ultrasonic "welding machines" currently manufactured. Hence, this program dealt with the extension of equipment capabilities rather than the development of new equipment.

An ultrasonic bonding system is complex in design but simple in operation. Figure 4 illustrates the instrumented laboratory version of the complete ultrasonic bonding system. The system can be subdivided into four major subsystems:

1. Electronics system (also called frequency converter).
2. Acoustics system (also called the dynamic system).
3. Mechanical system (also called the static clamping system; see Figure 5).
4. Auxiliary instrumentation (may not be employed with production-oriented apparatus).

A detailed listing of the features (as shown in Figure 4), characteristics, and engineering specifications for each of these subsystems is given in Appendix B.

A. INTERLAMINATE SPACING AS DETERMINED BY SURFACE ROUGHNESS

Diffusion bonding is a process whereby imperfect surfaces are forced into partial contact and the contact area is increased via various activation mechanisms. The starting contact point is dependent upon the surface shape (contour) and the microscopic surface roughness. Flat but rough surfaces will have a few large contact sites.

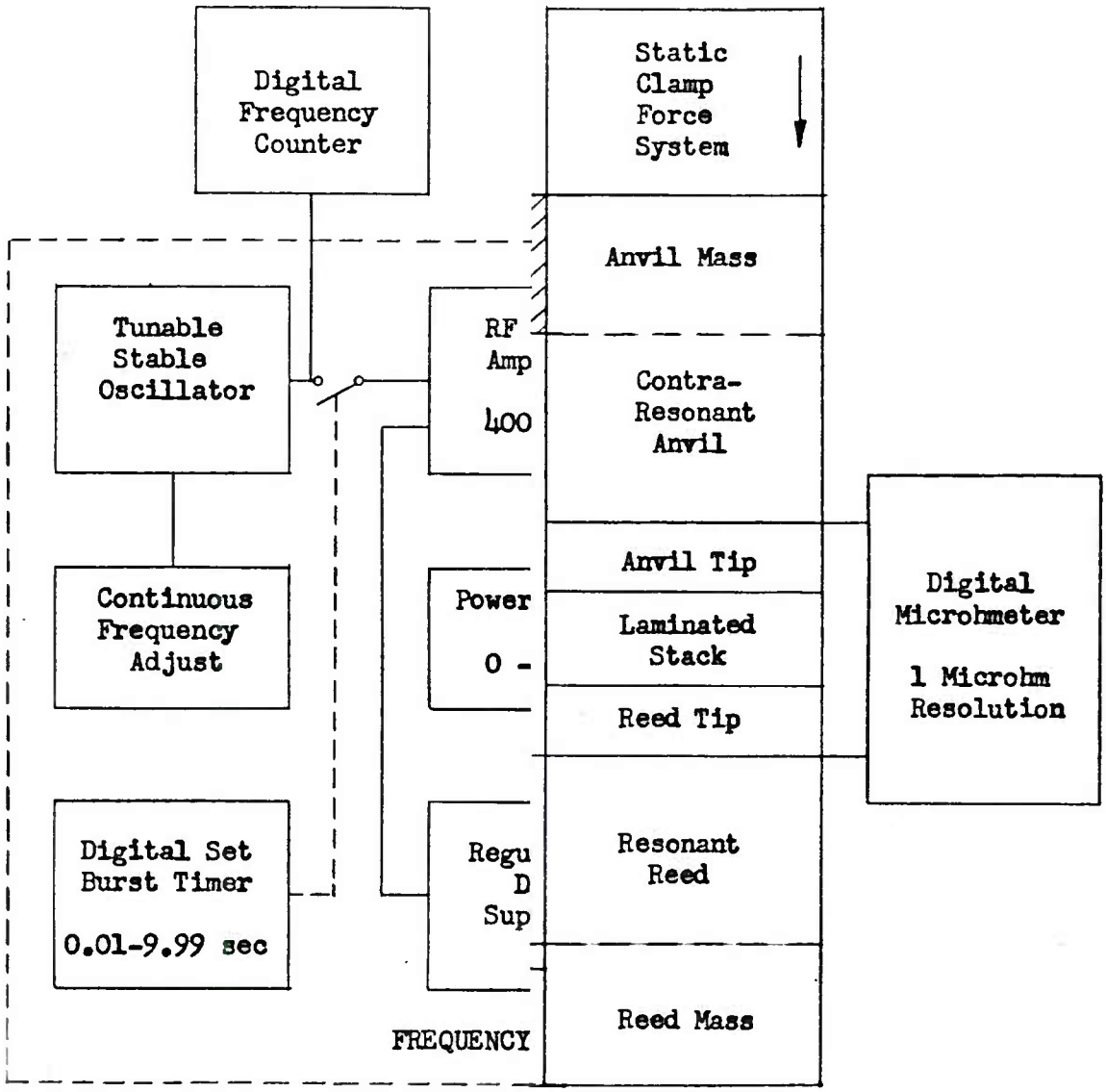
Digital
Frequency
Counter
Static
Clamp
Force
System
Anvil Mass
Tunable
Stable
Oscillator
RF
Amp
400
Contra-
Resonant
Anvil
Anvil Tip
Digital
Microhmeter
1 Microhm
Resolution
Continuous
Frequency
Adjust
Power
0 -
Laminated
Stack
Reed Tip
Digital Set
Burst Timer
0.01-9.99 sec
Regu
D
Sup
Resonant
Reed
Reed Mass
FREQUENCY

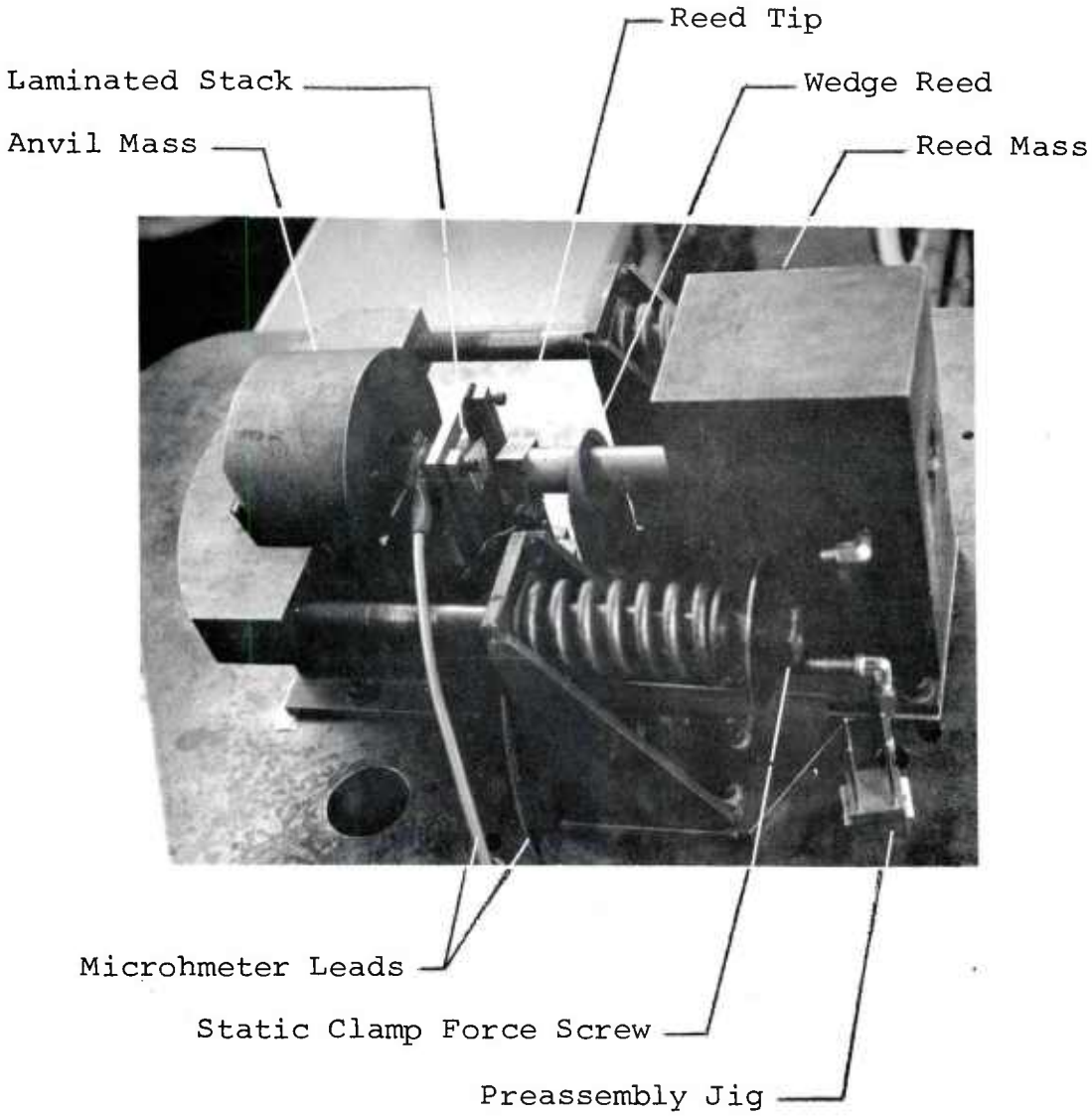

Figure 5. Top view of portion of diffusion bonding apparatus.

Localized plastic deformation of the contact sites is required to increase the number of contact sites and to increase the contact area. Ultrasonic activation provides the mechanism for inducing this localized plastic flow. Once each surface atom is brought into intimate contact with a metallic atom from the other surface, a bond can form. How close is intimate contact? About 4 angstroms (4×10^{-8} centimeters). This is the equilibrium distance between corner atoms of an aluminum single crystal having a face-centered cubic structure (see Appendix E). To better illustrate the smallness of this dimension, Table 3 was compiled to show representative surface roughnesses, film thicknesses, and atomic distances. The upper portion of Table 3 is arranged in progressive order of surface roughness from the 100-microinch lathe-turned steel to the 1-microinch surface of polished plate glass. The latter represents a lower limit for the mechanically scanned surface roughness profilometer type pickup. But even with this readily recognized "smooth" surface, the roughness is two-hundred-fold too large for large-area intimate contact.

Table 3 also shows that representative "thin films" on metallic surfaces are 10 angstroms thick. Such films need to be dispersed to provide intimate contact between virgin metal atoms. Aluminum surfaces oxidize within seconds to an Al_2O_3 film about 15 angstroms thick (see hexagonal lattice constants for Al_2O_3 in Table 3). This oxide layer thickness increases slowly by oxygen diffusion to a very stable, low-permeability film approximately 50 angstroms thick (30). After weeks of aging in air, the aluminum oxide layer changes little because the film is nonporous, ionically bonded, and relatively inert to atmospheric contaminants. Diffusion bonding of aluminum requires disrupting and dispersing this very stiff but brittle layer.

Ultrasonic activation induces plastic flow under the oxide layer in the vicinity of the contact sites, causing a very high stress within the oxide layer.* The oxide layer

(30) Seitz, F., The Physics of Metals, McGraw Hill Book Co., Inc., New York, 1943, p. 190.

*The shear modulus of Al_2C_3 is six times larger than for pure aluminum. Hence, at the aluminum shear yield point, the oxide film (which experiences the same displacement) has a shearing stress six times greater than the underlying aluminum.

TABLE 3. MICROGEOMETRY OF SURFACES AND FILMS

Material	Finish	Contour Notes	Surface Roughness (microinches)	Atomic Scale (angstroms) (Å)
Steel[a]	Lathe-turned	Regular 3-mil pitch	300 (pk-pk) 100 (rms)	
Steel[a]	Ground	Irregular	50 (rms)	
1145 Aluminum	Chemically etched	Random	32 (rms)	
Visible Light	Green (in air)	Wavelength	22	5600 Å
Stainless Steel[a]	Polished	Wavy	8 (pk-pk) waves	2000 Å
	(Amorphous layer 30 Å thick[b])	80-mil pitch	2 (pk-pk) ripple	500 Å
Plate Glass[a]	Ground and polished	Flat	~1 (pk-pk) ~0.4 (rms)	1 μin. = 254 Å
Metal[a]	"Thin film"		t = 0.04 μin. =	10 Å thick
Aluminum	Oxidized surface	Minimal thickness (monolayer)		15 Å thick
		Aged thickness		50 Å thick
Aluminum	fcc crystal	Lattice constant, cube side[c]		4.05 Å

(Continued)

TABLE 3 (Concluded)

Material	Finish	Contour Notes	Atomic Scale (angstroms) (Å)
Aluminum Oxide	Al_2O_3	Hex. lattice constants[c]	a = 4.8 Å c = 13 Å
Al^{+++} Ion		Ionic radii	0.5 Å
O^{--} Ion		Ionic radii	1.4 Å
ALUMINUM FLUIDIC LAMINATE	Photochemically etched	Diffusion bond interface spacing <0.02 μin	~4 Å

[a]Ref. 12. Jones, F. L., The Physics of Electrical Contacts, Oxford Press, 1957, p. 10.

[b]Ref. 1. Adam, N. K., The Physics and Chemistry of Surfaces, Dover Publ., 1968 Reprint.

[c]Ref. 34. Taylor, A. and B. J. Hagle, Crystallographic Data on Metal and Alloy Structures, Dover Publ., 1963.

fractures, releasing a flow of virgin aluminum through the opening toward the mating surface. Metallic bonding occurs where flowing paths intersect. The flow path length is dependent upon the initial surface separation distance, which in turn is dependent upon surface contour and roughness.

For comparison, Table 3 also shows the ionic radii of two (key) ions are under 2 angstroms. These radii establish lower limits on the closeness of "intimate contact."

B. SURFACE TOPOGRAPHY

Even optically polished surfaces do not present large area atomically intimate contact due to nonflatness, waviness, or other surface contours. Such surfaces are typically inspected with narrow-band light illuminating the interface between it and an optical flat. The spacing and shape of the interference fringes allow interpretation of the test surface contours. Good-quality optical flats are specified to be flat over a 2- to 6-inch-diameter region within 1/10 wavelength (2 microinches). Wringing of two such flat surfaces together still does not provide atomically intimate contact as required for diffusion bonding. Conditions are closer, however, since Johansson gauge blocks fall in this category and they will become bonded over local regions if stored in contact over extended periods of time.

Since it is impractical to consider fabricating optically polished and flat laminates for fluidic devices, bulk plastic deformation must be induced to cause the surface contours to coincide across each laminate interface. Ultrasonics provides the activation mechanism for the plastic shape changes required, as discussed later in this report.

With an ultrasonic energy density chosen for low compressive deformation, the average interface spacing would be reduced to about one-fifth the initial value, or 45 microinches. Figure 6 shows a photomicrograph of a six-layer assembly where the interface spacing varies from zero to 100 microinches, but averages about 50 microinches as predicted (note that 0.010 inch on a 200X enlargement equals 50 microinches). Figure 6 represents a stack cross section which is well consolidated via bulk plastic deformation, metallically bonded at spaced contact points and ionically bonded at some of the intermediate points. If this section came from a functional fluidic device, it is predicted that

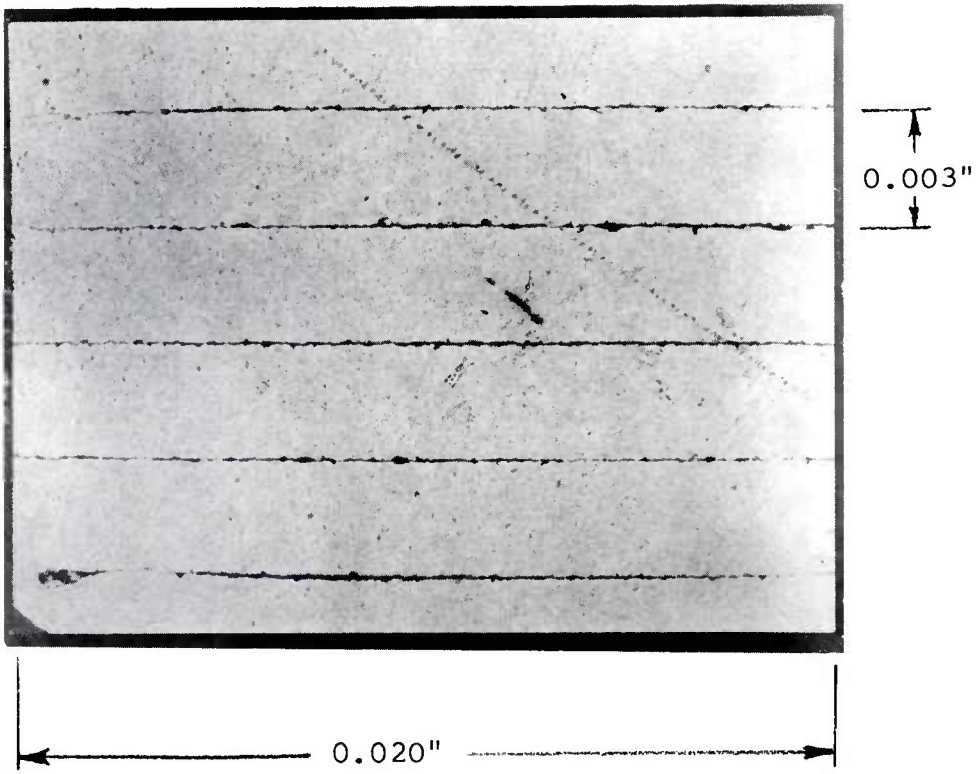

Figure 6. Sectional view of ultrasonically assembled etched aluminum laminates at 200X magnification (early, low-power example).

the leak rate would be acceptably low, i.e., less than a few percent of the volumetric flow rate being controlled. Leak rate measurements carried out in a later portion of this work are described in Appendix A.

C. INTERLAMINATE CONTACT AREA

The statistical model for surface roughness described in Appendix C lends itself to prediction of contact area versus interface spacing for both static loading (largely elastic deformation) and dynamic loading (largely plastic deformation). In turn, the contact area, number of contact sites, and contact size distribution can be used to predict both the electrical and the mechanical properties of the laminate assembly. Qualitatively, the predictions show a fundamental correlation between electrical resistance and shear strength of laminated stack assemblies.

Figure 7 is a large-scale model of two rough surfaces in contact. The model has single values for asperity geometry (i.e., peak height, peak spacing, peak shape, and peak placement along the surface plane). This model serves to illustrate several aspects of the analytical model presented in Appendix C, namely:

1. Initial contact sites are finite in number (three points are the extreme lower limit).

2. Initial contact areas are small until increased by static loading, dynamic shearing, or both.

3. Complete consolidation and 100 percent contact can be accomplished by surface conformation even though the surfaces are rough.

D. UNIFORMLY DISPERSED BONDING SITES

Conventional ultrasonic bonding induces atomically intimate contact over a large percentage of a finite bond region. Ultrasonically activated diffusion bonding (as developed for aluminum laminates) induces an array of bonded sites more or less uniformly dispersed throughout the overlap region. In Appendix C, it is shown that the percentage of area metallically bonded is small for etched aluminum contact surfaces. However, the localized bond strengths

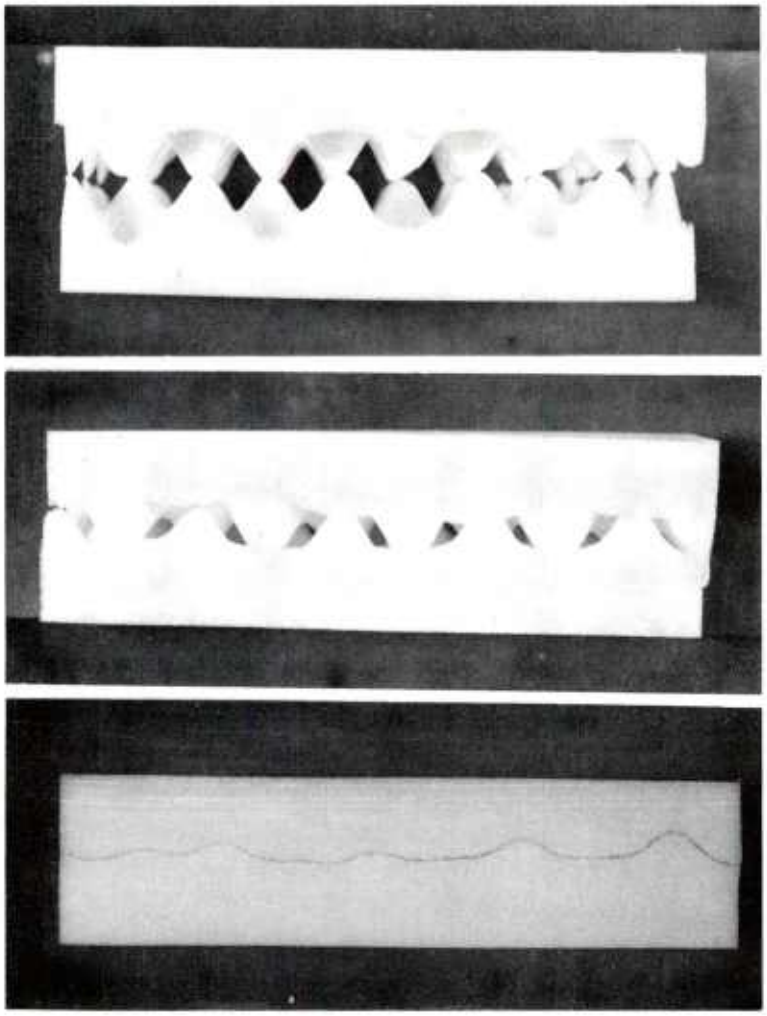

A. Initial zero-load contact

B. Contact with imperfect mating

C. Contact with complete consolidation

Figure 7. Model of rough surface multiple contact interface.

approach parent metal strength as found with conventional ultrasonic nuggets. With the statistically distributed surface peaks description of laminate bonding as consisting of a uniformly dispersed array of strongly bonded points, each of the experimental observations becomes understandable and self-consistent. Hence, trends in laminate bonding can be properly defined, and extrapolations to larger overlap areas and thicker stacks can be more reliably forecast.

Samples of the Army-supplied aluminum laminates (which had undergone photochemical etching to generate fluidic channels) were scanned with a Brush Surface Analyzer. The etched surface roughness averaged about 32 microinches. When two such surfaces are placed in contact at low clamping force, only a few extreme points touch, leaving an interface spacing which is relatable to the rms roughness value of each surface (see Appendix C).

E. SURFACE OXIDATION

Oxidation occurs first at the surface of a metal, and the resulting scale forms a barrier that tends to restrict further oxidation. For oxidation to continue, either the metal must diffuse through the scale to the surface, or the oxygen must diffuse through the scale to the underlying metal. The tendency for aluminum to oxidize is greater than for iron, but because the oxide barrier formed on aluminum is extremely adherent and quite impervious to diffusion, the rate of oxidation is rapidly decreased. Two factors contribute to this effect: (a) The aluminum and oxygen are very tightly bonded so that the aluminum ions cannot readily diffuse through the oxide layer toward the surface, and (b) the crystal structures of the aluminum oxide and of the aluminum can be oriented so that there is very little mismatch and considerable continuity from one phase to another. As a result, there is a strong coherency between the aluminum oxide surface and the aluminum metal (39). Because of this strong coherency, there is no fundamental need to completely expel the oxide from the interfaces to be bonded.

---

(39) Van Vlack, L. H., Elements of Material Science, Addison-Wesley Publishing Co., Reading, Mass., 1960.

IV. PRELIMINARY DIFFUSION BONDING STUDIES

Initially work progressed toward obtaining optimum impedance matching for effectively applying acoustic power to a stack of two and six aluminum foil test coupons. Several system limitations were revealed during this preliminary testing. The two aluminum foil stacks showed an indication of bonding activity having taken place. All testing was performed at room temperature, atmospheric pressure, and with mill-finish aluminum foil coupons which had not been surface-cleaned or polished.

With the ultrasonic array assembled as described earlier, initial evaluation was carried out to establish optimum acoustic impedance matching between the acoustic system and the frequency converter, using six aluminum foil (1145-H19 alloy) coupons interlaced to form a bond area approximately 1/2 inch square. Positioning pins were not installed in the tips for the initial tests. The system incorporated the original 2400-watt transducer assembly used on the previous contract. Optimum impedance matching was obtained at low input power levels but, because of the older design of the original transducer, voltage limitations were encountered when the system was driven at a 3000-watt level.

Six foil test coupons were made using a punch plate and were inserted on the positioning pins in an alternate pattern as depicted in Figure 8. The coupons were placed under a clamping force of 740 pounds and acoustic power was applied. Optimum impedance matching was obtained at input power levels up to 3000 watts. Acoustic energy (the product of power and time) could be increased by lengthening the time of the acoustic power burst. The frequency converter was capable of delivering 4000 watts continuous and thus induced no power limitation. The power monitor circuit, digital timer, and power delivery of the frequency converter all worked satisfactorily.

A. LAMINATE ALIGNING PINS

The anvil tip was modified to accept two test laminate positioning pins, and the reed tip was modified to provide two clearance holes for the positioning pins. The pins were placed in the anvil tip because this tip underwent less physical displacement with the application of acoustic power.

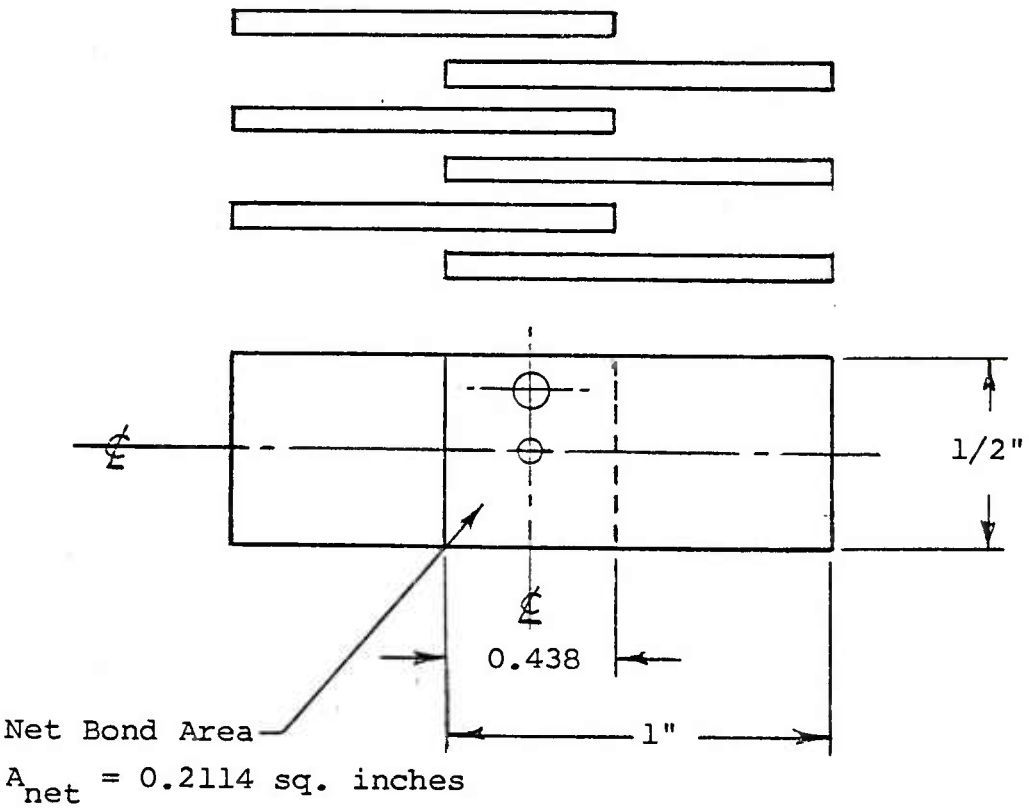

Figure 8. Aluminum test foil stack arrangement.

The hole pattern and pin diameter were made to accommodate the test laminate supplied by the US Army Armament Research and Development Command (ARRADCOM).

A punch plate was fabricated to make aluminum foil (1145-H19 alloy) coupons 1 by 1/2 by 0.0035 inch for preliminary tests. Positioning holes were punched in the exact location of those in the test laminates supplied by ARRADCOM.

B. INSTRUMENTATION

Temperature monitoring was added to the equipment via a Doric Scientific Model 410 digital temperature TRENDICATOR which would accept wire thermocouples. A thermocouple wire was placed in the anvil tip to provide a bulk temperature measurement of the acoustic tip area for monitoring the presence of acoustic power activity at the tips. Another thermocouple wire mounted on the transducer shell provided indication of excessive energy in the transducer.

The TRENDICATOR provided a temperature resolution of $\pm$ 0.1°C (or $\pm$ 0.1°F) and a response time of 0.3 second per reading at low temperature magnitudes, and 1.5 seconds per reading at a temperature of 3200°F. The fast response time was beneficial in measuring temperature rise during short bursts of acoustic power. This instrument had the further advantage that the cold junction temperature compensation was built in.

C. STATIC FORCE SYSTEM

The static force system was found to have a practical limit of 3000 pounds, because of the manual torque required to turn the 3/4-16 threaded rods. This limit applied to the insertion and removal of aluminum foil coupons or actual laminates on a short-time-interval series of tests. Larger static clamping forces could be achieved on an infrequent basis.

D. PRELIMINARY SYSTEM LIMITATIONS

1. Acoustic system: 2400 watts maximum continuous input with existing 2400-watt transducer.

2. Electronic system: 4000 watts maximum continuous output; set to operate at 2400 watts.

3. Static force system: 3000 pounds for repetitive testing.

4. Reed cooling system: For room-temperature tests, compressed air was used for cooling.

5. Anvil temperature monitoring: The thermocouple wire installed in the anvil tip provided immediate monitoring of bulk heating effects.

6. Sample temperature monitoring: A miniature shielded thermocouple bead in contact with the foil (or laminate) stack.

E. BONDING OF TEST COUPONS

Preliminary bonding experiments were carried out with laminates of test coupons made from 1145-H19 mill-finish aluminum alloy, 1 by 1/2 by 0.0035 inch. Test conditions for this series of experiments were as follows:

Room temperature

Atmospheric pressure

Overlap area: 0.2114 square inch

No special cleaning or polishing of specimens

Number of laminates: six

Reed and anvil tip material: stainless steel annealed

Tip surface: ground to about 6 microinch finish (rms)

Tip size: 2 inches diameter.

Initial experiments were carried out at several clamp force levels, ultrasonic power levels, and ultrasonic exposure times to serve as a guide for later tests. Data for this exploratory work are provided in Table 4.

Subsequent tests were made using the bonding parameters shown in Table 5, which also shows the compressive deformation of each sample after bonding.

TABLE 4. EXPLORATION OF DIFFUSION BONDING PARAMETERS

Static Clamp Force F (lb)	Static Stress σ (psi)	Total Acoustic Energy[a] E_{total} (watt-sec)	Total Coupling Time t_{coup} (sec)	Acoustic Power Input $P_{in(av)}$ (watts)	Average Ultrasonic Power Density (watts/in.^{2})	Normalized Exposure Time[b] t_{nor} (sec)
740	3,500	49,550	39.9	1240	2932	20.6
1110	5,250	200	0.5	400	946	0.08
1480	7,000	64,145	35.8	1789	4231	26.7
2220	10,501	104,540	42.3	2471	5844	43.5
2960	14,001	56,750	22.5	2522	5964	23.6

[a] E_{total} = Total energy into acoustic system ($E_{total} = \sum P_{load} \times t_{coup}$).

[b] t_{nor} = The time power is applied to acoustic system based on 2400 watts electrical power input: $\left(t_{nor} = \frac{E_{total}}{2400}\right)$.

TABLE 5. TEST COUPON BONDING DATA

Sample No.	Static Clamp Force F (lb)	Static Stress σ (psi)	Total Acoustic Energy* E_{total} (watt-sec)	Total Coupling Time t_{coup} (sec)	Acoustic Power Input* $P_{in(av)}$ (watts)	Average Ultrasonic Power Density* (watts/in.^{2})	Mean Compressive Deformation (percent)
3	2220	10,501	62,800	36	1744	8,251	9.9
4	2220	10,501	50,000	20	2500	11,825	2.4
5	2220	10,501	104,000	40	2600	12,298	3.7
6	2220	10,501	100,800	40	2520	11,920	9.9
7	2220	10,501	192,000	80	2400	11,352	14.3
8	2220	10,501	207,600	80	2595	12,275	8.6

*These data refer to RF load power (P_{RF}) into the acoustic system.

To obtain an early indication of the peel strength associated with each layer, some of the samples were subjected to a simple peel test in which no fixture was used to keep the pull angle or bend radius constant. Adjacent layers in the coupon stack were secured in the jaws of an Instron tensile testing machine so that each layer formed a 90-degree angle with the bonded portion of the stack. Maximum peel strengths for Sample #3, for progressive layers from the reed tip side, were 4.0, 4.0, and 0.5 pounds; for Sample #5: 5.0, 6.5, 8.0, and 5.0 pounds; and for Sample #7: 8.0, 10.0, 10.5, and 6.5 pounds (see Figure 8 for stack assembly).

In addition, a tensile test was performed on the layer of Sample #3 closest to the anvil tip. The parent metal strength was 38.5 pounds, and the test coupon single-layer strength was 40.5 pounds, which shows close agreement. It was noted that this layer broke at the bond seam. Since this sample was bonded with lower energy input than the other samples in the series, no further tensile tests were performed; it was anticipated that the individual layers of the samples bonded at higher energy levels would likewise break at the bond seam at a tensile strength approximating the parent metal strength.

F. BONDING OF TEST LAMINATES

Since effective bonding was achieved with the test coupons, further bonding tests were carried out with actual test laminates, using the same bonding conditions as for the coupons:

Room temperature

Atmospheric pressure

Overlap area: 0.2114 square inch

No special cleaning or polishing of specimens

Reed and anvil tip material: stainless steel annealed

Tip surface: ground to about 6 microinch finish (rms)

Tip size: 2 inches diameter.

Samples #9 through #12 were subjected to the same bonding parameters as the test coupons, but the compressive deformation was substantially greater than for the coupon series. Consequently the static clamping force was reduced by half for the remainder of the tests (Table 6).

Before any changes were made to the test fixture, bonded specimens were prepared with 6, 12, and 18 laminates to determine the maximum number of laminates that could be handled with the existing laminate retainer pin design and to obtain an early indication of the effect of the number of laminates on bond quality with the selected test parameters. As shown in Table 6, ultrasonic coupling time was progressively increased for each laminate group.

G. EFFECTIVENESS OF TEST FIXTURE

After the above samples had been prepared, the acoustic system was disassembled to correct noise that had developed in the reed and anvil tip area. It was found that the joint between the force-insensitive mount and the test fixture sealing flange and also the joint at the base of the wedge coupler had worked loose. The effect of these loose joints on the acoustic system was to reduce acoustic power transmission efficiency. The power delivered to the laminate stack is the product of the input power ($P_{in(av)}$) and a constant (K). The constant, however, is the product of all the coupling coefficients associated with each joint in the acoustic system, starting with the transducer and ending with the anvil.

The results of acoustic system performance calculations predicted that a threefold increase in the acoustic power (P_A) was obtained from the reworked system.

The total acoustic energy (E_{total}) into the acoustic system was varied by varying the number of 4-second power bursts. The total coupling time (t_{coup}) is the product of the number of power bursts (N) times 4 seconds per power burst.

As the bonding experiments progressed, the test laminates began bonding to the drive reed and anvil tips. This demonstrated that the tip material must be changed from 303 stainless steel to a material with greater yield strength

TABLE 6. SMALL TEST LAMINATE BONDING DATA

Test laminates consisted of ARRADCOM-supplied 3-mil-thick laminates chemically etched with process resolution chart pattern.

Laminate size: 1/2 x 1 inches
Overlap region: 1/2 x 1/2 inches
Interface area: 0.211 square inches

Sample No.	Static Clamping Stress (psi)	Total Acoustic Energy* (watt-sec)	Total Coupling Time (sec)	RF Load Power (watts)	Average Ultrasonic Power Density* (watts/in.^{2})	Mean Compressive Deformation (percent)
6-LAMINATE STACKS						
9	10,500	48,000	20	2440	11,500	24.4
10	10,500	50,000	20	2500	11,800	--
11	10,500	47,600	20	2380	11,200	32.4
12	10,500	98,400	40	2460	11,600	37.4
13	5,250	46,000	20	2300	10,800	14.8
14	5,250	43,200	20	2160	10,200	12.5
15	5,250	83,600	36	2320	10,900	22.6
16	5,250	88,000	40	2200	10,400	24.7
17	5,250	181,600	80	2270	10,700	30.8
18	5,250	166,000	80	2075	9,800	33.3
12-LAMINATE STACKS						
19	5,250	47,600	20	2380	11,200	18.0
20	5,250	43,200	20	2160	10,200	18.4
21	5,250	76,800	40	1920	9,000	12.7
22	5,250	87,200	40	2180	10,300	13.3
23	5,250	172,800	80	2160	10,200	22.1
24	5,250	182,800	80	2285	10,800	27.9

(continued)

TABLE 6 (Concluded)

Sample No.	Static Clamping Stress (psi)	Total Acoustic Energy* (watt-sec)	Total Coupling Time (sec)	RF Load Power (watts)	Average Ultrasonic Power Density* ($watts/in.^2$)	Mean Compressive Deformation (percent)
18-LAMINATE STACKS						
25	5,250	49,200	20	2460	11,600	12.3
26	5,250	48,400	20	2420	11,400	10.7
27	5,250	97,600	40	2440	11,500	21.5
28	5,250	84,400	40	2110	9,900	17.9
29	5,250	188,000	80	2350	11,100	28.1
30	5,250	174,800	80	2185	10,300	28.6

*These data refer to RF load power (P_{RF}) into the acoustic system.

and with a textured finish instead of a smooth finish on the tip faces.

The test data indicated certain trends. There was an increase in compressive deformation with increase in total energy input. The number of laminates used with the test coupons was six, and the clamping force was 2220 pounds. The test laminates bonded under the same conditions showed a higher compressive deformation than did the test coupons, indicating an increase in coupling of acoustic power to the laminate stack. At a clamping force of 1110 pounds, the compressive deformation decreased with a decrease in total energy input and in general decreased with an increase in the number of laminates in a stack.

The bond quality as determined visually appeared to improve with reduced clamping force and with reduced energy input. The minimum energy required for a good visual bond depended on the number of laminates in a stack.

H. SUMMARY OF OBSERVATIONS

1. The trends suggested that clamping force and possibly input power should be reduced to arrive at a minimum achievable compressive deformation with "good bonding" under the existing test conditions.

2. A new tip design and acoustic system improvements should increase coupling of acoustic power to the laminate stack.

3. The design of the laminate retaining pins limited the working number of laminates in a stack to 18 (with 3-mil-thick laminates). Pin length was arbitrarily chosen to accommodate a stack thickness of 60 mils early in the program and does not represent a system limit.

V. BONDING STUDIES WITH LAMINATES OF INCREASING AREA

Improvements were made to the acoustic bonding system, and the modified system was used to prepare a total of 26 bonded laminate samples with 1/2 by 1/2 inch overlap area. A dramatic improvement in bonding performance was obtained.

An energy input level (E_{total}) of approximately one-fourth of that used previously was applied to the test laminates. Comparable percent compressive deformation was obtained, substantiating earlier predictions. Also, bonds with significantly less compressive deformation were achieved as the total input ultrasonic energy level was reduced.

As a result of the improved efficiency of the acoustic system, experimental data were obtained for observing the effect on visual bond quality and compressive deformation by varying the following parameters:

	Constant	Variable
a.	Clamping Force (F) No. of Laminates (N) Laminate Thickness (L) Bond Area (A) RF Load Power (P_{load})	Bonding Time (t) and Input RF Excitation Energy (E_{total})
b.	Total Input Ultrasonic Energy (E_{total}) No. of Laminates (N) Laminate Thickness (L) Bond Area (A) Bond Time (t) RF Load Power (P_{load})	Clamping Force (F) (fourfold range)

	Constant	Variable
c.	Static Compressive Stress (σ)	Bond Area (A) (fourfold range)
	Average Ultrasonic Power Density Input (P/A)	
	Bond Time (t)	

In-situ electrical resistance measurements of the various laminate stacks were obtained during the bonding cycle. A bench model pneumatic press was set up to obtain static electrical resistance measurements (under reproducible contact force conditions) to determine if a trend relating electrical resistance to bond quality could be ascertained.

A. TEST COUPONS

Using the newly modified acoustic system, tests were first made on coupons of 1145 aluminum foil, 3 mils thick. The frequency and power levels of Samples #3 and #4 (Table 5) were used as a starting point. The test conditions were as follows:

Room temperature

Atmospheric pressure

Overlap area: 0.2114 square inch

No special cleaning or polishing of specimens

Number of layers: six

Reed and anvil tip material: M2 tool steel heat-treated to Rc 60-62

Tip surface: EDM 200

Tip size: 1-1/8 inches square.

During the tuning and impedance matching procedure, a total energy input of $E_{in(total)} = 37{,}600$ watt-seconds* was applied to the first test coupon stack in a series of time

* 1 watt-second = 1 joule.

bursts while optimizing electrical drive parameters. This sequence was terminated because the metal in the bond area was excessively distorted and compressed to the extent that the bond area was increased to almost twice the original size. This overdone sample serves to illustrate the results of ultrasonically induced superplasticity over prolonged periods or at high energy density. As predicted, significantly more acoustic power was being coupled to the test coupon stack than was the case with earlier samples (#3 and #4). Analysis of the modified acoustic system estimated a threefold increase in available acoustic power (P_A). From the extreme compressive deformation of Sample #31, as well as the system analysis, it was concluded that the acoustic power (P_A) increased by a factor of 4 to 1.

B. ETCHED LAMINATE BONDING CONDITIONS

Having defined a range for the ultrasonic energy input (E_{total}), testing was resumed on the etched laminates. Test conditions were the same as those listed above, except that the overlap area was increased.

Three overlap areas were examined: 1/2 by 1/2 inch; 1/2 by 1 inch; and 1 by 1 inch. An optimum operating frequency and proper impedance match were achieved for each overlap area. Bonding conditions for the three areas are given below:

	Small Stack	Intermediate Stack	Large Stack
Overlap area (A), ($in.^2$)	0.25	0.5	1.0
Clamping force (F), (pounds)	555	1110	2220
Average load power (P_L), (watts)	600	1200	2400
Number of laminates (N)	6	6	6
Laminate thickness (L), (inch)	0.005	0.005	0.005

	Small Stack	Intermediate Stack	Large Stack
Stack thickness (NL), (inch)	0.030	0.030	0.030
Compressive stress (σ = F/A), (psi)	2220	2220	2220
RF power density (δ = P_L/A), (watts/in.^{2})	2400	2400	2400
Bond time (t), (seconds)	3.34	3.34	3.34
Energy density, (joules/in.^{2})	8016	8016	8016

C. SMALL-SIZE ETCHED LAMINATES

The second series of tests was made with laminates having an overlap area of 1/2 by 1/2 inch. The RF excitation energy (ultrasonic input) was an order of magnitude less than that previously used. E_{total} was 12,000 joules and less at an RF load power input, P_{RF}, of 600 watts (Table 7), instead of the previcus 175,000 joules and less at an RF load power input of 2400 watts (Table 6).

This first examination of bond area versus bond quality was performed keeping compressive stress (σ), RF power density (δ), and bond time (t) constant. A simple linear scaling model would predict constant bond quality, while previous ultrasonic experience would predict a nonlinear degree of deformation. The results shown in Table 7 reveal a nonlinear deformation relationship.

Examination of Figure 9 shows that good visual bond quality was being obtained in the 1000-joule range for the conditions annotated on the graph. It would be desirable to undertake auxiliary tests that would yield quantitative results on bond quality. The stack electrical resistance measurement was considered one means of achieving this goal.

TABLE 7. COMPRESSIVE DEFORMATION VERSUS STATIC CLAMP FORCE FOR TEST LAMINATES

Test laminates consisted of ARRADCOM-supplied 3-mil-thick laminates chemically etched with process resolution chart pattern.

Laminate size: 1/2 x 1 inches
Overlap region: 1/2 x 1/2 inches
Interface area: 0.211 square inches

Sample No.	Static Clamp Force (lb)	Static Compr. Stress (psi)	Total Acoustic Energy* (watt-sec)	Total Coupling Time (sec)	RF Load Power (watts)	Average Ultrasonic Power Density* ($watts/in^2$)	Mean Compressive Deformation (percent)
6 LAMINATES							
32	2220	10,500	13,600	48	283	1340	21.6
33	2220	10,500	6,000	12	500	2365	19.4
34	2220	10,500	2,400	4	600	2838	14.2
35	2220	10,500	1,000	2	500	2365	10.9
36	1110	5,250	12,800	20	640	3027	20.3
37	1110	5,250	5,400	9	600	2838	22.7
38	1110	5,250	2,400	4	600	2838	11.7
39	1110	5,250	1,200	2	600	2838	6.1
40	555	2,625	12,400	20	620	2932	29.5
41	555	2,625	6,000	12	500	2365	16.8
42	555	2,625	2,000	4	500	2365	18.1
43	555	2,625	1,200	2	600	2838	9.5

*These data refer to RF load power (P_{RF}) into the acoustic system.

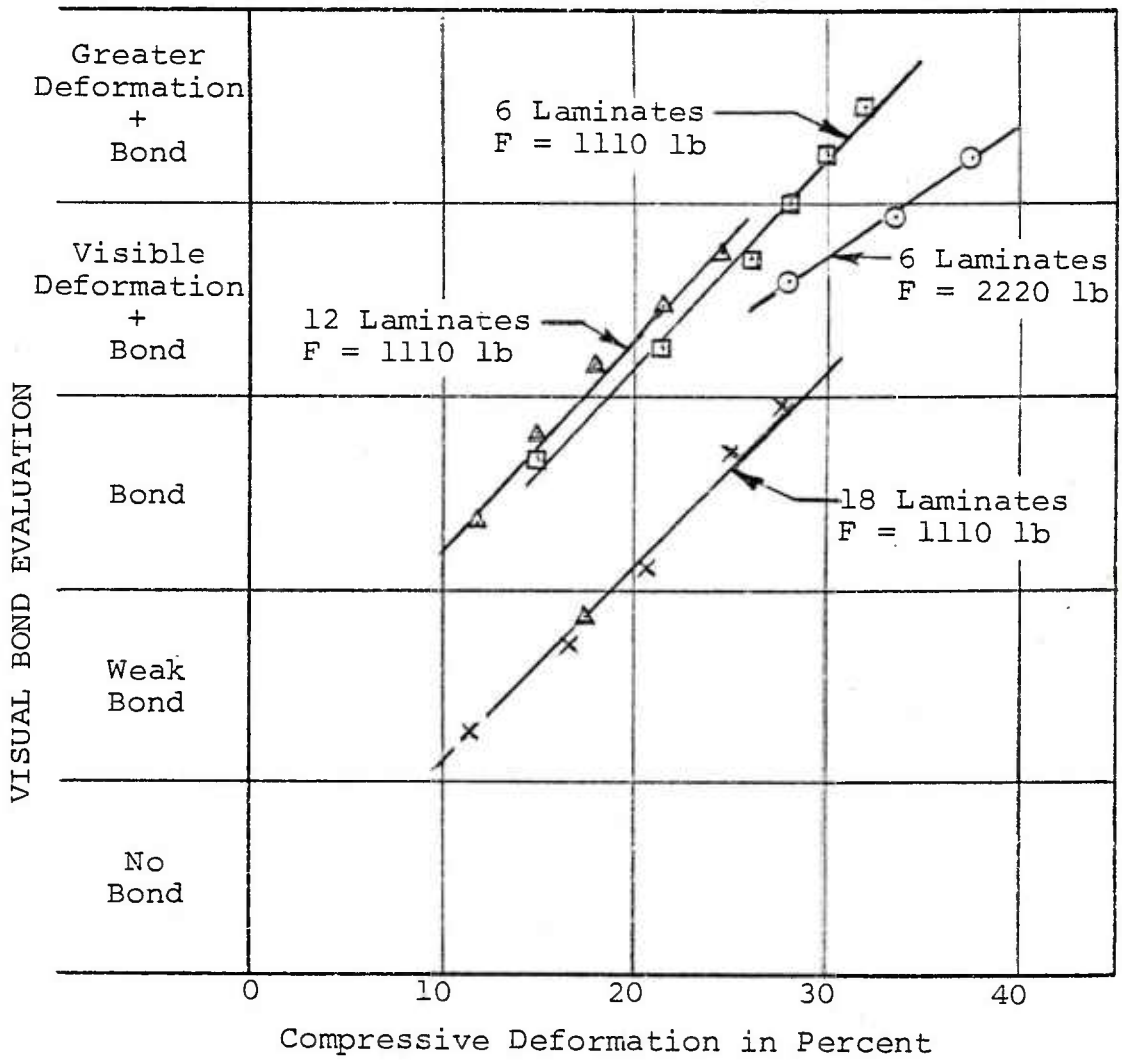

Figure 9. Visual bond quality versus compressive deformation (representative for 3-mil etched laminates, 1/2 by 1/2 inch)

D. INTERMEDIATE-SIZE ETCHED LAMINATES

A third series of tests was made on etched laminates having a 1/2 by 1 inch overlap area. As noted, the RF load power for this series was increased from 600 to 1200 watts, since the overlap area was doubled, while the compressive stress was held constant (2200 psi). Again good-quality bonds were obtained (Table 8) but with substantially reduced deformation.

In-situ measurements of the electrical resistance of the laminate stack were made on samples obtained during this series. Figure 10 shows typical results of the total RF input energy versus the assembly electrical resistance. Note the dramatic drop in resistance as the oxide interface is dispersed and the metallic bond is formed at the intermediate energy levels. The total resistance measured included contributions from the copper shim electrodes, the reed and anvil tips, the laminate stack, and the contact resistances for the 1/2 by 1 inch contact areas. The fixture resistance represents a major portion of the final assembly resistance: over 80 percent, as shown in Figure 10. Because of the relatively high fixture resistance, an interim goal for the face-to-face stack resistance was set at under 100 microhms. Subsequent analysis and photomicrographs show that the goal should have been more stringent (e.g., under 10 microhms).

E. LARGE-SIZE LAMINATE BONDING

Attempts to bond 1.0 by 1.5 inch etched laminates with 1.6-inch-square tips were not successful due to the large operating frequency shifts introduced by the massive tips. Attempts to operate at abnormally low frequencies (e.g., at 14.1 kilohertz with 15-kilohertz transducers) also led to large impedance mismatches which limited the available RF load power.

Static electrical resistance measurements were made of the extra large laminate stack assemblies obtained during these experiments. Representative results are summarized in Table 9. Those in the first group (Samples #61 to #64) were produced using the 1.5 by 1.5 inch tips and the larger 3.2 kilowatt (rms) transducer. Overall, the power delivered was not sufficient to obtain good bonding for the area.

TABLE 8. FUNDAMENTAL BONDING PARAMETERS FOR VARIOUS SIZE TEST LAMINATES

Sample No.	Static Compr. Stress (psi)	Total Acoustic Energy (watt-sec)	Total Coupling Time (sec)	RF Load Power (watts)	Average Ultrasonic Power Density (watt/in.^{2})	Mean Compr. Deform. (%)	Bond Area (appr.) (in.^{2})	Contact Area Shape*
48	2220	2004	3.34	600	2400	18.7	0.25	
49	2220	2004	3.34	600	2400	23.1	0.25	
50	2220	4008	3.34	1200	2400	1.3	0.5	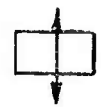
51	2220	4008	3.34	1200	2400	1.2	0.5	
56	2220	8016	3.34	2400	2400	2.3	1.0	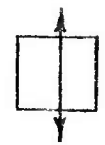

*The laminate stacks were always oriented with the acoustic shearing displacement parallel to the laminate minor axis. When the contact region has an aspect ratio of 2 to 1, the laminate orientation becomes more critical.

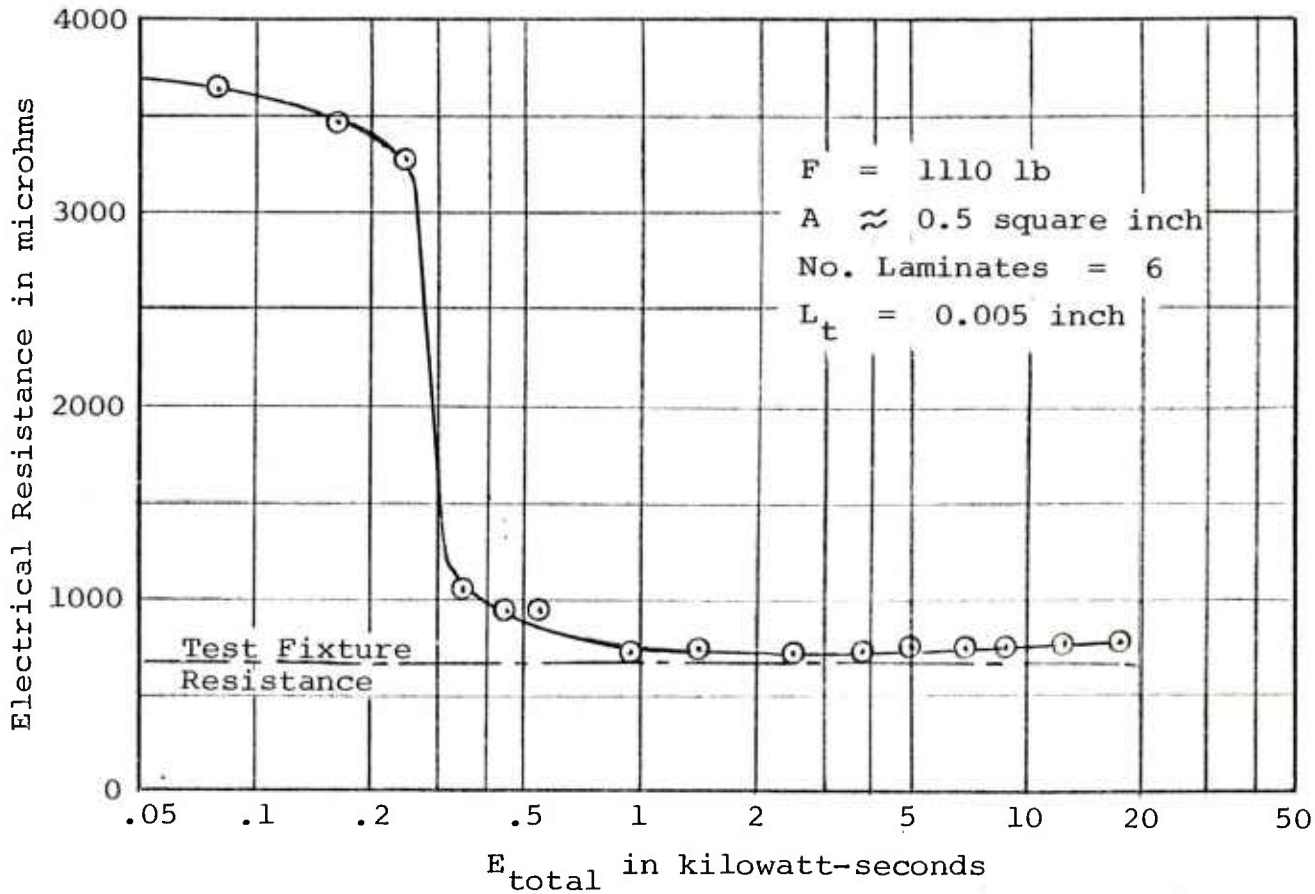

Figure 10. Electrical resistance of laminate assembly as a function of ultrasonic energy input.

TABLE 9. STATIC ELECTRICAL RESISTANCE MEASUREMENTS ON ASSEMBLED STACKS

Sample No.	No. of Laminates	Bond Area ($in.^2$)	$*R_{sample}$ in microhms at Static Loads of 78 lb	157 lb	314 lb	157 lb	78 lb	Visual Bond Quality
REPRESENTATIVE SAMPLES OBTAINED FROM DIFFUSION BONDING TEST FIXTURE								
76	6	1.0	46	26	11	16	30	Good bond
78	12	1.0	56	32	17	22	38	Good bond
Cu Electrodes			142	136	132	134	139	Calibration
61	12	1.5	4,785	2,171	1,147	1,140	2,417	Weak bond
62	6	1.5	2,761	1,182	377	540	945	Weak bond
63	12	1.5	245,000	170,000	70,000	110,000	155,000	No bond
64	6	1.5	221,000	250,000	90,000	120,000	500,000	No bond
Cu Electrodes			125	119	113	115	118	Calibration
REPRESENTATIVE SAMPLES OBTAINED FROM STANDARD SCNOBOND 4-KW SPOT WELDER MODEL W-4000								
W3	6	1.0	603	299	128	162	313	Good bond Laminates skewed
W7	9	1.0	951	394	163	204	411	Good bond Laminates skewed
W4	12	1.0	670	324	118	143	301	Good bond Laminates skewed

$*R_{sample} = R_{measured} - R_{Cu\ electrodes}$.

New (lower mass) tips 1.1 inches square were made for use on 1.0 by 1.1 inch laminates. Impedance matching, power delivery, and bonding results were better. With the addition of a larger, higher power transducer (3200 watts, as described in Appendix B), much better bonding results were obtained. Many parametric bonding studies were conducted at load power levels of 2500 to 3100 watts. Because the solid overlap area was approximately 1 square inch, the power density values were numerically similar to the load power readings.

By way of comparison, it was observed that a good visual bond was produced for each of the bond areas tested, and that the compressive deformation obtained in samples with bond areas of 0.5 and 1.0 square inch was substantially less than that obtained in samples with a 0.25-square-inch interface area (Table 8). Since the 1/2 by 1 inch samples and the 1 by 1 inch samples listed in Table 8 were obtained under one set of test conditions only, no conclusions relative to optimization of bond energy for larger laminates could be drawn at that time.

It was also observed, with respect to the largest (1 by 1.1 inch) area, that another system limit was defined, i.e., the maximum peak voltage rating of the 2400-watt transducer of 2500 volts (zero to peak) was reached in attempts to deliver the 2400 watts dictated by the test criteria.

In summary, visually good-quality bonds were obtained with three different size contact areas, without excessive deformation, within a few seconds ultrasonic bonding time, on as-received surfaces, without special atmospheres, on etched foil fluidic laminate stacks made from 1145 aluminum alloy, as supplied by ARRADCOM.

F. DIFFUSION BONDING TESTS ON A STANDARD W-4000 SPOT WELDER

As noted in Appendix B, the ultrasonic diffusion bonding system differed acoustically and mechanically from the more conventional ultrasonic spot welders.

During the period when the diffusion bonding system was undergoing mechanical changes, a Sonobond standard W-4000 metal spot welder was used for acoustic design comparison tests. Table B-4 in Appendix B summarizes the key

design features and differences for the two systems. To facilitate recommendations toward ultrasonically activated diffusion bonding of larger laminates and thicker stacks, these differences were evaluated directly by laminate bonding tests.

The most pronounced effect was the skewing of the laminates within a stack during bonding on the W-4000 welder. A variety of stack clamping approaches were tried, including pop rivets and binder head screws, with little success. A review of the welder revealed a "kick" at the reed tip at medium to high power levels. This kick was a visible forward jerk of the reed tip relative to the anvil tip, probably induced by a static couple associated with the offset clamping force axis and the moving head design. Each time a kick was observed, the upper laminates were skewed forward with reference to the lower laminates. The skewing was too severe to provide meaningful high-power tests as planned.

However, medium power tests typified by data in Table 10 show a few interesting differences. The effective transducer impedance on the W-4000 welder was consistently lower than for the diffusion bonding system. This lower impedance had the advantage of requiring lower drive voltages to reach similar load power levels (as shown in Table 10). The lower impedance occurs because of the different flexural mode of vibration designed into the two resonant reeds. Consequently, future diffusion bonding systems would perform best if the reed design were similar to the W-4000 and the static force were applied via a moving anvil. This combination corresponds to the new M-8000 spot welder made available within the last 6 months. Unfortunately, the latest M-8000 welder was shipped before it could be evaluated for diffusion bonding.

In-situ stack resistance measurements also showed the effects of laminate skewing as the final value increased with each skewing increment (Samples W3 to W7 in Table 9). The revised diffusion bonding system (operated at medium power) produced a six-layer stack with a stack resistance ($\lesssim$ 200 microhms) manyfold lower than obtained on earlier tests. Stack resistance measurements confirmed the presence of better bonds as seen by visual examination of surfaces and edges.

TABLE 10. BONDING CHARACTERISTICS OF TWO TYPES OF ULTRASONIC WEDGE-REED SYSTEMS

Bonding Tests 1 x 3 Inch Laminates 1 x 1 Inch Overlap 6-Laminate Stack	Revised Diffusion Bonding System (Moving Anvil)	Standard W-4000 Metal Spot Welder (Moving Head)
LAMINATE ALIGNMENT		
General Comments	Simple rubber-lined picture frame Clamp adequate	Laminate skewing, despite clamps, bolts, rivets
Cause of Skewing	None, due to rigidly mounted acoustic system	Minute clearance in moving head dovetail slide
BONDING TESTS		
	Specimen #66	Specimen #69
Operating Frequency	14,370 Hz	14,230 Hz
Frequency Shift re 15 kHz	- 630 Hz	- 770 Hz
RF Load Power	2000 watts	2200 watts
Effective Transducer Impedance	1480 Ω	1120 Ω
Transducer Drive Voltage	3300 V (0-pk)	2900 V (0-pk)
In-Situ Stack Resistance		
Initial (before RF)	2200 μΩ	3800 μΩ
Final (after RF)	700 μΩ	830 μΩ
Note: Fixture resistance of ~600 μΩ included in data		Note: Higher resistance indicative of smeared interfaces during skewing

Flexural rigidity tests made on samples assembled on the W-4000 spot welder at higher bond energy levels (5400 joules) showed higher stiffness, indicating a larger percentage of interface area bonded (see Figure 14). These results suggest additional studies should be conducted at still higher energy density levels for the larger laminated stacks.

G. BONDING TIME VERSUS EXTRUSION TIME

The 1-1/8-inch-square tips originally made for the 1/2 by 1/2 inch overlap laminates were tried without the two aligning pins. Bonding with extended time (3-4 seconds) at medium power caused the aluminum to partially extrude into the vacant pin holes. Reducing the bond time to 1 second produced very little extrusion and good-appearing bonds when the load power was above the threshold value. It became apparent that a trade-off exists between time required to form a diffusion bond and the allowable time for extrusion of unsupported areas. The optimum time appeared to be in the order of 1 second. While this conclusion needed verification via sectioned stack assemblies, it did appear a promising way of minimizing fluid channel collapse while providing low-leak assemblies.

Electrical resistance measurements on samples from this group (Samples #76 and #78 in Table 9) showed uniformly low values (< 60 microhms), approaching the range where acceptable leak rate samples should be obtained.

H. STACK ASSEMBLY BY SUBGROUPS

Since thickness limitations do exist with each ultrasonic system, it is appropriate to ask if subgroups of laminates can be bonded separately and then combined. From a simple energy density viewpoint, subgroups offer no advantage because the final stack assembly thickness limitation still exists. However, because of the energy threshold phenomena, assembly of bonded subgroups into the total stack could extend the stack thickness limit.

The interassembly of active element laminates with fluid channel and manifold laminates can lead to unsupported regions involving more than one layer. Interface bonding

at unsupported regions is weaker than at supported regions. For this reason, the last test conducted during this program consisted of assembling stacks via the subgroup approach. Four layers of active elements plus two bonding manifolds constituted one subgroup (see Figure 11). A second subgroup consisted of four layers of fluid channels and a final manifold. These two subgroups were then assembled into the active device stack at the same power density levels employed for the subgroups. Stack resistance measurements indicated the same final value was obtained as for the earlier assemblies made with a single power burst. Visual examination of the exhaust port channels and the images of the underlying channels showed less distortion for the subgroup approach, as shown in Figures 19 and 20. Optimization via stack resistance and visual deformation revealed that shorter power bursts would lead to both low distortion and low stack resistance.

The reduced distortion effect is understandable in terms of the time required for material flow during plastic deformation associated with laminate distortion. For power bursts under 1/2 second, very little distortion occurred. By employing 1/2-second bursts for each subgroup and the final assembly, each laminate was exposed to ultrasonic activation for 1 second total. But only half of the total time involved attempts to bond multiple layers of unsupported regions.

The original photographs of the top and bottom views of assembled active device stacks (Figure 12) show surface texture differences which reveal the underlying fluid channel and control geometry. This X-ray-like portrayal is due to the heavy impression of the tip EDM surface upon the best supported regions. The unsupported regions do not replicate the EDM texture and hence leave a contrasting image.

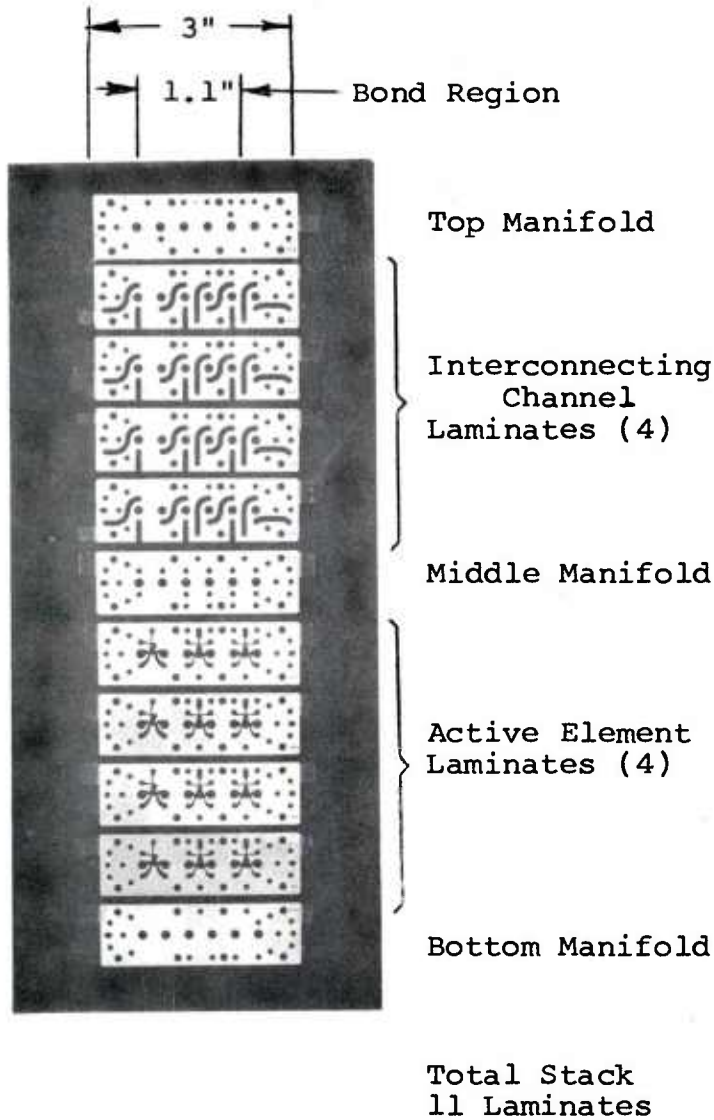

Figure 11. Array of 5-mil etched laminates as assembled for active element tests.

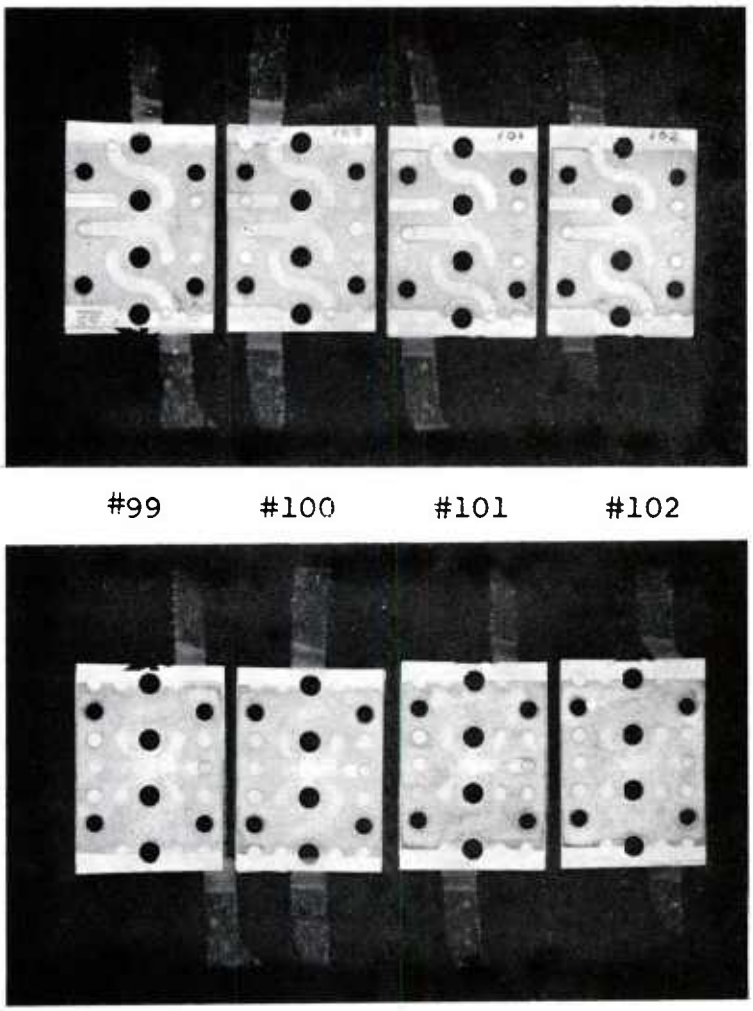

Figure 12. Top and bottom views of assembled stacks containing an active fluidic circuit.

VI. CHARACTERISTICS OF BONDED LAMINATES WITH UNIFORMLY DISPERSED BONDING SITES

A. TENSILE-SHEAR STRENGTH

Through the use of chemically roughened surfaces, initial contacts between surfaces become widely separated but with uniform concentration over interface areas large compared with the peak roughness values. Initially, the site concentration is very low, giving an apparent low strength per unit area of overlap. The bond strength at each bond site, however, may be of "nugget" quality. In fact, the total bond averaged over the contact area (only) is expected to equal parent metal strength.* It is the low bond site concentration density which facilitates large area laminate bonding at relatively low acoustic power densities.

Tensile-shear testing of 3-mil-thick 1/2 by 1/2 inch laminate assemblies was attempted early in the study. The bond interface shear strength exceeded the parent metal strength of the thin laminates in each assembly tested. These tests only defined a lower limit to the tensile-shear strength where:

Parent metal breaking load, $P_b = t\ w\ \sigma_u$

t = laminate thickness = 0.003 inch

w = laminate width = 0.5 inch

σ_u = ultimate tensile strength = 23,000 psi

P_b = 35 pounds. (See Appendix E.)

---

*Tensile-shear testing of 1/2 by 1/2 inch laminate assemblies was abandoned early in this program when the samples all failed in the parent metal outside the overlap region. No quantitative data on bond strength could be obtained under those conditions. These early tests did establish lower limits to the apparent strength.

B. COMPRESSIVE DEFORMATION

Each of the laminate stack assemblies has been measured for compressive deformation (i.e., permanent stack thickness change) at several locations within the overlap region. These measurements were made manually with a standard micrometer (0.0001 inch vernier) to provide guidance in defining "excessive deformation." Conventional ultrasonic bonding can often be accomplished with only a few percent compressive deformation. However, the maximum spacing shown on Figure C-2 indicates that a minimum of 8 percent would be required to establish full area contact on etched-surface 3-mil laminates.*

Elastic solids in compressive loading exhibit a lateral expansion due to the Poisson effect. This lateral expansion could have the effect of reducing the fluid channel cross section. However, with etched-surface laminates, the Poisson effect will start at zero and increase toward a value of 0.5 (pure plasticity) as the interface gap approaches zero. In other words, the Poisson effect will be small for the initial 8 percent compressive deformation.

C. PEEL STRENGTH

The apparent peel strength of a laminate stack assembly with 1 percent interface contact area will appear low, as reported in Table 11. But the effective peel strength over a small bond site can correspond to nugget quality. It is apparent that conducting peel tests without defining contact area will have little value. Since the functional fluidic device is not exposed to peel-type loading, peel tests were abandoned except for model confirmation data.

---

*A typical interface spacing of 225 microinches per laminate interface equals:

$$\text{For } t = 3 \text{ mils}, \quad \frac{225 \times 10^{-6} (N - 1)}{3 \times 10^{-3} N} \times 100\% \simeq 7.5\%.$$

$$\text{For } t = 5 \text{ mils}, \quad \frac{225 \times 10^{-6} (N - 1)}{5 \times 10^{-3} N} \times 100\% \approx 4.5\%.$$

TABLE 11. PEEL STRENGTH IN MULTI-LAYER TEST COUPONS

0.0035 x 1/2 x 1 inch coupons
1/2 x 1/2 inch overlap area

1145-H19 Unetched Sample No.	Layer from Drive Reed Tip	Maximum Peel Strength (lb)	Peel Strength (lb/inch)
3	1	4.0	8
	2	4.0	8
	3	0.5	1
	4	*	*
5	1	5.0	10
	2	6.5	13
	3	8.0	16
	4	5.0	10
7	1	8.0	16
	2	10.0	20
	3	10.5	21
	4	6.5	13

*This layer was subjected to tensile test mentioned in accompanying text.

D. FLEXURAL STIFFNESS

Tensile-shear tests and peel strength tests were not found to be adequately sensitive to small changes in bonding parameters. Neither would be useful for parametric optimization studies. A brief review of flexural stiffness calculations suggested that a standard three-point loading fixture might provide a means of nondestructive mechanical evaluation of assembled stacks. Figure 13 shows a miniature fixture used for exploratory measurements.

Force-deflection measurements were made on a few assemblies using fixed spaced drill rods to apply line contact loading over the central portion of the stacks. Figure 14 shows the very low stiffness (70 pounds per inch) measured for loosely stacked laminates (12 layers) where a 1-pound force produced a 0.014-inch deflection.

Similar deflection on bonded specimen #98 required a force of 21 pounds (giving a flexural stiffness of 2200 pounds per inch). Hence the interface bonding obtained with 0.8 second ultrasonic activation increased the flexural stiffness by more than twentyfold. A solid aluminum bar with the same dimensions as the laminated stack (11 layers) would have a stiffness of 18,000 pounds per inch, which is 121 times the loose stack. This shows that the percent interface area bonded at low energy (e.g., specimen #98) is small but finite.

A higher bond energy sample (#W-4) assembled on the W-4000 spot welder gave 50 percent higher stiffness (0.010 inch deflection with 24 pounds force = 3700 pounds per inch). Thus, these stiffness measurements confirm that a significant fraction of the interface area is bonded at low ultrasonic energy and that both the stiffness and the bond area increase as the bond energy increases.

E. SINGLE NUGGET VERSUS DISPERSED SITE BOND AREA LIMITATIONS

With conventional ultrasonic metal bonding, the largest weld spot dimension is smaller than the diameter of the resonant reed. Rectangular bar tips typically have a weld length of 60 percent of the reed diameter or less. Spherically crowned spot weld tips typically generate an oval-shaped nugget less than 50 percent of the reed diameter.

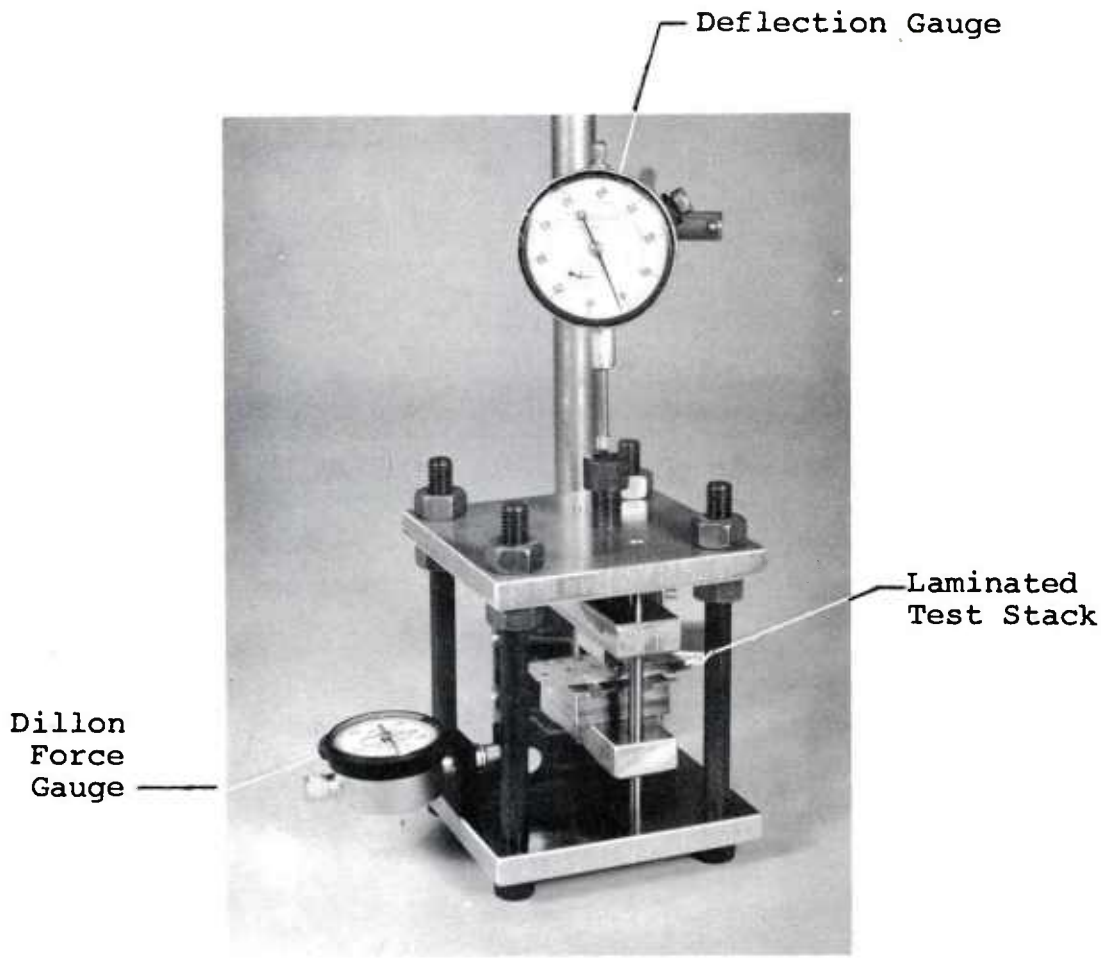

Figure 13. Miniature flexural loading fixture.

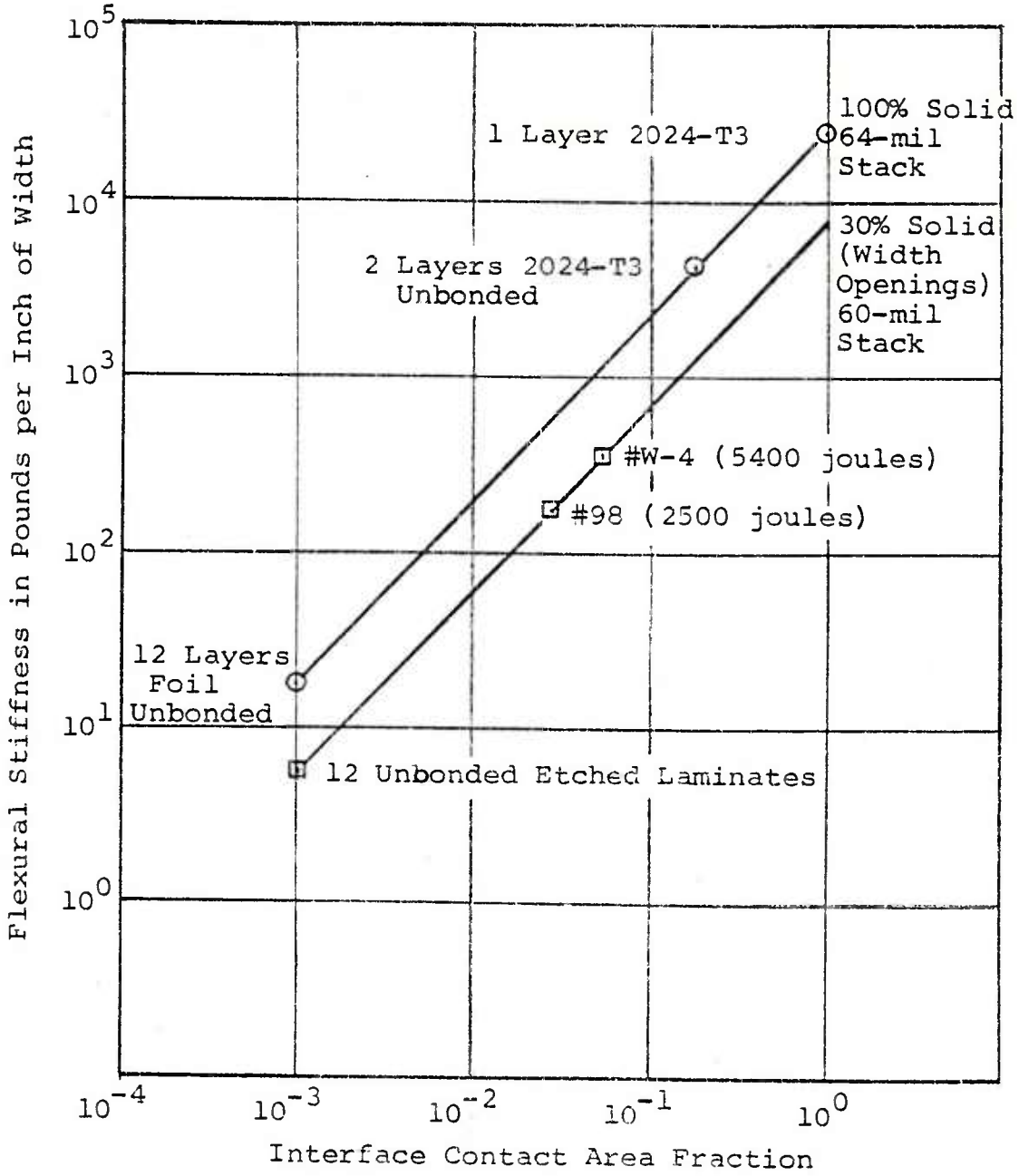

Figure 14. Flexural stiffness of laminated aluminum stacks.

Table 9 shows data from laminates bonded with a 1 x 1 inch overlap area using the diffusion bonding system having a 1-1/8-inch-diameter reed. Clearly the 1.4-inch diagonals on the above laminates extend beyond the reed diameter, yet the corners responded as if equally active with the central region. Because of the distributed bonding sites associated with the etched foil surfaces, the conventional size limitations no longer apply and possibly may be exceeded by severalfold. The statistically random surface texture created by chemical etching suggests that the average bond strength will be uniformly distributed over the full overlap region.

Other system design factors also affect the bond area limitations. The static clamping force system (discussed on page 29) was rather severely limiting. Figure 15 shows the available compressive stress versus spring compression for several stack sizes. Since a compressive stress level in the order of 2000 psi is indicated so far, stack sizes larger than 1 by 1.5 inches will require modifications to the screw-spring system.

The acoustic power density available is determined by the RF load power available from the frequency converter (see Appendix B) and the RF excitation rating of the transducer. Figure B-1 shows the RF power densities available for various stack sizes, for two transducer sizes, and for different frequency converter ratings.

By modifying the system to accommodate the larger tension-shell transducer (rated 5 kilowatts at 50 percent duty cycle), stack sizes up to 1.0 by 1.5 inches can be activated at power densities of 2400 watts per square inch. This power density has produced good results for several stack sizes. The optimum power density is yet to be determined, but should be a similar order of magnitude.

F. RELATIVE LEAK RATE

Two roughened surfaces in light contact will present a tortuous path to fluid flow along the interface. As the contact area increases due to ultrasonically activated plastic deformation of the larger peaks, the resistance to fluid flow would increase. The engineering trade-off between average bond strength, total compressive deformation, and fluid leak rate now envisioned suggests that a

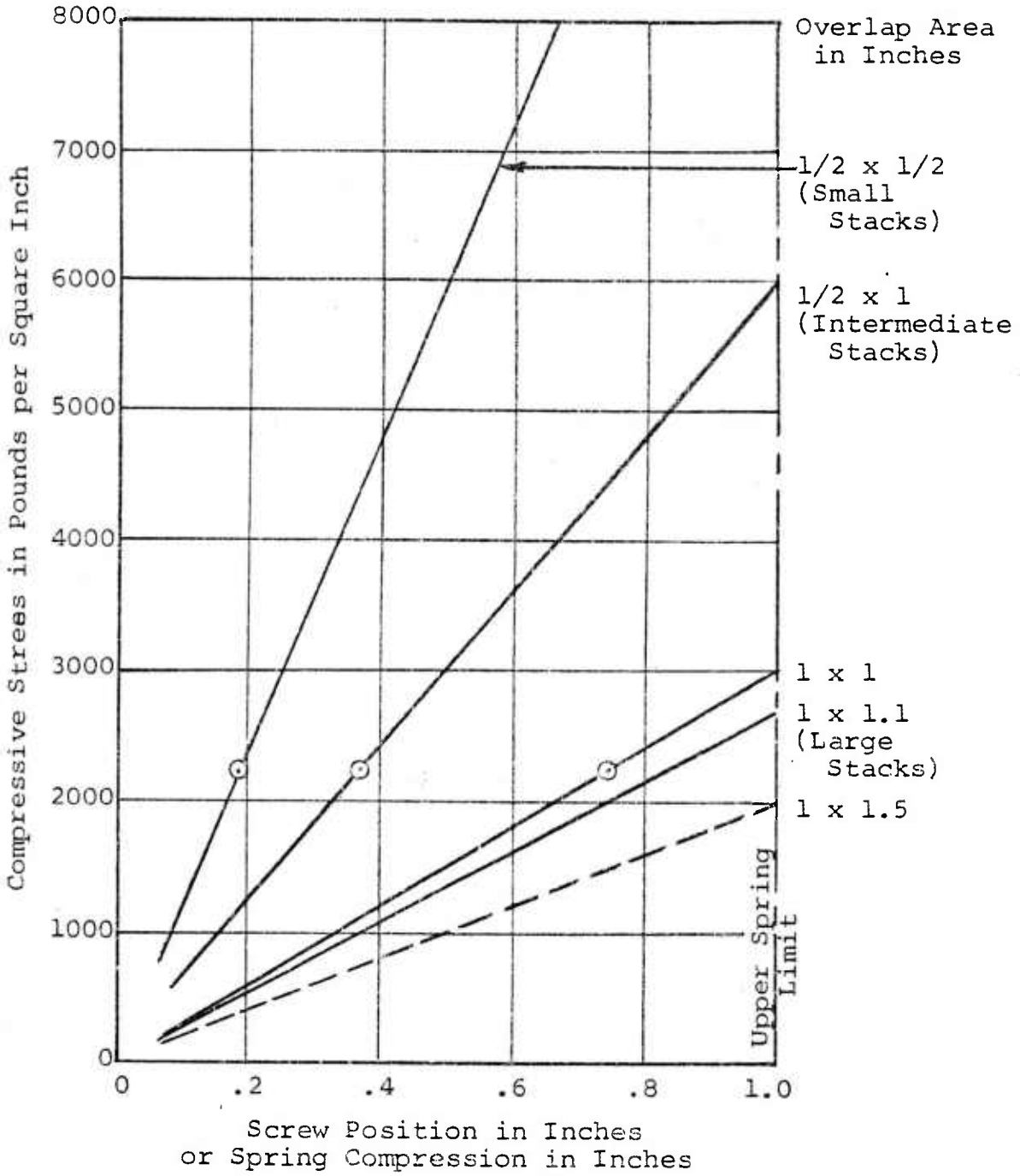

Figure 15. Static clamp force system characteristics.

compromise will be selected where the fluid path will be diffusion. Dushman (7) shows that the gaseous flow rate through a porous solid can be defined by the following equation:

$$F = \frac{7.282 \times 10^{-6}}{\eta} Aa + \frac{0.1636}{\sqrt{M}} \quad (cm^3/sec),$$

where η = shear viscosity of gas,
M = molecular weight of gas,
Aa = gas pressure in atmospheres.

For air (with a pressure differential of 7 psi):

$$\text{Viscosity, } \eta = 1.845 \times 10^{-4} \text{ poise}$$
$$M = 29$$
$$Aa = 0.5 \text{ atmospheres}$$

$$\text{and } F_1 = \frac{7.282 \times 10^{-6}}{1.845 \times 10^{-4}} \times 0.5 + \frac{0.1636}{\sqrt{29}}$$
$$= 0.050 \text{ cm}^3/\text{sec} = 0.006 \text{ scfm.}$$

1. Soap Bubble Leak Tests

A simple but effective test for leaks consists of applying soap film along the exterior surfaces of a pressurized device. The creation of soap bubbles clearly defines the presence of a leak. To establish the order of magnitude of the leak rate, the following assumptions were made:

Bubble shape = sphere
Bubble size = 2 mm diameter
Bubble formation rate $\approx$ 1 per second
Gaseous flow rate, $F = \frac{\text{bubble volume}}{\text{formation rate}}$

---

(7) Dushman, S., Scientific Foundations of Vacuum Technology, J. Wiley & Sons, Inc., New York, 1958, p. 118.

$$F_b = \frac{4}{3} \pi r^3 / BPS$$

$$F_b = 0.004 \text{ cm}^3/\text{sec.}$$

In comparison, the gaseous volumetric flow rate through a duct of uniform rectangular cross section which simulates a fluidic channel is given by the Hagen-Poisseuille law (8) as:

$$Q = \left(\frac{\Delta P}{\Delta L}\right) \frac{1}{2\mu} \left[\frac{ab}{2(a+b)}\right]^2 ab \quad (\text{cm}^3/\text{sec})$$

where a = duct width

b = duct height

ab = duct cross-sectional area

ΔL = duct length

ΔP = pressure differential across channel length

μ = shear viscosity (poise)

$\frac{ab}{2(a+b)}$ = hydraulic radius.

For air at 25°C, $\mu = 180 \times 10^{-6}$ poise (dyne-sec/cm^2)

Let $a = 0.2$ cm

$b = 5 \times 3$ mils $= 0.006$ cm

$\Delta L = 1$ cm

$\Delta P = 7$ psi $= 4.8 \times 10^5$ dyne/cm^2.

Then:

$$Q = \left(\frac{4.8 \times 10^5}{1}\right) \frac{1}{2 \times 180 \times 10^{-6}} \left[0.0029\right]^2 \times 0.2 \times 0.006$$

$$Q = 13 \text{ cm}^3/\text{sec},$$

and the relative leak rate F/Q is small:

$$\frac{F_1}{Q} = \frac{0.05 \text{ cm}^3/\text{sec}}{13 \text{ cm}^3/\text{sec}} = 0.004 = 0.4\%$$

(8) Eshbach, O. W., Handbook of Engineering Fundamentals, 2nd Ed., J. Wiley & Sons, Inc., New York, 1965.

$$\frac{F_b}{Q} = \frac{0.004 \text{ cm}^3/\text{sec}}{13 \text{ cm}^3/\text{sec}} = 0.0003 = 0.03\%.$$

Two 12-layer assemblies consisting of S-shaped fluid channels and enclosing manifold plates were sent to ARRADCOM for leak testing. Unfortunately, the manifold holes did not align with the leak test fixture holes. After drilling holes in the laminated assemblies, both were subjected to the soap bubble leak test. Only one developed small bubbles at a fluid pressure of 5 pounds per square inch. This small leak may have been introduced by laminate burr distortions during drilling.

It is clearly evident that additional leak testing and related bond parameter optimization should be conducted during the next program.

G. ELECTRICAL RESISTANCE

An introduction to an analytical model for the electrical resistance of aluminum laminates is presented in Appendix D. Table 12 summarizes the analysis showing that the constriction resistance associated with the localized contact sites was of major importance. It was also shown that the effective value of constriction resistance depends upon:

a. Number of contact sites
b. Distribution of contact sites
c. Area of contact at each site
d. Height of contact sites relative to base plane
e. Concentration of oxide particles within the interface region.

Each of these parameters also has a pronounced effect upon mechanical strength and acoustic response. Hence, in-situ monitoring of stack resistance during ultrasonic bonding does provide a direct measure of the mechanical properties generated.

Measurement of laminate stack resistance has been greatly facilitated through the use of a digital microhmeter with a resolution of 1 microhm (1×10^{-6}) ohms. This

TABLE 12. CALCULATED AND MEASURED VALUES OF LAMINATE STACK RESISTANCE

Electrical Resistance Characteristics	Calculated Stack Resistance	Static Fixture Resistance Measurements	Dynamic Resistance Measurements: Initial (with Static Clamp Force Only)	Dynamic Resistance Measurements: Final (After Ultrasonic Activation)
FILM RESISTANCE (single 15 μin. oxide layer)	$R_F = 10^{11}$ μΩ			
THREE-CONTACT CONSTRICTION RESISTANCE N = 6, M = 3 a = 16 μin.	$2(R_c)\frac{6}{3} = 45{,}000$ μΩ	~50,000 μΩ at 5 psi		
MULTIPLE CONTACT SITES		Readable to 1 microhm		
N = 6, M = 50 a = 16 μin.	$2(R_c)\frac{6}{50} = 2700$ μΩ	3500 microhms at 150 psi	8000 microhms at 2000 psi	
N = 6, M = 1000 a = 48 μin. (max) a = 16 μin. (min)	$2(R_c)\frac{6}{1000} = 30$ μΩ	90 microhms at 1200 psi	1000 microhms	<100 microhms at 2000 psi
BASELINE DATA	Ohmic Resistance	Electrode Calibration Static Fixture	Electrode Calibration Bonding Fixture	
N = 30, t = 5 mils N = 6, t = 3 mils (A = 0.25 sq in.)	$R_o = 0.8$ μΩ $R_o = 0.1$ μΩ	100 - 300 microhms	500-600 microhms at 2000 psi	

N = number of laminates t = laminate thickness A = laminate overlap area
M = number of contact sites G = surface roughness = 32 μin. (rms) a = contact disk radius

high resolution permits measurement of primary effects such as bond contact area, secondary effects such as pressure and temperature dependence of stack resistance, and possibly even third order effects involving nonlinear dependencies.

The high sensitivity of the microhmeter permits measurements of resistance effects usually considered negligibly small. For example, it was reported in Appendix D that the resistance of copper foil 10 mils thick by 1 inch wide was 90 microhms for a 1-inch clip lead spacing, and further that the ohmic resistance of 59 microhms and a spreading resistance of 30 microhms fully describes the origin of the measured values. Obviously, if the microhmeter can reliably measure the resistance in a short section of copper foil, it can also measure a variety of effects in aluminum laminated stack assemblies.

Figure 16 illustrates measurements made on unbonded laminated stacks while statically loaded within the ultrasonic bonding system. A hysteresis type result was found as resistance measurements were made with both increasing and decreasing loads. During initial loading, the larger surface peaks made contact with the opposite surface and were plastically deformed. This localized plastic deformation caused a reduction in the constriction resistance which largely remained as the loading was reduced.

Figure 17 shows that the entire stack resistance versus static load curve moves to higher values as the number of laminates (and interfaces) increases. It should be noted that the initial (low load) value of stack resistance is in the order of thousands of microhms and increases in proportion to the number of interfaces. It should also be noted that even with very high compressive loads, the final stack resistance of unbonded assemblies remains at several hundred microhms. After bonding, the corresponding stack resistance is manyfold lower (see Table 12). Hence, the stack resistance measurements can distinguish between contact area changes induced by static pressure and those permanently induced by ultrasonic bonding.

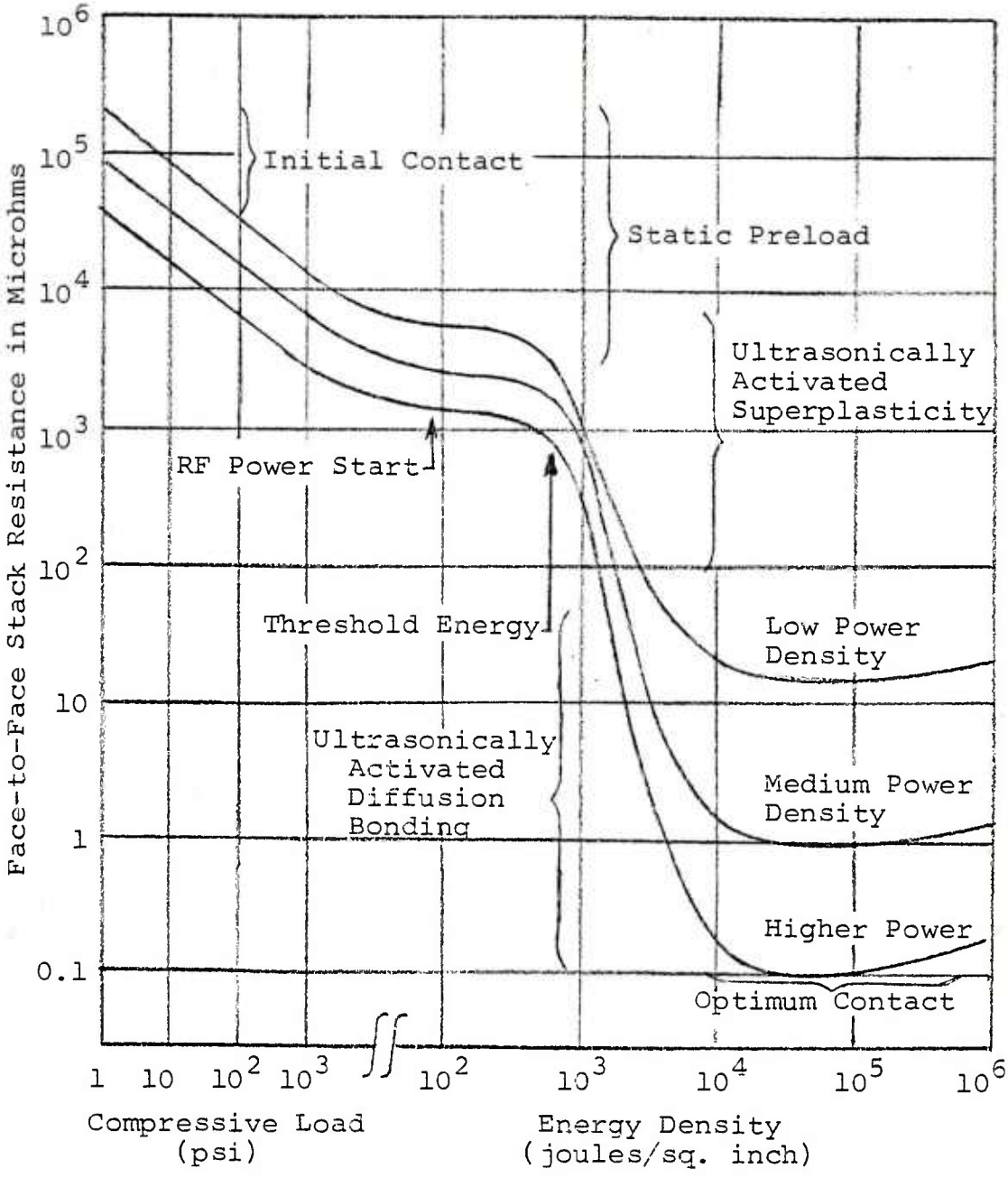

Figure 16. Static and dynamic effects upon laminated stack resistance.

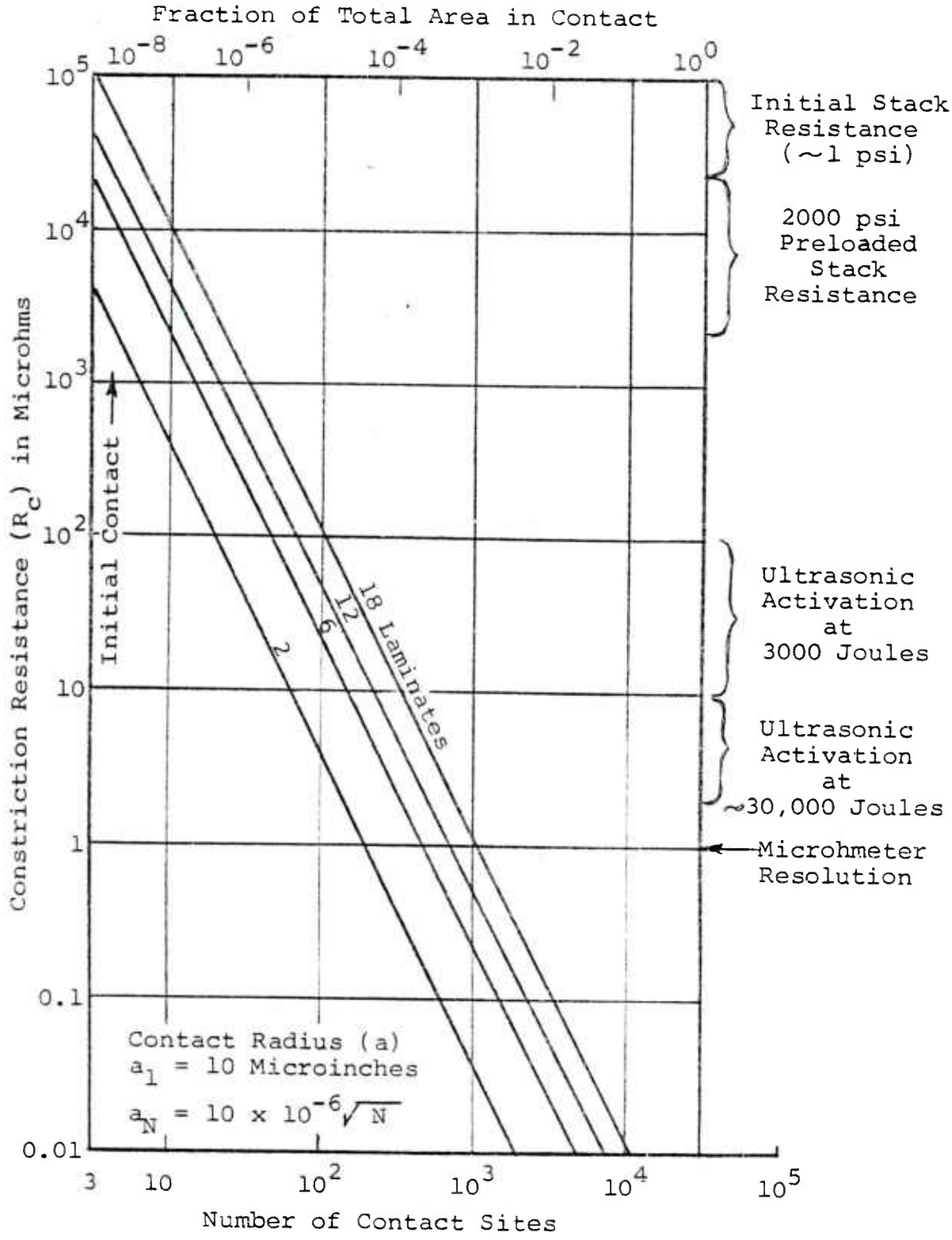

Figure 17. Constriction resistance in multilaminated stacks.

VII. PHOTOMICROGRAPHIC ANALYSIS OF LAMINATE ASSEMBLIES

Because of the relatively high cost of mounting, sectioning, and photographing, photomicrographic analysis has been conducted on a limited scale. Figure 6 is a photomicrograph of a six-layer stack cross section at 200X magnification near the center of specimen #59b. This stack was assembled with low power and shows a well-consolidated region with localized metallic bonds near the left and right hand extremes (about 0.02 inch apart). Interfaces are clearly evident over much of the region as would be expected for roughened contact surfaces that are incompletely bonded. The interface gap appears to vary from 0 to 100 microinches but may average near 32 microinches. Better consolidation and greater bond areas were obtained on later specimens as the bonding process was improved.

Based upon the randomly roughened surfaces of etched aluminum foil, each cross-section view of low-energy assemblies will have a different arrangement of contact sites. The average fraction of interface shown with metallic bonds present is related to the statistically distributed roughness values, the compressive load applied during bonding, the ultrasonic power level relative to the power threshold, and the ultrasonic energy density.

Figure 6 is a representative cross section for the compromise bonding conditions selected, i.e., low compressive deformation, low ultrasonic energy density, and short-duration bonding times. Nugget quality metallic bonds are seen over approximately 10 percent of the exposed interface. This value is quite consistent with the randomly dispersed bonding site model discussed earlier in this report.

Table 13 shows the effect upon bonding parameters of different bond area definitions, i.e., overlap area, solid area, true contact area. It can be seen that the dispersed bond site model predicts energy densities corresponding to those required in conventional ultrasonic bonding to produce nugget quality. This model also shows that the compressive loading falls just below the static yield stress, but with the onset of ultrasonically induced superplasticity, the dynamic yield point is exceeded.

TABLE 13. BOND PARAMETERS VERSUS BOND AREA DEFINITION

Specimen 59b Six 3-Mil Layers Characteristics	Nominal Overlap Region	Interface Area Less Open Channels	Rough Surface Contact	Dispersed Metallic Bond Contact
STACK SIZE	1/2 x 1/2 in.			
Interface area, sq in.	$A_1 = 0.25$	$A_2 = 0.212$	$A_3 \approx 0.05$	$A_4 \approx 0.02$
% Area Contact		$A_2/A_1 = 85\%$	$A_3/A_2 \approx 24\%$	$A_4/A_2 \approx 10\%$
RF POWER				
Load Power, watts	500 W			
Power Density	2000 W/sq in.	2400 W/sq in.	10 KW/sq in.	10 KW/sq in.
Nugget Quality				8-20 KW/sq in.
Bond Time, seconds	2 seconds			
BOND ENERGY				
Total RF Energy	1 KJoule = 4 KJ/sq in.	1 KW-second		
Bond Energy Density		4.7 KJ/sq in.	20 KJ/sq in.	20 KJ/sq in.
Nugget Quality				8-20 KJ/sq in.
STATIC LOAD				
Clamp Force	1100 pounds			
Compressive Stress	4400 psi	5200 psi	22,000 psi	22,000 psi
Tensile Yield Stress				25,000 psi
Compressive Yield Stress				~26,000 psi
STACK RESISTANCE				
Stack + Fixture	611 $\mu\Omega$ (final value, in situ)			
Stack Only	111 $\mu\Omega$			
Area Resistance A x R	28 $\mu\Omega$-sq in.	24 $\mu\Omega$-sq in.	6 $\mu\Omega$-sq in.	2 $\mu\Omega$-sq in.

Figure 18 shows an end sectional view of the same specimen shown in Figure 6. It can be seen that metallic bonding occurred over a larger fraction of the exposed interface, being pronounced at the upper and lower interfaces. Consolidation appears complete over the three central interfaces, indicating a very low leak rate assembly.

Some of the photomicrographs showed the effects of highly textured reed and anvil tip surfaces. At high bond energies, some of the stack upper surfaces show a tip penetration in the order of 20 percent of a single 3-mil layer. This corresponds to 600 microinches, which appeared too rough for this application. A scanning surface profilometer gave a surface roughness on these tips of 280-300 microinches (rms) as compared with the 6-10 microinches (rms) used at the beginning of this study. A geometric mean between these two extremes (about 50 microinches rms) appeared to be a better compromise. However, attempts to generate tip surfaces to this roughness by electrical discharge machining (EDM) and hand lapping were not successful. Further attempts to generate 50-microinch surfaces were abandoned when the abnormally high electrical impedances were traced to imperfect tip-to-stack acoustic coupling.

Figure 19 shows a magnified (25X) view of a 12-layer stack edge containing an exhaust port. The edge shown is the unetched and untouched exposed edge of the assembled stack as removed from bonding. The minor distortion of the cover plates over the unsupported fluid channel was kept small by the choice of bonding parameters, namely:

RF load power:	2700 watts
Bonding time:	1.0 second
Bond energy:	2700 joules
Static clamp force:	2200 pounds.

Figure 19 also shows that simple aligning procedures provide exhaust port sides as straight as the etched variations would allow.

Figure 20 shows the magnified (25X) edges of three stacks assembled with different bond times and bond energies. Each of these stacks contained 11 layers total with four layers containing an active element. The four active layers had one exhaust port shown in Figure 20. It can be seen that the fluid channel remained over 90 percent open in each case.

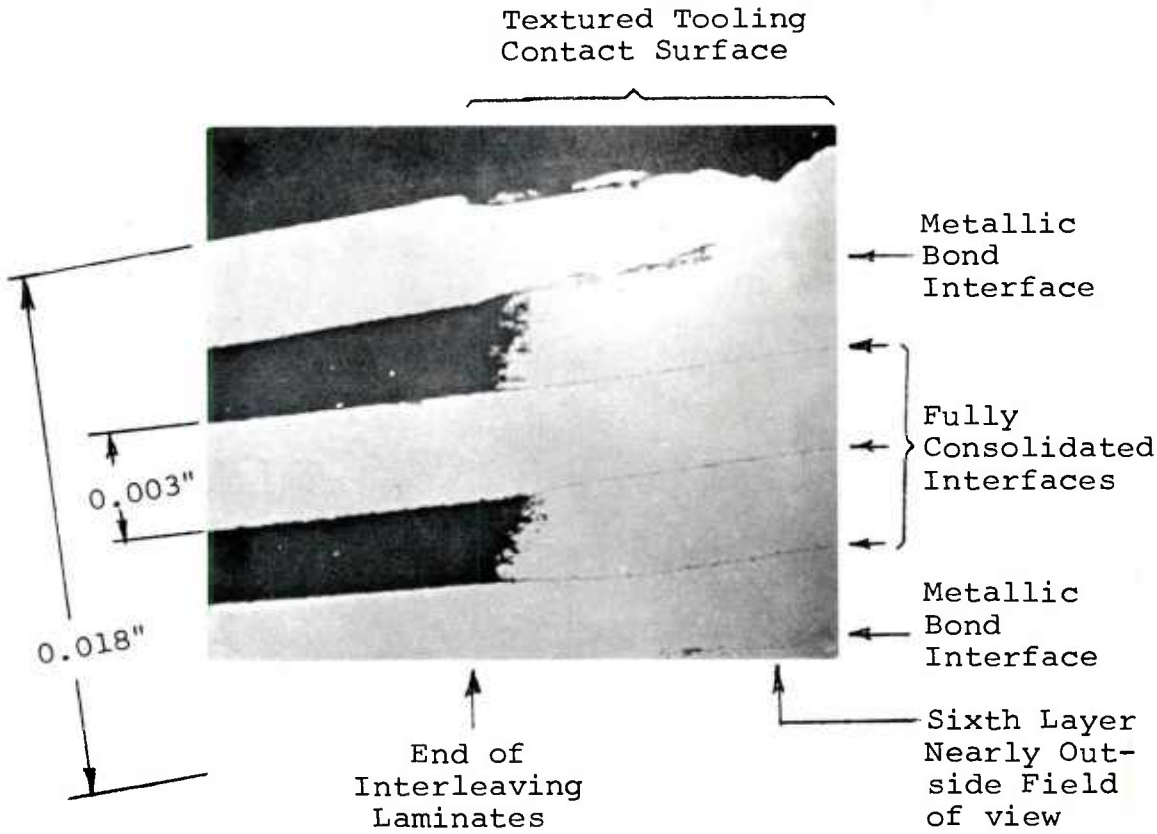

Figure 18. End sectional view of ultrasonically bonded aluminum laminates at 200X magnification.

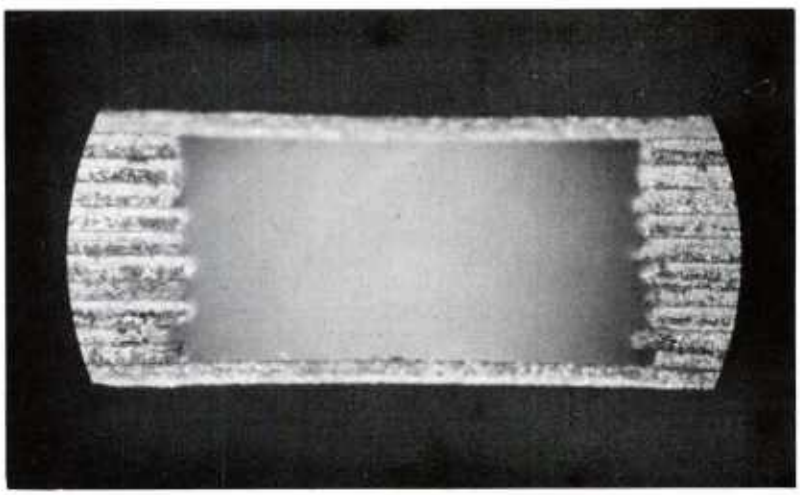

Specimen #83 (12 layers)

Figure 19. Magnified (25X) view of exhaust port with as assembled edges.

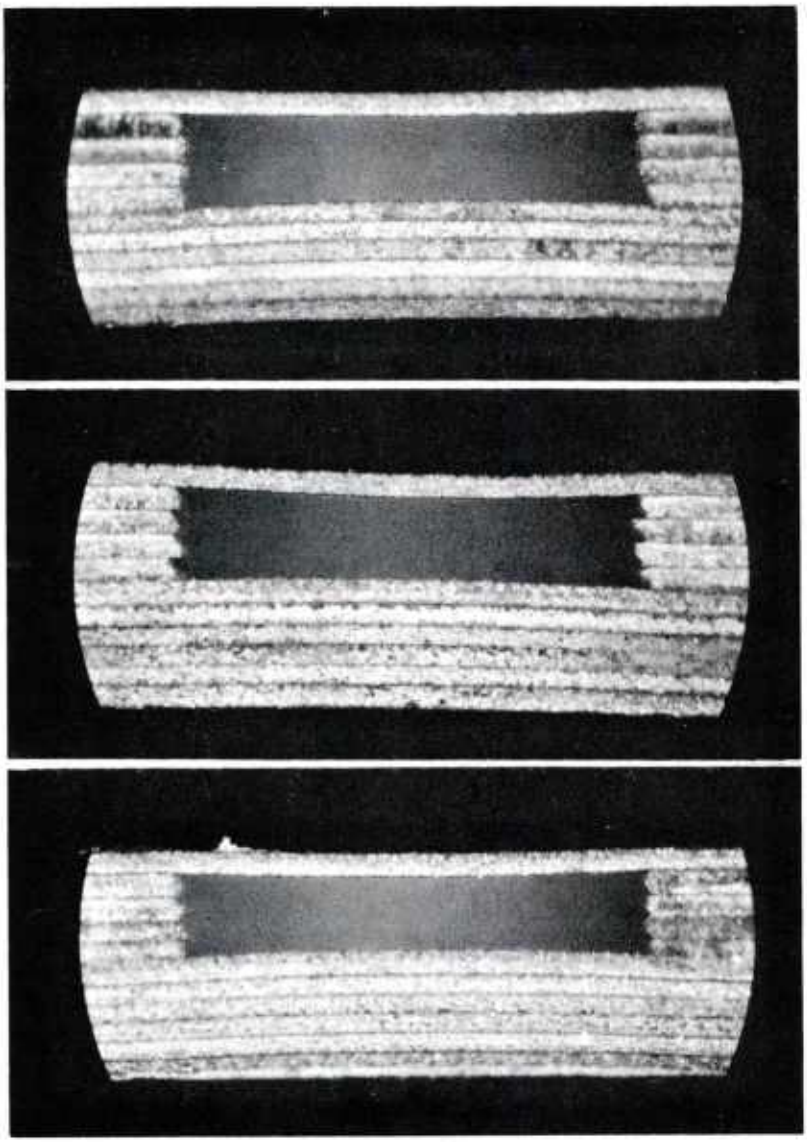

Figure 20. Magnified (25X) view of active exhaust ports with as-assembled edges (11 layers).

Figure 21 shows a magnified (50X) sectional view of the exhaust port and solid stack region of specimen #83 (same as shown in Figure 19). These views show a fully consolidated and bonded assembly with only minor distortion of the unsupported layer regions. Specimen #83 was prepared for photomicrography by casting in clear epoxy resin, sawing through the assembly, belt sanding, coarse grinding, polishing, and etching as a subcontracted service.

Figures 22 and 23 provide a magnified (50X) comparison of cross sections bonded at different bond energy levels. These specimens were prepared by casting, sawing, and coarse grinding only. These sectioned surfaces show more grinding marks and gouges than the etched surface in Figure 21. Both specimens (#87 and #89) show nearly complete consolidation but incomplete interface bonding as would be expected for the short bonding times employed.

Figures 19 through 23 are photomicrographs made at the end of this program. The information presented suggests that the bond parameter optimization might have appeared better at higher bond energies than the 3000 joules employed.

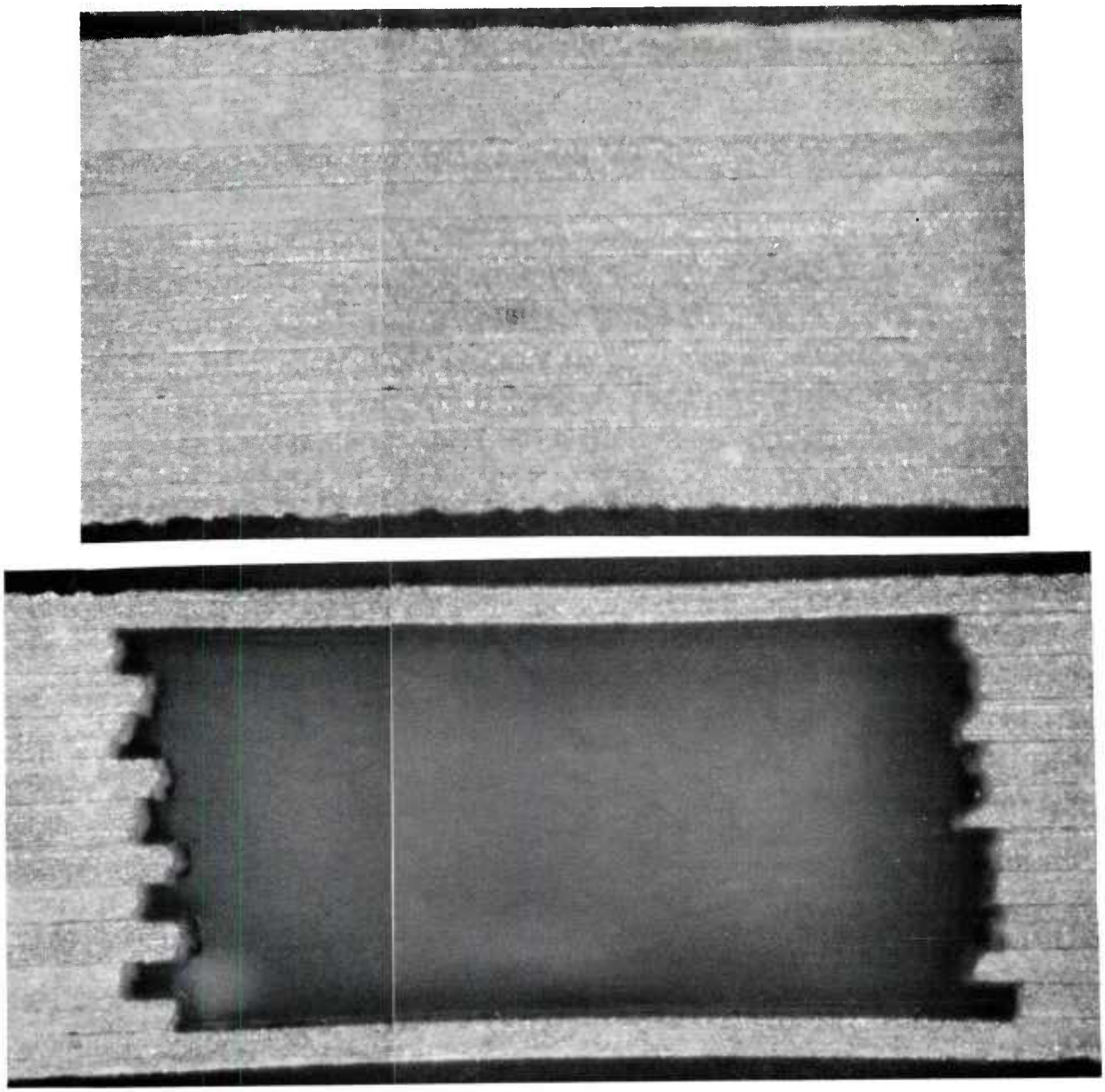

Specimen #83 (polished and etched)

Figure 21. Magnified (50X) sectional view of exhaust port and adjacent solid section.

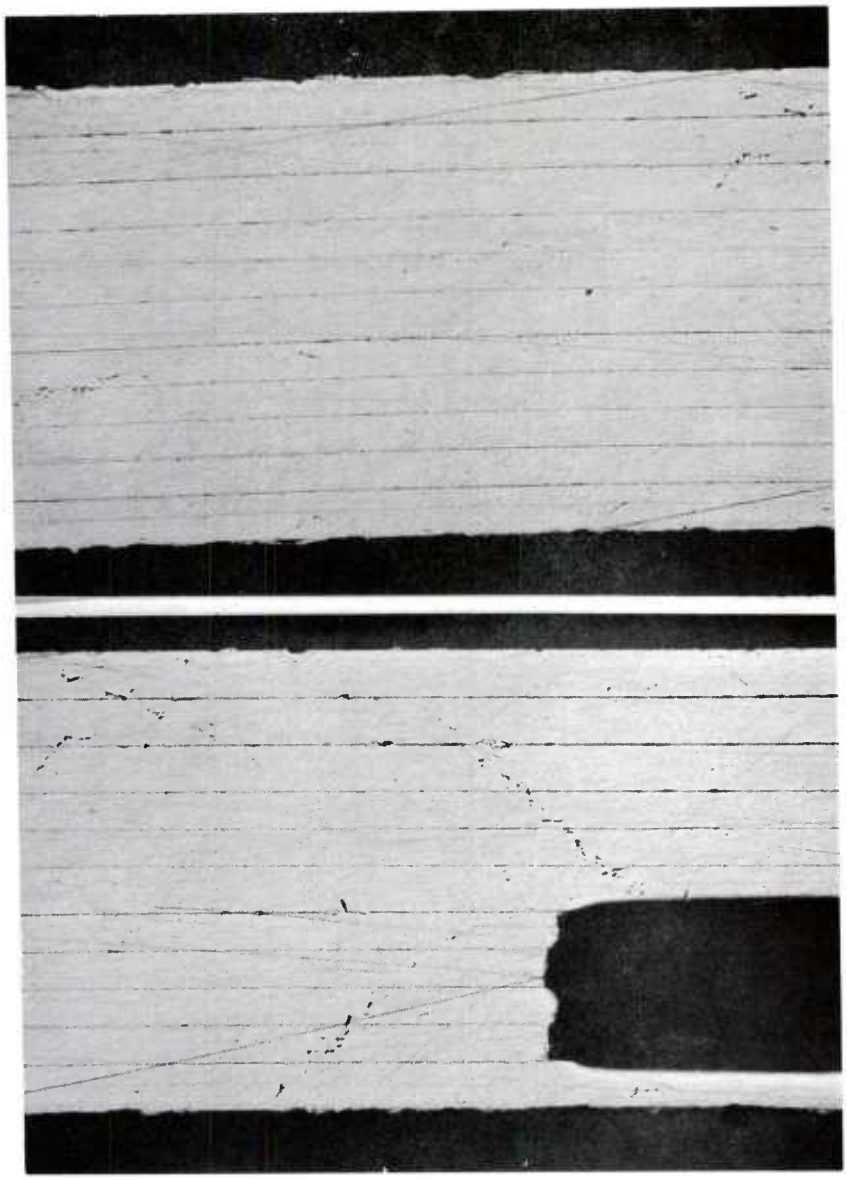

Specimen #87 (3600 joules)

Figure 22. Magnified (50X) sectional views of active device assembled at medium energy

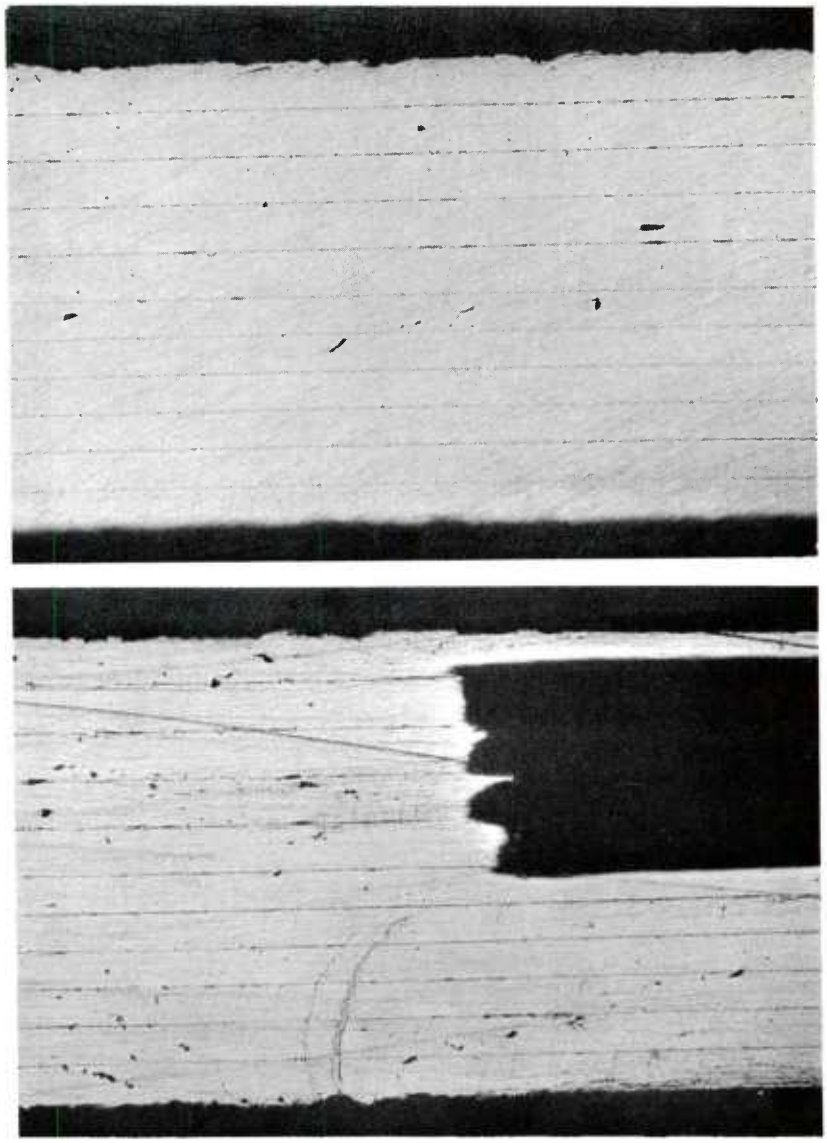

Specimen #89 (2000 joules)

Figure 23. Magnified (50X) sectional view of active device assembled at low energy.

VIII. REVIEW OF ULTRASONICALLY ACTIVATED DIFFUSION BONDING

The physical model of two roughened surfaces in partial contact can be quantitatively described by a statistical distribution of surface peak heights, surface concentration, and interpeak distances (see Appendix C). This model of uniformly dispersed bonding sites provides an explanation for the apparent low bond energy requirements found with fluidic laminates. As was shown in Table 8, the actual bond energy density utilized for assembly of aluminum laminates agrees well with conventional ultrasonic bonding requirements when the true contact area is carefully defined. This conceptual breakthrough permits extrapolation of bonding parameters to larger areas and thicker stacks with much better confidence than before. Both the uniformly dispersed bonding site model and the experimental evidence show a linear increase in ultrasonic power requirements with increasing laminate size and increasing stack thickness.

The analytical model also aids in understanding the mechanical properties created by diffusion bonding. The parent metal bond strength is present, and it is dispersed via many contact points over the entire overlap region. Hence, if the full stack size is used for area averaging, the strength appears low. The local bond strength, however, is equal to the more conventional ultrasonically bonded nugget.

The present analytical model presents a clear picture of the engineering trade-off available between percent area bonded, permanent deformation, leak rate, and mechanical strength (Table 14). It is apparent that the thickness deformation should be greater than the 8 percent required just to reduce the interface gap associated with unnested, randomly roughened surfaces. Furthermore, the initial 8 percent of thickness change will have very little effect upon the fluid channel geometry.

Measurement of the electrical resistance of laminated assemblies across the full area of the overlap region provides both confirmation of the model predictions and status of the bonding process. Figure 16 summarizes the resistance trends versus the assembly stages. Static clamping

TABLE 14. BOND ENERGY VERSUS RESPONSE TRADE-OFFS FOR ULTRASONICALLY ACTIVATED DIFFUSION BONDED STACKS

	Low Bond Energy <4000 Joules	Medium Bond Energy 4K < E < 40K	High Bond Energy >40,000 Joules
MECHANICAL			
Peel Strength	L	M	H
Shear Strength	L	M*	H
Flexural Stiffness (I)	L	M	H
Compressive Set	L*	M	H
% Area Bonded	L	M*	H
ELECTRICAL			
Stack Resistance (I)	M	L*	L
FLUIDIC GEOMETRY			
Relative Leak Rate	M	L*	0
Channel Distortion	0	L*	M
Change in Flow Resistance	0	L*	M
FLUIDIC DEVICE			
Amplifier Gain	?	H	M
Bias Flow	H	M	L

*Interim project goals
I = quality indicator
L = low; M = medium; H = high.

forces reduce the initially high resistance to the several thousand microhm level. But compressive loading alone will not cause the stack resistance to reach the very low values associated with metallic bonding (under 10 microhms over 1 square inch).

Figure 16 dramatically illustrates the threshold energy level effect (i.e., the minimal energy level at which dynamic yielding occurs) which precedes the onset of ultrasonically induced superplastic deformation of the contact sites. In this region, bond area increases rapidly with bond energy until the stack resistance falls by more than tenfold. Then, the bond area increases more slowly at the expense of increasing compressive deformation. Within the lower valley lies the engineering trade-off region cited earlier. For example, specimen #59b shown in section view in Figure 6 had a final stack resistance of 110 microhms (Table 12) and an average compressive deformation of 9.4 percent. Figure 16 shows that the bonding should have been continued for twice as long (double the bond energy density) to obtain minimal stack resistance. Such a schedule was applied to specimen #59a, wherein the stack resistance was reduced to about 80 microhms and the deformation increased to 12.3 percent. Note that when the area resistance product is calculated (16 microhm-square inches), a "good bond" value is obtained. Features of this good bond are:

a. Low intralayer distortion: $12.3 - 8.0 \approx 4\%$.
b. Practical bond area: $<<100$ microhms.
c. Acceptable leak rate: $< 5\%$.
d. Minimal fluid channel changes: $0.5 \times 4\% \approx 2\%$.
e. Nonfragile assembly: Can be handled.
f. Suitable for manifold assembly: Flat exterior surfaces.

A. LIMITING FEATURES OF PREVIOUS ULTRASONIC BONDING SYSTEM

1. Stack Thickness Limitation

The bonding apparatus used to develop small-stack bonded assemblies consisted of a single wedge-reed acoustic

system with a passive contra-resonant anvil support. Since ultrasonic energy was transmitted into the laminated stack from only one face, a severe stack thickness limitation was imposed. We propose to increase the bondable stack thickness by using a driven wedge-reed system on both faces of the laminate stack. The relative phasing will be chosen to maximize the net shearing displacement (e.g., opposite faces will be excited 180 degrees out of phase).

2. Laminate Length Limitation

The largest lateral dimension of a bonding tip on a wedge-reed system is fundamentally limited to a small fraction of an acoustic wavelength. At a 15-kilohertz operating frequency, the longitudinal wavelength in steel is about 13 inches. Acoustic design guidelines suggest tip dimensions should not exceed 1/8 wavelength or about 1.6 inches at 15 kilohertz. We propose to extend the maximum lateral dimension by using an array of abutting tips, each driven by a separate wedge-reed system. Previous experience with abutting bar tips for fabricating leak-tight seam welds in aluminum heat exchangers has confirmed the merit of the abutting approach.

The alternative of operating at much lower frequencies would be more costly in terms of acoustic engineering design time. At this time, it appears more appropriate to utilize the existing 15-kilohertz acoustic know-how.

3. Laminate Area Limitation

The largest area laminate which could be bonded was established by the available acoustic power density, which was in turn limited by the maximum excitation voltage that could be safely imposed upon the 4-kilowatt transducer. We propose to modify the Sonobond tension-shell transducer design to permit operation at voltages higher than the present 3000-volt (zero to peak) breakdown limit. This will facilitate the utilization of the full power-handling capability of this transducer. We were unable to exploit the 5-kilowatt, 50-percent-duty-cycle transducer rating due to the combination of high effective electrical impedance of the larger area laminate stack and the high voltage breakdown limitation.

IX. THE PROPOSED NEW LARGE-STACK BONDING SYSTEM

Several approaches could be considered appropriate for the development of a diffusion bonding system for large fluidic stacks. In order to maximize chances of success, we have selected a low-risk equipment development approach. This approach utilizes much of the existing ultrasonic technology associated with 15-kilohertz wedge-reed metal bonding systems developed at Sonobond.

Having systematically defined, in quantitative terms, each of the existing bonding system limitations, we are able to describe the ultrasonic system needed to bond larger laminate stacks.

A. STACK-CONTACTING BONDING TIPS

We propose each driven face shall consist of a symmetrical array of four abutting tips, each driven by a separate wedge-reed system for a total of eight wedge-reed acoustic subassemblies, as indicated in Figure 24. Nominal tip size will be 1.5 inches square to provide an array face size of 3 by 3 inches. Any pair of adjacent tips may be employed for studies on 1 by 3 inch laminates.

Abutting tips are proposed to reduce plate-mode vibrations expected with large face dimensions. While separate tips will necessitate extra alignment provisions to permit mounting in a common plane, separate tips will allow standard acoustic joints between reed and tip, which are essential to efficient acoustic transmission at high power densities.

B. ACOUSTIC SUBSYSTEM FOR ULTRASONIC ACTIVATION

The ultrasonic transducers to be employed will correspond in physical size to the standard 4-kilowatt tension-shell design. Because of the 4.5-inch shell diameter, a simple parallel array of four transducers can not be placed on 1.5-inch centers.

We propose to rotate the acoustic axes within a common plane so that each pair forms the oblique sides

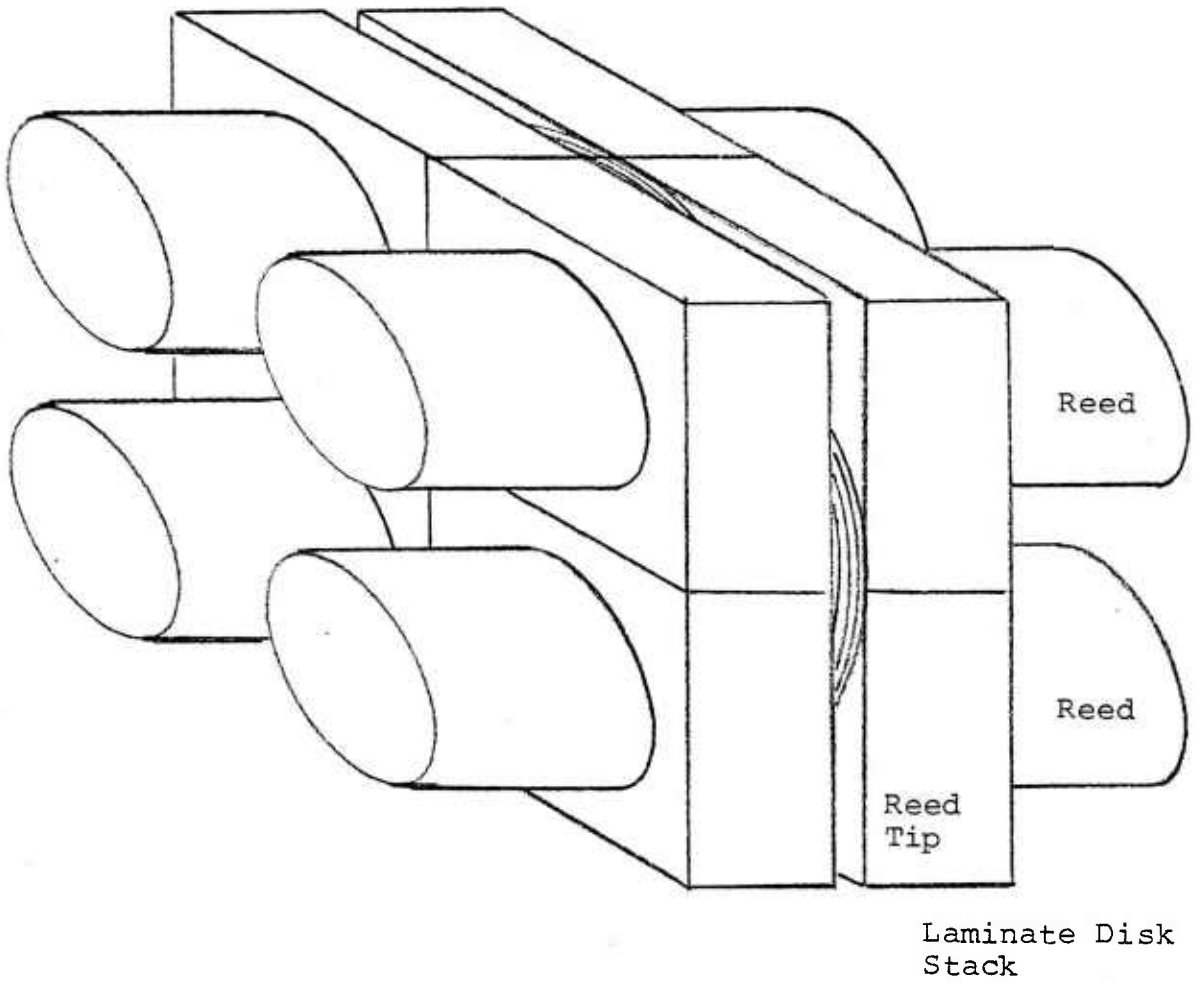

Figure 24. Abutting reed-tip bonding array for 3-inch laminates.

Since the actual bonding time with ultrasonic activation is 4 seconds or less, it appears appropriate to consider sequential or alternate excitation of the acoustic subassemblies. For example, alternate excitation of each stack face array would reduce the RF power requirements from 32 kilowatts to 16 kilowatts while increasing the total bonding cycle to 8 seconds. This appears to be a reasonable approach with only a small sacrifice in stack thickness capabilities.*

We propose to use sequential excitation of acoustic assemblies within a single face array. Single wedge-reed acoustics or pairs of wedge-reed acoustics would be excited in a time-sequencing cycle. Sequential excitation would permit the use of a single 8-kilowatt frequency converter for all sizes of laminates and stack thicknesses within the system capabilities.

D. STATIC CLAMPING FORCE SUBSYSTEM

The original bonding apparatus was designed to fit inside a commercial bell jar to provide a high-vacuum atmosphere. This design inhibited the use of conventional pneumatic or hydraulic clamping force systems. A pair of tension bolts and compression springs was arranged to provide a manually adjustable clamping force. However, this manual procedure was tedious, lacked high precision and repeatability, and was severely limiting in the maximum force available. Since diffusion bonding has been accomplished without high vacuum by using ultrasonic activation, we propose to delete the high vacuum limitations and return to more conventional clamping force systems.

E. LAMINATE STACK SIZE GOALS

Having had several discussions relative to fluidic device applications and representative sizes thereof, we

---

*Alternate face excitation should double the stack thickness capability while simultaneous excitation would more than double it due to superimposition of dynamic shearing stresses near the stack control layers.

present the following stack size goals as useful and realistically achievable:

1. Maximum laminate length: 3 inches.
2. Maximum laminate diameter: 3 inches.
3. Maximum laminate diagonal: 3.2 inches (corresponding to diagonal of 1 by 3 inch laminate layer).
4. Maximum laminate bond area: 5 square inches (corresponding to 70 percent solid contact on 3-inch-diameter laminate layers).
5. Maximum stack thickness: > 0.100 inch (to be experimentally defined).

F. SUMMARY OF CHARACTERISTICS

Table 15 summarizes the characteristics of the proposed large-stack bonding system in comparison with linear extrapolations computed from small-stack data obtained on this program.

TABLE 15. PROJECTED BONDING SYSTEM REQUIREMENTS

Characteristic	Extrapolation from Small Stack Study	Proposed Large Stack System
1 x 3 Inch Laminates	Overlap = 3 $in.^2$	Contact A = 2.4 $in.^2$
Tip Size	1.0 x 1.5 in.	1.5 x 1.5 in.
Contact Area per Tip	< 1.5 $in.^2$	1.2 $in.^2$
No. Active Tips	Two per face	Two per face
No. Wedge-Reed Assemblies	Four	Four
Clamp Force @ 2200 psi	6600 pounds	7500 pounds
High Voltage Limit, Z = 1000 Ω	2200 V rms 3200 V (0-pk)	4 KV (0-pk)
High Voltage Limit, Z = 1500 Ω	2700 V rms 3900 V (0-pk)	4 KV (0-pk)
RF power @ 2400 $W/in.^2$	7200 watts	8 kilowatts
Transducer Rating	2 x 4 KW/face	4 x 5 KW
3-Inch-Diameter Laminates	Overlap = 7 $in.^2$	Contact A = 5 $in.^2$
Tip Size	1.5 x 1.5 in.	1.5 x 1.5 in.
Contact Area per Tip	< 1.5 $in.^2$	1.25 $in.^2$
No. Active Tips	Four per face	Eight
No. Acoustic Assemblies	Four per face	Eight
Clamp Force @ 2200 psi	13,200 pounds	15,000 pounds
High Voltage Limit	Same as above	Same as above
RF Power @ 2400 $W/in.^2$	12 KW/face	16 KW
Stack Face Excitation	Single face	Alternating faces
Transducer Rating	4 x 4 KW/face	8 x 5 KW

X. CONCLUSIONS

A. LOW POWER INVESTIGATION

1. Ultrasonically activated diffusion bonding can be accomplished with aluminum foil laminates at room temperature and with ambient atmospheric conditions.

2. At energy density levels of 3 kilowatts per square inch (20 KW/cm^2), stack thicknesses of 60 mils can be bonded within a few seconds.

3. The aluminum oxide surface layer normally present on aluminum laminates does not require removal for ultrasonic bonding.

4. Textured laminate surfaces resulting from the photochemical etching process employed to fabricate fluid channels, etc. are preferred over mill-rolled surfaces for ultrasonic bonding.

5. As-received laminate surfaces can be bonded without cleaning or special surface preparation. However, the bond energy required is lower for freshly cleaned surfaces.

6. With fixed-head, moving-anvil ultrasonic systems, laminate alignment can be maintained with as few as two pins. Steel dowel pins in the anvil tip were adequate and did not inhibit local bonding.

7. Ultrasonic bond energy requirements increased almost linearly with the number of laminates in the stack.

8. Ultrasonic bond energy requirements increased linearly with overlap area for sizes up to 1.0 by 1.1 inches.

9. Commercial aluminum foil alloy type 1145-H19 is one of the best choices for ultrasonic multi-laminate bonding.

10. Engineering trade-offs do exist between bond strength, relative leak rate, and relative distortion of fluid channel paths. If small leak rates

can be tolerated, minimal channel distortion is obtainable.

11. Laminated stacks can be assembled in subgroups to minimize local distortions in unsupported regions. However, time and materials ran out before this approach could be fully evaluated.

12. Laminate dimensions larger than the bonding tips inhibit uniform bonding near the laminate overhang.

13. No evidence of non-uniformity in bonding was found along planar interfaces within the confines of the bonding tips.

14. The face-to-face electrical resistance of laminated stacks provides a quantitative measure of the interface metallic contact area from the rudimentary three points upwards over several orders of magnitude.

15. Commercially available digital microhmeters provide a fast convenient resistance measuring system with resolutions of 1 microhm and a high degree of repeatability.

16. Microhmeters provide the means for in-situ monitoring the diffusion bonding progress, especially during the critical early stages.

17. Fundamental relationships exist between final stack resistance and degree of interface bonding with laminated aluminum stacks.

18. Static compressive stresses of 2000 psi reduce laminated stack resistance values from a few hundredths of an ohm to a few milliohms. However, ultrasonic activation reduces the stack resistance by a thousandfold to a few microhms (12 layers of 1 by 1 inch area).

19. The wedge-reed ultrasonic system provides a good method for modularizing apparatus toward larger stack diffusion bonding. The moving-anvil ultrasonic system is superior to the moving-head system in terms of preserving laminate alignment.

20. Ultrasonically activated diffusion bonding of laminates up to 3 inches in diameter is technically feasible and practically attainable within the state of the art.

21. Ultrasonic diffusion bonding of laminated stacks is amenable to high-volume production requirements.

22. Energy costs associated with ultrasonic diffusion bonding are a small fraction of those associated with thermally activated diffusion bonding.

23. The final analysis reveals higher bond energy should be employed during the assembly of laminated stacks for leak testing or active device testing. These studies should be conducted prior to the design of ultrasonic bonding systems for the assembly of larger or thicker stacks.

B. INCREASED POWER INVESTIGATION

1. In-situ testing and monitoring of stack leak integrity is a viable quality assurance technique.

2. Bonding results with leak-test specimens showed inconsistencies which are believed to be attributable to variations in part cleanliness, presence of burrs, and heating of the tooling.

3. In general, ultrasonic bond energy requirements increased with the number of stack laminates.

4. The delivery of higher bond energy is related to the capability of aligning the laminate stack with suitable constraint to prevent interlaminate slip; with the pin alignment method used, the laminates were severely compromised at power levels exceeding RF load power of 3500 watts.

5. Ultrasonically activated diffusion bonding of aluminum foil laminates has the potential for assembling fluidic stacks if suitable stack handling equipment is provided.

6. An interim program is recommended to ascertain the optimum stack handling technique for the ultrasonic joining of fluidic elements in order to achieve a production specification for assembly of fluidic stacks.

REFERENCES

1. Adam, N. K., The Physics and Chemistry of Surfaces, Dover Publications, Inc., New York, 1968 Reprint.

2. Alcoa Aluminum Foil, Aluminum Company of America, Inc., Pittsburgh, PA, 1960.

3. Blank, G.F., "A Practical Guide to Diffusion Bonding." Mater. Design Eng., Oct. 1966, p. 76-79.

4. Bradfield, G., "Use in Industry of Elasticity Measurements in Metals with the Help of Mechanical Vibrations." Notes on Applied Science No. 30, National Physical Laboratory, London, 1964.

5. Dienes, G.J., "On the Temperature Dependence of the Activation Energy for Diffusion." Acta Met., Vol. 13, 1965, p. 433.

6. Dixon, H.S. and R. Holm, "Electrical Conductors and Contacts." Engineering Materials Handbook, Section 19, McGraw-Hill Book Co., New York, 1958.

7. Dushman, S., Scientific Foundations of Vacuum Technology. J. Wiley & Sons, Inc., New York, 1949.

8. Eshbach, O. W., Handbook of Engineering Fundamentals. 2nd Ed., J. Wiley & Sons, Inc., New York, 1965.

9. Girifalco, L. A. and H. H. Grimes, "The Theory of Diffusion in Strained Systems." NASA TR-R-38, Lewis Research Center, National Aeronautics and Space Administration, Cleveland, Ohio, 1958.

10. Hanlein, S. L., W. M. Hinckley, and F. P. Stecher, "Comparison of Mechanical and Acoustical Properties for Selected Nonferrous, Ferrous and Plastic Materials." NOLTR 70-141, U. S. Naval Ordnance Laboratory, July 1970.

11. Herring, C., "Diffusional Viscosity of a Polycrystalline Solid." J. Appl. Phys., Vol. 21, May 1950, p. 437-445.

12. Jones, F. L., The Physics of Electrical Contacts. Oxford Press, London, 1957.

13. Jones, J. B., N. Maropis, J. G. Thomas, and D. Bancroft, "Phenomenological Considerations in Ultrasonic Welding." Welding J., Vol. 40, July 1961, p. 289s-305s.

14. Joshi, K. C., "The Formation of Ultrasonic Bonds Between Metals." Welding J., Dec. 1971, p. 840-848.

15. Kameoka, Y. and J. E. Bonhomme, "Very High and Very Low Resistances--Why and How They are Measured." Hewlett-Packard J., March 1971.

16. Keller, D. V., "Adhesion Between Atomically Pure Metallic Surfaces, Part IV." Semi-Annual Report, Syracuse University Research Institute, Syracuse, NY, July 1966.

17. Kerner, E. H., "The Electrical Conductivity of Composite Media." Proc. Phys. Soc. (London), Vol. B69, 1956, p. 802-807.

18. Kinzel, A. B., "Solid Phase Welding." 25th Annual Meeting, American Welding Society, 1944.

19. Knight, J. W., Kaiser Aluminum Foil. Kaiser Aluminum Co., Oakland, CA, 1958.

20. Kolsky, H., Stress Waves in Solids. Oxford Press, London, 1953.

21. Kragelskiy, I. V., N. B. Demkin, and N. M. Mikhin, Computing The Contact Areas of Stationary and Sliding Contacts." Electrical Contacts, NASA TT F-339, National Aeronautics and Space Administration, Dec. 1965, p. 77-91.

22. Maropis, N., "The Design of High-Power Ceramic Transducer Assemblies." IEEE Trans. Sonics and Ultrasonics, Vol. SU-16, July 1969, p. 132-136.

23. Mason, W. P., Physical Acoustics and the Properties of Solids. D. Van Nostrand Co., Inc., New York, 1958.

24. Miller, M. A., "Joining Aluminum to Other Metals." Welding J., Aug. 1953, 12 p.

25. Ogden, H. R. et al., "Study of Bonding Fundamentals." BMI-1101, Battelle Memorial Institute, Columbus, Ohio, June 1956.

26. Pelleg, J., "On the Relation Between Diffusion Coefficients and Grain Boundary Energy." Phil. Mag., Vol. 14, Sept 1966, p. 595-601.

27. Pitney, K. E., Ney Contact Manual. J. M. Ney Co., Bloomfield, Conn., 1973.

28. Quinn, T. F. J., "The Importance of 'Tribology' in Selecting Materials for Wear." Mater. Eng., Vol. 85, April 1977, p. 58-61.

29. Ruoff, A. L., "On Strain-Enhanced Diffusion in Metals. III, Interpretation of Recent Experiments." J. Appl. Phys., Vol. 34, Sept 1963, p. 2862-2872.

30. Seitz, F., The Physics of Metals. McGraw Hill Book Co., Inc., New York, 1943, p. 190.

31. Spurgeon, W. M., S. K. Rhee, and R. S. Kiwak, "Diffusion Bonding of Metals." Bendix Technical J., Spring 1969, p. 24-41.

32. Stark, J. P., "Diffusion and Melting in Solids." Acta Met., Vol. 13, Nov. 1965, p. 1181-1185.

33. Storchheim, S., "Some Studies of Al-Cu and Al-Zr Solid State Bonding." Trans. AIME J. Metals, Vol. 203, August 1955, p. 891-894.

34. Taylor, A. and B. J. Hagle, Crystallographic Data on Metal and Alloy Structures. Dover Publications, New York, 1963.

35. Thomas, J. G., "Investigation of Production Practicability of Bonding Fuel-Element End Caps to Nickel-Plated Uranium Slugs by Ultrasonic Techniques." Report RLOO-65-8, Aeroprojects Inc., West Chester, PA, AEC Contract DDR-203, August 1966.

36. Thomas, J. G., "Ultrasonically Accelerated Diffusion Bonding of Beryllium." Research Report 71-22, Aeroprojects Inc., West Chester, PA, Navy Contract N00156-70-C-1613, July 1971.

37. Thomas, J. G., "Development of an Ultrasonically Augmented Diffusion Bonding Process for Fluidic Control Assembly Fabrication." Research Report 74-1, Aeroprojects Inc., West Chester, PA, Army Contract DAAA-21-73-C-0243, Jan. 1974.

38. Toth, L. E. and A. W. Searcy, "Activation Energies for Diffusion in Pure Metals and Concentrated Binary Alloys." Trans. Met. Soc. AIME, Vol. 230, June 1964, p. 690-694.

39. Van Vlack, L. H., Elements of Material Science. Addison-Wesley Publishing Co., Reading, Mass., 1960.

APPENDIX A

SUPPLEMENTARY EVALUATION

After completion of the previously described work, additional experimentation in ultrasonically assisted diffusion bonding was carried out primarily to supply extended baseline data for evaluation of the process and to evaluate leak rate as a function of the bonding parameters. The additional work consisted of the following tasks:

a. Design and fabrication of laminates suitable for leak testing.

b. Modification of the ultrasonic bonding equipment to achieve higher power capability and necessary tooling modifications to accommodate the leak test laminates.

c. Evaluation of the modified equipment at power levels up to 8 rms kilowatts, and bonding and evaluation of test laminates.

d. Assembly and evaluation of functional fluidic laminate stacks.

1. TEST LAMINATES

In a fluidic device, it is important that liquid flow through the channels with minimum leakage. In the earlier work, little consideration had been given to evaluating the leak rate of ultrasonically bonded assemblies. In this supplementary phase, studies were made to optimize bonding conditions for minimum leak rate assemblies.

Sonobond personnel, with assistance from ARRADCOM and Harry Diamond Laboratory personnel, designed a test laminate stack that would permit in situ leak testing while the stack was still clamped in the bonding machine. Monitoring the leak rate by this means would permit determining the change in leak rate with changing power density.

The leak test laminates were configured to simulate the bonding conditions which would be typical of fluidic logic devices in circuitry; that is, large open areas simulating

manifolding, small fine gaps simulating nozzles and control ports, and the circular cutout to simulate the distance between passages within a circuit.

The assembly consisted of four identical center laminates and two cover plates, as shown in Figure A-1. All laminates were made from 1145-H19 aluminum alloy. Each was 0.0045 inch thick, providing a total package thickness of 0.0270 inch. The assembly was 1.200 inches square and had four through-holes for mounting in the bonding machine. The layer adjacent to the anvil had a small-diameter hole for leak testing. The laminates were fabricated by a photo-etch process by Tech-Etch, Plymouth, Massachusetts. For all stack assemblies, the etched side of the layer was oriented toward the reed tip.

2. EQUIPMENT AND MODIFICATIONS

Earlier studies had indicated that the ultrasonic bonding equipment, which had a maximum power delivery capability of 2400 RF watts, was marginal for bonding 1-inch-square laminates. Before bonding the leak test packages, this equipment was modified to accept higher power levels.

The original welding machine had a wedge-reed coupling system that was driven by a single 3.2-kilowatt piezoelectric ceramic transducer. This was replaced by a dual-drive system incorporating a "Y" transition coupler, shown in Figure A-2. The reed member was driven by two identical 3.2-kilowatt transducers (Figure A-3) capable of accepting in excess of 7 kilowatts input power on a 50 percent duty cycle. The new assembly operated satisfactorily with a 4-kilowatt frequency converter and subsequently with two 4-kilowatt frequency converters for the higher power levels.

The reed and anvil tips were modified to accept the test laminates. The reed tip, shown on the left in Figure A-4, had a flat surface. The anvil tip, on the right in Figure A-4, contained the pins for alignment of the laminates, as well as an input-output manifold for the in-situ monitoring of the leak rates.

3. LEAK TESTS

Eight (8) test laminated packages were bonded at various ultrasonic energy levels and clamping forces as shown in

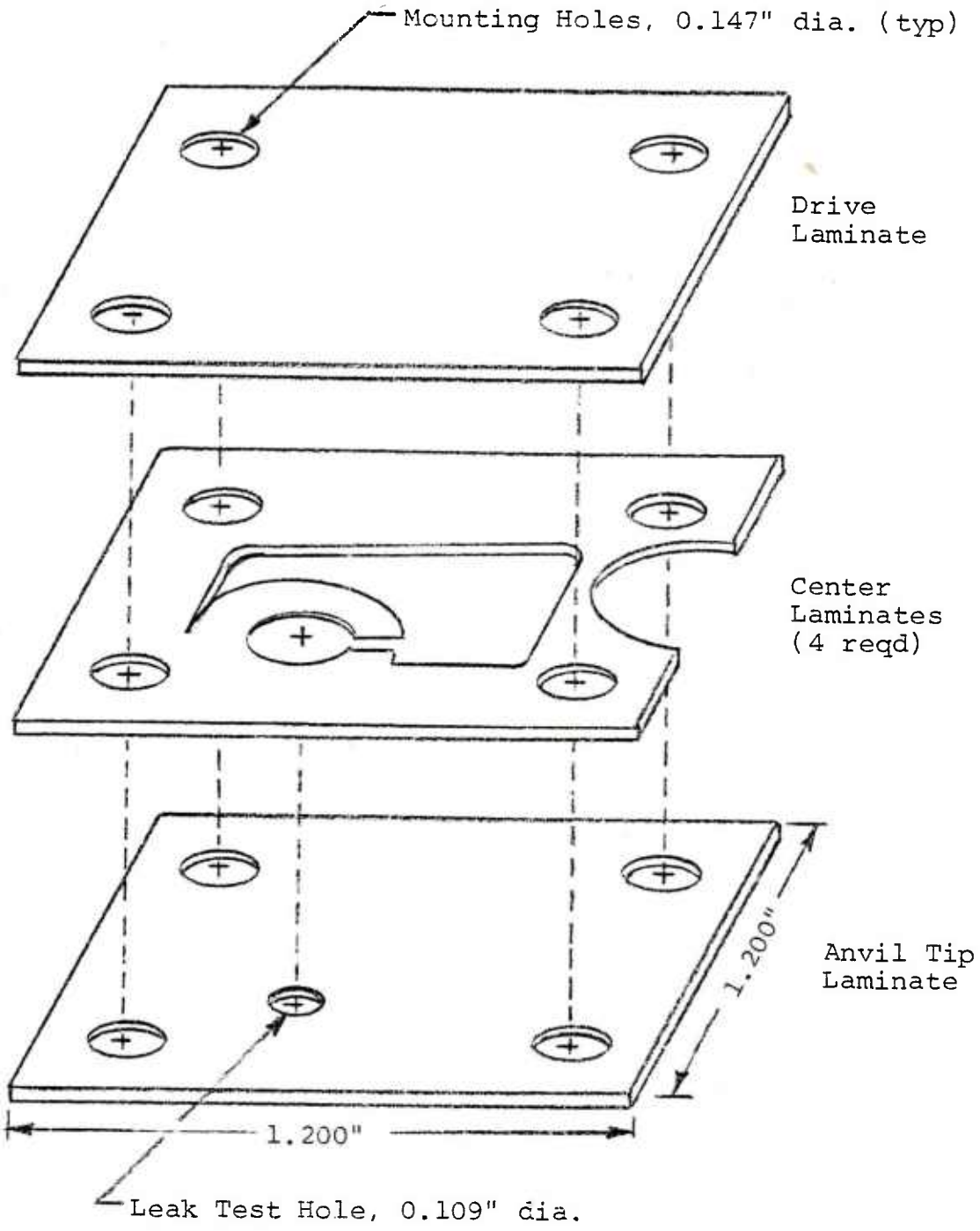

Figure A-1. Configuration of leak test package.

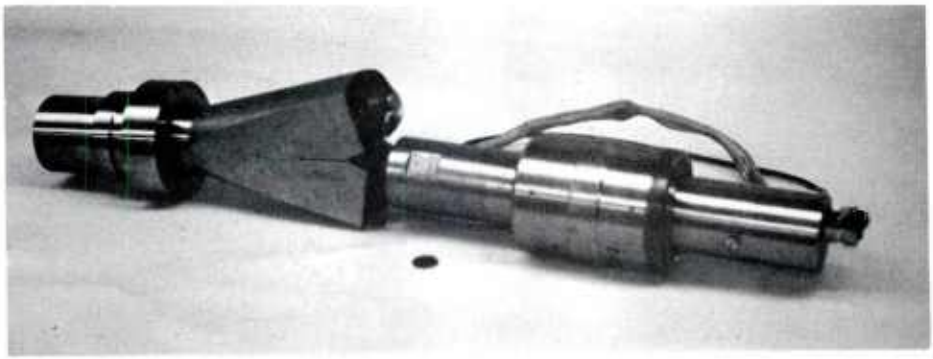

Figure A-2. Dual-drive transducer-coupling system incorporating "Y" transition coupler.

Figure A-3. 3.2 Kilowatt transducer assembly. Two such transducers were used to drive the high power system.

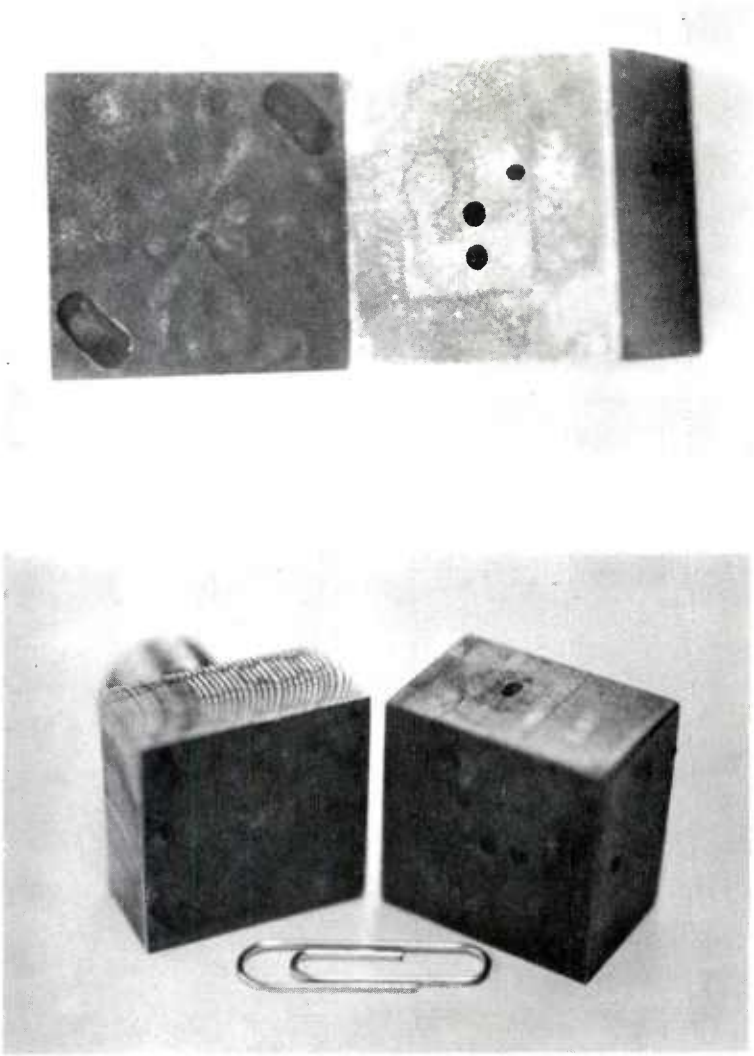

Figure A-4. Reed (left) and anvil (right) modified to accept leak-test laminates.

Table A-1. These were subjected to leak tests before removal from the ultrasonic bonder. For comparison, several assemblies clamped in the machine at similar clamping forces without ultrasonic application were also leak tested.

The leak tests were performed with a Digital Pressure Decay Leak Tester Assembly System, Model 326G-50, manufactured by S. Himmelstein & Co., Elk Grove Village, Illinois. This equipment is shown in Figure A-5.

The results are presented in Table A-1. As noted, the ultrasonically bonded packages showed an order of magnitude improvement in leak rate over the clamped but unbonded packages in the limited number of tests conducted. Average leak rates for the bonded assemblies were less than 0.05 cubic inch per second. The results, however, were compromised by the limited number of packages available for the program. Individual test results varied as much as 2 to 1 at the same bonding conditions.

4. FUNCTIONAL FLUIDIC ASSEMBLIES

For further evaluation of the ultrasonic bonding process, Harry Diamond Laboratories provided two types of functional fluidic element assemblies:

a. Six-laminate assembly, 0.040 inch thick
   Top cover 0.105 inch thick
   Bottom cover 0.0095 inch thick
   Four inner laminates each 0.005 inch thick.

b. Four-laminate assembly, 0.040 inch thick
   Top cover 0.0105 inch thick
   Bottom cover 0.0095 inch thick
   Two inner laminates each 0.010 inch thick.

The tools evolved for bonding these assemblies are shown in Figure A-6. The anvil tip, as with the earlier tools, contained pins for alignment of the laminates during bonding.

The laminates were ultrasonically bonded at conditions selected on the basis of the leak test results, i.e., at high power levels up to about 7000 watts. Even though the total package thickness was the same for both types of assemblies, much better bonding appeared to be obtained with the four-laminate packages.

TABLE A-1. LEAK TEST PACKAGES

RF Load Power (watts)	Static Clamp Force (lb)	Total Coupling Time (sec)	Test Pressure (psi)	Leakage*	
				(psi)	($in.^3$/sec)
Unbonded	2220	--	45	12.4	0.519
3500	2220	3.0	45	0.65	0.027
4700	3000	2.0	40	0.94	0.039
4700	3000	0.5	40	0.79	0.033
5600	2700	1.0	40	1.03	0.043
6600	3000	1.0	40	0.60	0.025
6600	3000	1.25	40	0.83	0.035
7100	3000	1.0	40	0.43	0.018
6700	3200	1.0	40	0.58	0.024

*Each leak test value represents an average of 3 to 5 samples made at the same conditions.

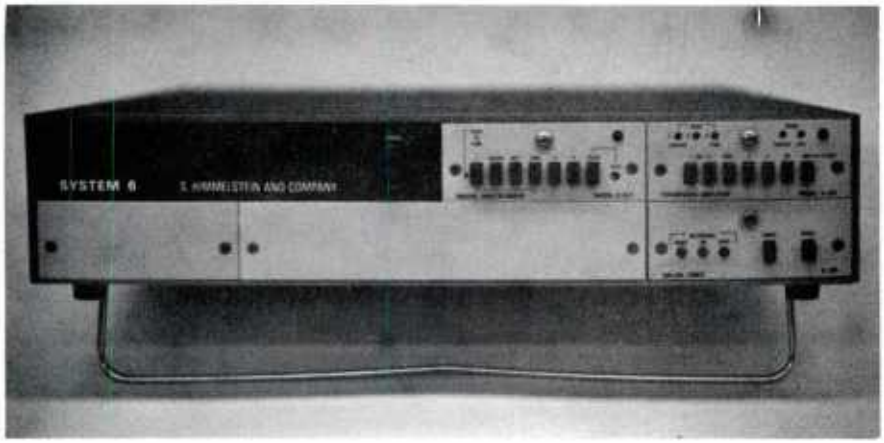

Figure A-5. Leak test assembly system.

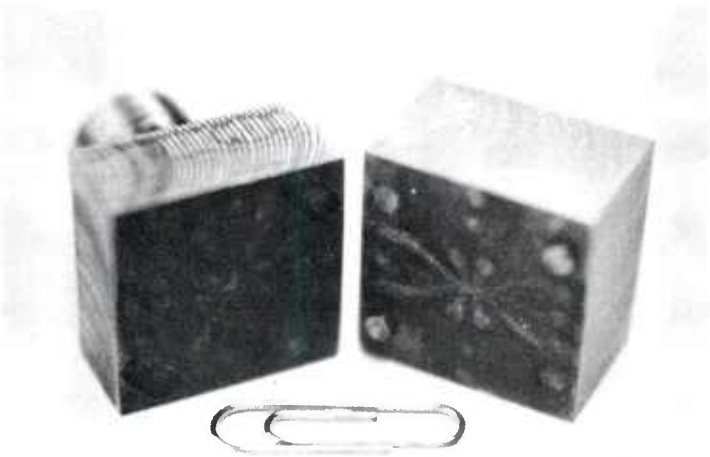

Figure A-6. Reed (left) and anvil (right) tips for bonding functional fluidic element assemblies.

Both types reacted differently from the test laminates prepared for leak testing. During ultrasonic application at high power levels, the laminates shifted and deformed in contact with the alignment pins. Efforts to proceed at power levels up to 6000 watts resulted in complete destruction of the laminates. This had not occurred in the earlier work, and substantial unanticipated effort was directed to re-evaluating the bonding parameters to achieve minimum deformation. This activity consumed the supply of functional laminates on hand.

Harry Diamond Laboratories supplied additional packages for continuation of the work. One type consisted of four laminates, prepared by fine blanking, and a second type consisted of seven laminates, prepared by photo-etching.

These laminates were bonded with the tools shown in Figure A-5, at the conditions noted in Table A-2. In all instances, the clamping force was 3200 pounds, which was the maximum available with the equipment. After three of these assemblies were bonded, the alignment pins were found to be deformed and were replaced. Initially the new pins improved alignment, but as load power was increased, the laminates were again subjected to damage with high power ultrasonic application.

The bonding results, included in Table A-2, were not consistent. Measured power delivery into the assemblies varied even when the same power settings were used. For some unidentified reason, coupling of ultrasonic power into the assemblies was not consistent. There may have been variations of cleanliness of the parts, burrs may have been present on some of the laminates, the packages may have been non-uniformly sensitive to the slight heating of the tooling, or combinations of these or unidentified factors may have been present.

An analysis of the 23 packages which were programed for inclusion in Harry Diamond Laboratory circuits indicated that success on this program would have been achievable only by investigation of a large population of specimens which were joined under optimum conditions that were never reached within the framework of this program. For example, where improved alignment and light to fair bonds were achieved, the next effort was to increase the power to achieve better bonds with minimized leak rates. The immediate result, however, was a tearing of the laminates at the alignment pin.

TABLE A-2. ULTRASONICALLY ASSISTED DIFFUSION BONDED FLUIDIC PACKAGES

Part No.	No. Layers	Mfg. Method	RF Load Power (watts)	Total Coupling Time (sec)	Analysis		
					Visual Inspection		Destructive Inspection
					Alignment	Bond	Internal
1	4	Fine blanked	2200	1.3	Poor	--	--
2	4	Fine blanked	800	1.3	Minimum shift	Light	--
3	4	Fine blanked	1400	1.3	Some shift	Light	--
Anvil Pins Replaced							
4	4	Fine blanked	1400	1.3	Improved	Light	--
5	4	Fine blanked	2500	1.3	Improved	Light	--
6	4	Fine blanked	3000	1.3	Improved	Fair	Light bond
7	4	Fine blanked	4500	1.3	Shift	Good	--
8	4	Fine blanked	4400	0.5	Shift and tearing	--	--
9	4	Fine blanked	3300	0.5	Slight shift	Fair	--
10	4	Fine blanked	3400	0.3	Slight shift	Fair	--

(continued)

TABLE A-2 (Concluded)

Part No.	No. Layers	Mfg. Method	RF Load Power (watts)	Total Coupling Time (sec)	Analysis		
					Visual Inspection		Destructive Inspection
					Alignment	Bond	Internal
11	4	Fine blanked	3500	0.15	Shift	--	Inner laminates bonded; cover plates poor'
12	4	Fine blanked	3400	0.15	Shift	Fair	--
13	4	Fine blanked	2700	0.15	Shift	--	Split inner laminates
14	4	Fine blanked	3000	0.15	Slight shift	Fair	--
15	4	Fine blanked	3000	0.15	Slight shift	Fair	--
16	7	Etched	(2400 (3600	0.15 0.5	Very poor	No bond	Piece split and shifted
17	7	Etched	(3600 (3800	0.15 0.3	--	No bond	--
18	7	Etched	3800	0.5	Very poor	--	Piece split
19	7	Etched	2800	1.5	--	No bond	--
20	7	Etched	2800	1.5	Poor	Light	Cover unbonded
21	7	Etched	2800	1.5	Poor	Light	Cover unbonded
22	7	Etched	3600	2.0	Slight shift	Light	--
23	7	Etched	3600	2.0	Very poor	Light	Badly damaged

It was apparent that an alternate alignment procedure must be evolved to accommodate the relative motion between the parts during ultrasonic activation. Program limitations did not permit investigation of alternate alignment means to facilitate the use of higher power levels. It is recommended that an interim investigation in this regard be undertaken in order to maximize the process and facilitate a production specification for assembly of fluidic stacks.

APPENDIX B

CHARACTERISTICS OF ULTRASONICALLY ACTIVATED DIFFUSION BONDING SYSTEMS

Ultrasonic metal bonding equipment can be categorized in general terms by:

a. RF power rating (e.g., 2400 or 4000 watts)

b. Mode of dynamic motion (e.g., lateral drive, wedge-reed, torsional, seam welder disk-coupler)

c. Fixed or moving portion of static clamping system (e.g., moving head versus moving anvil)

d. Method of dynamic isolation (e.g., tuned resonant isolation mounting).

During this program, three combinations of these four features have been employed for diffusion bonding studies, and a fourth combination has been proposed for future applications to larger fluidic stack assemblies. This appendix serves to list the engineering characteristics of the equipment used, citing the distinguishing features.

Table B-1 lists the features of the electronic subsystem called the frequency converter. The same electronics system has been used throughout this program.

Table B-2 lists the characteristics of the accustic subsystem used during the initial phase of this program. About midway in the study, a higher power transducer was installed. Data for this transducer are listed in Table B-4 under M-8000 tension-shell transducer.

Toward the end of this program, diffusion bonding tests were conducted on a Sonobond metal spot welder Model W-4000. Table B-4 provides a comparison between the features of the moving anvil system used for most of these studies and the W-4000 spot welder. Table B-3 shows that the static clamp force system is significantly different from the newer spot welders like the M-8000 (see Table B-5).

TABLE B-1. CHARACTERISTICS AND PRACTICAL LIMITATIONS OF ELECTRONICS PORTION OF ULTRASONIC DIFFUSION BONDING SYSTEM

POWER AMPLIFIER

RF load power limit:	4000 watts (rms)
LED display:	100-watt increments
Display scale:	0 to 5000 watts (rms)
RF reflected power overload set point:	1500 watts (rms)
RF drive circuit impedance:	50 ohms (nominal)
RF drive circuit maximum voltage:	450 volts (rms)
RF duty cycle rating:	Continucus duty
Weld timer - digital set:	0.01 to 99.99 seconds
resolution:	0.01 second

IMPEDANCE MATCHING

High voltage transformer #A8650023

RF power rating:	4000 volt-amperes
Number primary taps:	4 } Hard wired
Number secondary taps:	4 } Hard wired
Turns ratio range:	4.5/1 to 10.8/1
Impedance ratio range:	20/1 to 116/1
Duty cycle:	Continuous duty

Intermediate transformers (2) #SA-30457

RF power rating (each):	1650 volt-amperes
Number secondary taps:	5 (hard wired)
Turns ratio range (each):	1/0.58 to 1/1.12
Impedance ratio range (each):	1/0.33 to 1/1.25

Composite impedance matching range:	330 to 7250 ohms
Composite impedance matching increments:	± 20%

TABLE B-2. CHARACTERISTICS AND PRACTICAL LIMITATIONS OF ACOUSTICS PORTION OF ULTRASONIC DIFFUSION BONDING SYSTEM

MEDIUM-POWER TRANSDUCER

Tension-shell design with piezoelectric ceramic

RF power rating:	3600 watts @ SWR $\leq$ 3.5, 50% duty
	2400 watts @ SWR $\leq$ 3.5, 100% duty
RF high voltage rating:	2500 volts (0 - peak)
Drive coupler size:	2-1/4 inches diameter
Piezoelectric active area:	4 square inches

WEDGE-REED ASSEMBLY

Two-piece, tapered joint reed-mass design

Fixed mounted reed-mass assembly

Slide-mounted contra-resonant anvil assembly

Isolation-mounted wedge coupler

Reed power rating:	4000 watts, 50% duty
Reed size:	1-1/8 inch diameter
Reed cross section:	Circular
Maximum spot weld size:	5/8-inch bar shape
Maximum diffusion bond size:	1.1 x 1 inches
Reed tip material:	M-2 tool steel, heat-treated to Rockwell Rc = 60
Reed tip size:	1-1/8 x 1-1/8 inches square
Reed tip texture:	EDM 200 surface (Reports 4 ff)
	Surface grind, 6 µin. (Report No. 3)

ANVIL ASSEMBLY

Reed-mass type contra-resonant anvil design

Anvil reed size:	1-1/4 inch diameter

TABLE B-2 (continued)

ANVIL ASSEMBLY (cont.)

Anvil tip size:	1-1/8 x 1-1/8 inches square
Anvil tip texture:	EDM 200 surface (Reports 4 ff)
	Surface grind, 6 μin. (Report No. 3)

TABLE B-3. CHARACTERISTICS AND PRACTICAL LIMITATIONS OF MECHANICAL PORTION OF ULTRASONIC DIFFUSION BONDING SYSTEM

STATIC CLAMP FORCE SYSTEM	
Coplanar tension screws with compression springs (for incorporation inside high-vacuum system)	
Adjusting screw thread:	3/4-16 NF
Compression spring constant (two springs, each):	1500 pounds/inch
Maximum static clamp force:	3000 pounds
Clamp force settability:	± 2 pounds
Clamp force indicator:	Micrometer type dial (100 divisions) and scale (1/64-inch divisions)
TEMPERATURE MONITORING SYSTEM	
Thermocouple sensors with digital readout	
Thermocouple type J:	Chromel-alumel
Cold junction compensation:	Electronic
EMF conversion:	Analog to digital converter
Temperature display: Doric Model 400 Trendicator	4-1/2 digits (°C) 1999.9°C full scale
Temperature resolution:	0.1° Celsius
Temperature accuracy:	± 0.5° Celsius
Thermocouple selection: Doric Model 405	10-channel push-button
Temperature monitoring sites:	a. Laminate face in contact with anvil tip b. Bore hole in reed tip c. Transducer shell near air exhaust port

TABLE B-4. DESIGN COMPARISON OF TWO TYPES OF ULTRASONIC BONDING SYSTEMS

Characteristics of Acoustic Subsystem	Revised Diffusion Bonding System (Moving Anvil)	Standard W-4000 Metal Spot Welder (Moving Head)
ULTRASONIC TRANSDUCER	Tension-shell	Same
Drive Coupler Size	Tapered; 2-1/4" dia.	Standard; 2-11/16" dia.
RF Power Rating,		
SWR $\leq$ 3.5	5000 watts, 50% duty	Same
SWR $<$ 2.5	4000 watts, 100% duty	Same
SWR $<$ 3.5	3200 watts, 100% duty	Same
Acoustic Axis	Vertical	Horizontal
RESONANT REED + MASS	Two-piece	One-piece
Vibrational Mode	First Flexural Overtone	Second Flexural Overtone
Reed Diameter	1 inch	Same
Reed Cross Section	Circular	Same
Reed-to-Mass Joint	Ground Taper	Solid
Reed Axis re Mass	Center 4" x 8.25" Face	Center 4.5" x 5" Face
Mass Volume	4" x 5" x 8.25" = 165 $in.^3$	4.5" x 5" x 7.6" = 171 $in.^3$
Reed Tip Size	1-1/8" square	Same
WEDGE COUPLER		
Reed Attachment	Brazed Socket	Same
Coupler Support	Elmore Mounting	None

TABLE B-4 (continued)

Characteristics of Acoustic Subsystem	Revised Diffusion Bonding System (Moving Anvil)	Standard W-4000 Metal Spot Welder (Moving Head)
STATIC FORCE SYSTEM	Two Compression Springs	Hydraulic
Force Adjustment	Two Adjustable Screws	Pressure Regulator
Moving Element	Anvil System	Acoustic System (Head)
Static & Acoustic Axes	Coplanar	1" Offset Planes
FREQUENCY CONVERTER	EGB-4200	Same
RF Power Rating	4000 watts	Same

TABLE B-5. GENERAL SPECIFICATIONS FOR SONOBOND M-8000 WEDGE-REED ACOUSTIC SYSTEM

REED-MASS

Nominal Resonant Frequency (with tip):	15.0 ± 0.3 kHz
Vibrational Mode:	Flexural overtone
Construction:	One-piece for low loss
Material:	High-fatigue-strength steel alloy
Reed Cross Section:	Flat oval
Mass Mounting:	Four bolt holes plus aligning keyway
Tip End:	Conical contact surface; over 50% of conical surface in contact with tip
Tip End Acoustic Gasket:	Dead-soft copper washer, nominal 0.003-inch thickness
Tip Mounting:	1/2-20 NF-3 stud, rolled threads, high-strength steel

WEDGE COUPLER

Nominal Resonant Frequency (to reed centerline):	15 kHz, matched to reed
Vibrational Mode:	Longitudinal fundamental
Acoustic Design:	High mechanical amplification, acoustic impedance match to reed
Material:	Selected stainless steel alloy
Transducer End Diameter:	2-11/16 inches, flat, smooth surface
Transducer Coupling:	3/4-16 NF-3 stud, high-strength steel
Coupler Acoustic Gasket:	Dead-soft copper washer, nominal 0.003 inch thick

TABLE B-5 (continued)

WEDGE-REED JUNCTION

Recessed Socket:	Metallurgically bonded
Acoustic Axes:	$90^{o} \pm 0.5^{o}$

REED-TIP

Standard Material:	M-2 tool steel heat-treated to Rockwell Rc 60-62
High-Temperature Material:	Udimet 700
Design - Custom:	Sonobond proprietary, stringent acoustic and shop specifications
Contact Geometry:	a. Spherical radius b. EDM texture c. Custom bar protrusion d. Diamond cross-hatch ("waffle pattern")

M-8000 TENSION-SHELL TRANSDUCER

Nominal Resonant Frequency, (f_r):	15.0 $\pm$ 0.3 kHz (matched to wedge-reed assembly)
Vibrational Mode:	Longitudinal, 3/2 wavelengths long
Construction:	Heavy-duty, fully enclosed
Material:	Stainless steel alloy
Mechanical Bias:	Preloaded in hydraulic press, maintained via tension shell
Active Elements:	Piezoelectric ceramic
Maximum Internal Temperature:	$200^{o}C$ (nominal Curie temperature = $340^{o}C$)
Cooling Provisions:	Forced air cooling between active elements, air flow rate 2 std cubic feet per minute at 80 psi. MUST BE CLEAN AND DRY AIR

TABLE B-5 (continued)

M-8000 TENSION-SHELL TRANSDUCER (cont.)

RF High-Voltage Rating:	3000 volts (0 - peak) 2100 volts (rms)
RF Power Rating:	5000 watts @ SWR $\leq$ 3.5, 50% duty
	4000 watts @ SWR $<$ 2.5, 100% duty
	3200 watts @ SWR $<$ 3.5, 100% duty
Drive Coupler Size:	Standard: 2-11/16 inch diameter
	Tapered: 2-1/4 inch diameter
Wedge-Coupler Attachment:	3/4-16 NF-3 stud, high-strength steel
Front Coupler Acoustic Gasket:	Dead-soft copper washer, nominal 0.003 inch thickness
Static Shunt Capacitance, (C_o):	$6.5 \pm 0.6) \times 10^{-9}$ farads
Front Coupler Acoustic Impedance:	39×10^5 acoustic ohms (cgs)
Recommended Parallel Inductance:	$L = \frac{0.9}{(2 f_r)^2 C_o} \approx 15$ mhy

WEDGE-REED AND TRANSDUCER ACOUSTIC SYSTEM IN M-8000 WELDER

Nominal Design Frequency:	15.0 ± 0.5 kHz
Approximate Operating Frequency Shift with Power Level:	- 0.1 kHz/KW
Approximate Operating Frequency Shift with Temperature:	- 4 Hz/$^\circ$C or - 0.03%/$^\circ$C

TABLE B-5 (concluded)

WEDGE-REED AND TRANSDUCER ACOUSTIC SYSTEM IN M-8000 WELDER

Vector Admittance Locus Plot (VALP), typical data with reed tip and transducer:

f_o = 14.8 kHz
A = 3.6 millimhos
Q $\approx$ 200

f_o = frequency of zero reactance (test voltage = 3.0 V_{rms})

A = admittance = reciprocal of impedance

Q = acoustic quality = $\frac{\text{elastic energy stored}}{\text{energy dissipated}}$

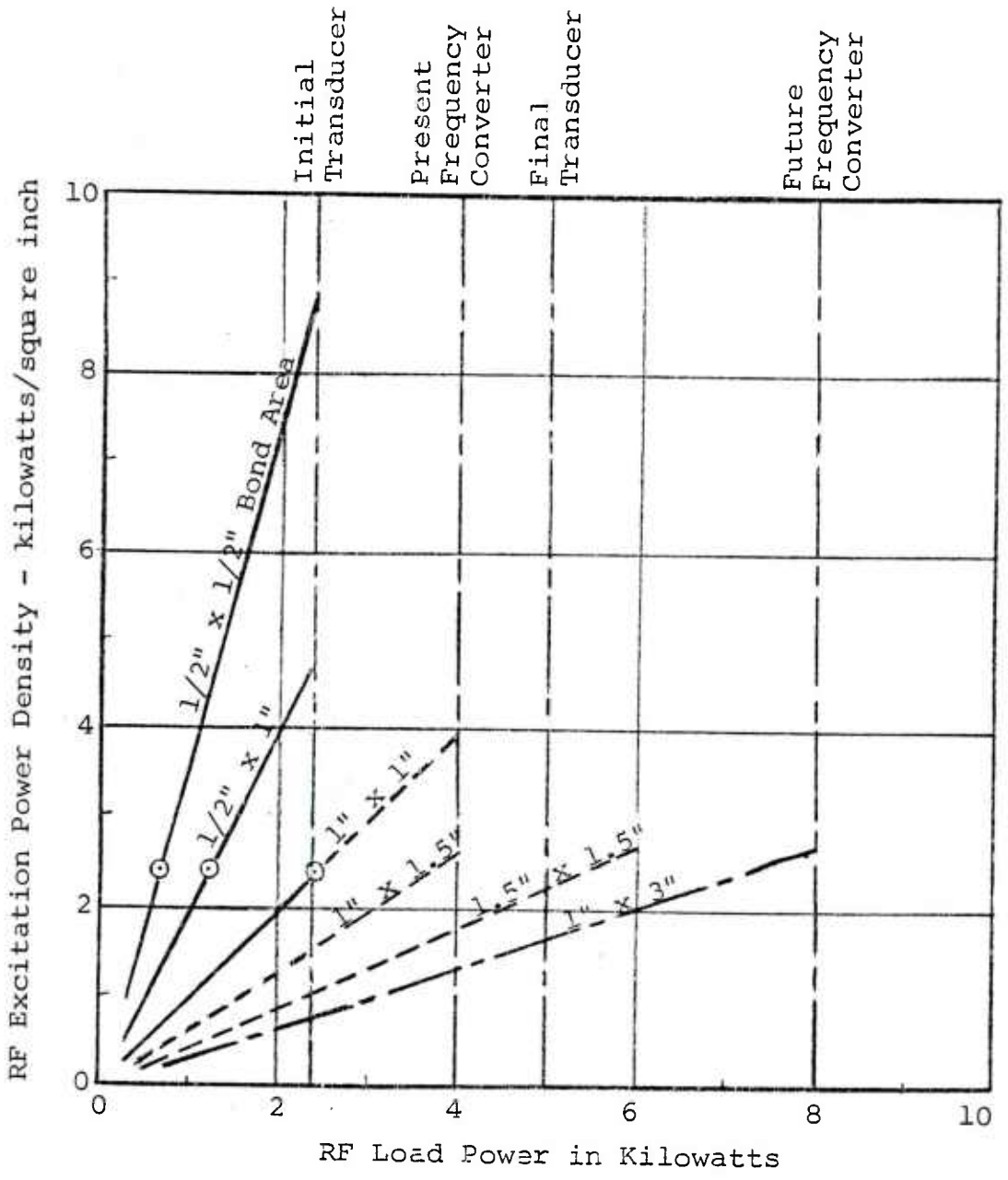

Figure B-1. Power delivery characteristics of ultrasonic system.

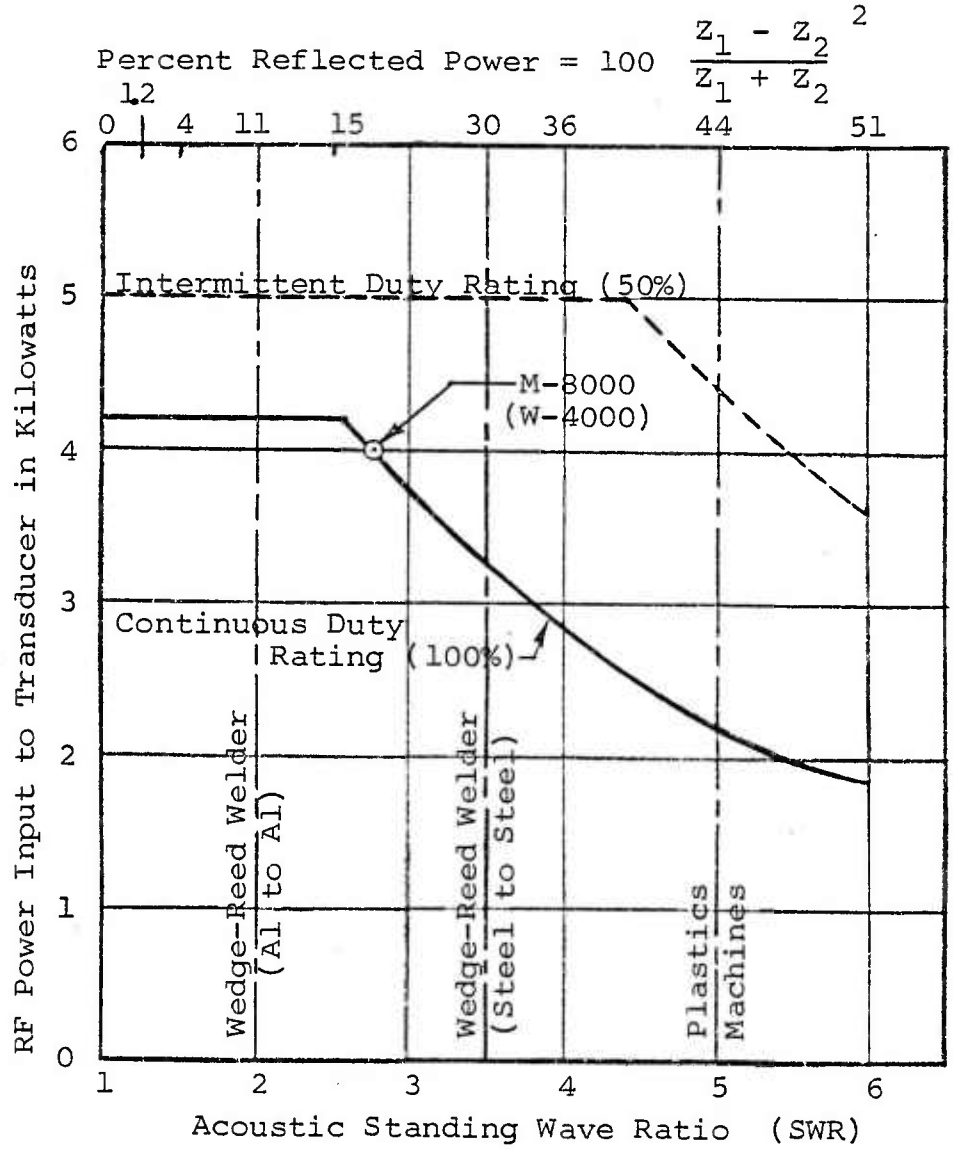

Figure B-2. Ultrasonic transducer power rating versus SWR for Sonobond 3200-watt tension-shell design

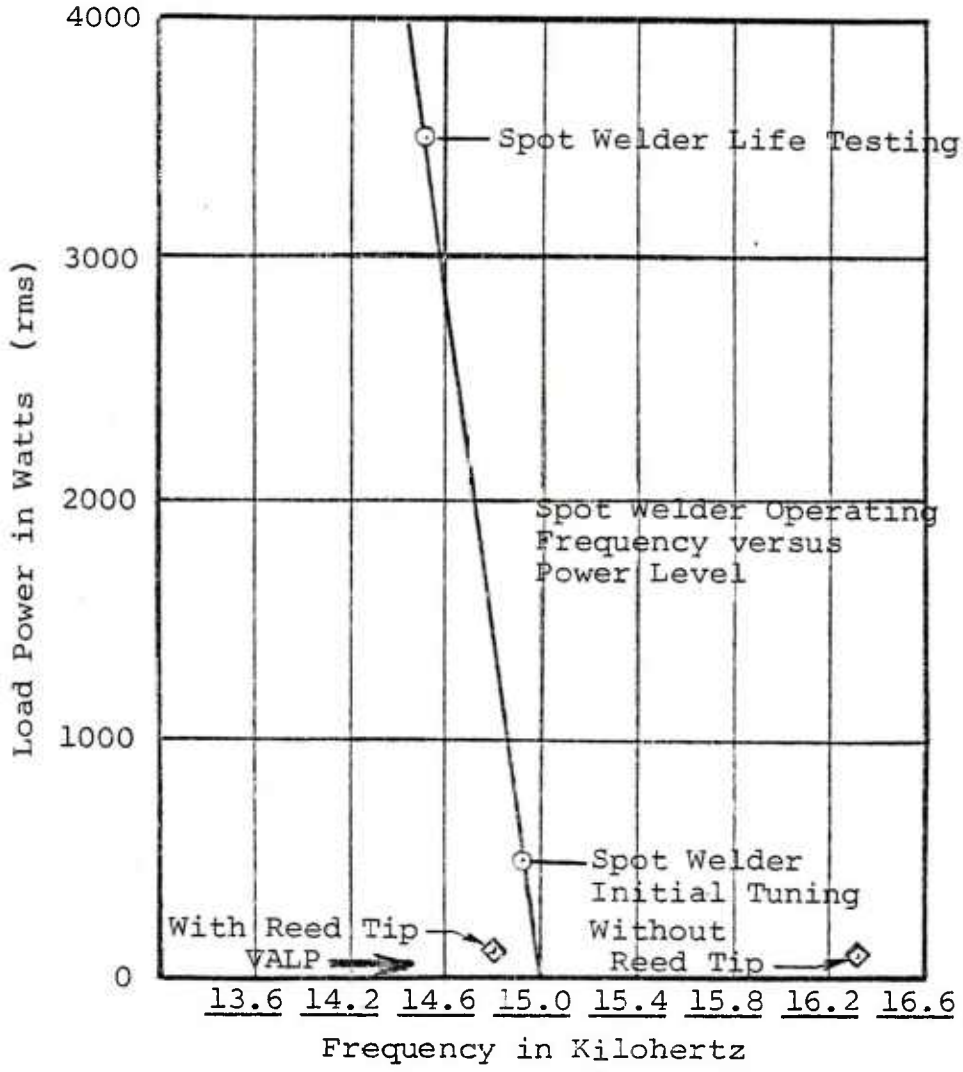

Figure B-3. Characteristics of M-8000 acoustic system.

APPENDIX C

STATISTICAL CHARACTERISTICS OF UNIFORMLY DISPERSED BONDING SITES

Conventional ultrasonic bonding induces atomically intimate contact over a large percentage of a finite bond region. Ultrasonically activated diffusion bonding (as developed for aluminum laminates) induces an array of bonded sites more or less uniformly dispersed throughout the overlap region, as shown in Figure 7. The percentage of area metallically bonded would be small in the laminate case. However, the localized bond strengths are expected to approach parent metal strength as found with conventional ultrasonic nuggets. With this description of laminate bonding as consisting of a uniformly dispersed array of strongly bonded points, each of the experimental observations becomes understandable and self-consistent. Hence, trends in laminate bonding can be properly defined and extrapolations to larger overlap areas and thicker stacks can be more reliably forecast.

Samples of the ARRADCOM-supplied aluminum laminates (which had undergond photochemical etching to generate fluidic channels) were scanned with a Brush Surface Analyzer. The etched surface roughness ranged from 20 to 50 microinches (rms) averaging about 32 microinches (see Table 3). When two such surfaces are placed in contact at low clamping force, only a few extreme points touch, leaving a spacing about equal to the sum of the peak roughness of very-low-probability large peak sizes and the rms value:

$$\text{Initial spacing} \simeq 32\ \mu\text{in. rms} + 32\ \mu\text{in. rms} \times 1.4\ \frac{\text{pk}}{\text{rms}} \times 4\ \text{sigma} \simeq 200\ \text{microinches}$$

(for 32 μin. rms).

Figure C-1 shows the probable occurrence of peak values for a randomly roughened surface having a normal (Gaussian) type size distribution. The probability of finding sizes larger than a value (Y_{PK}) can be calculated from the exponential relationship:

$$\text{Probability} = \exp\left(\frac{-Y_{PK}^2}{2\,Y_{rms}^2}\right).$$

This expression can be used to calculate the relative probability of finding three large peaks from one surface in contact with the average contour of the second surface. Based on average number of peaks per square inch (about 1.2×10^9 peaks per square inch for 32 microinch rms surface), the initial spacing between surfaces can be predicted to be near 200 microinches. As the static clamping force increases, the number of contact sites increases very rapidly, nearly tenfold per 10 microinch compression (see Figure C-2).

Since the total contact area is proportional to the sum of the squares of the contact diameters, contact area increases more rapidly than the number of contact sites.

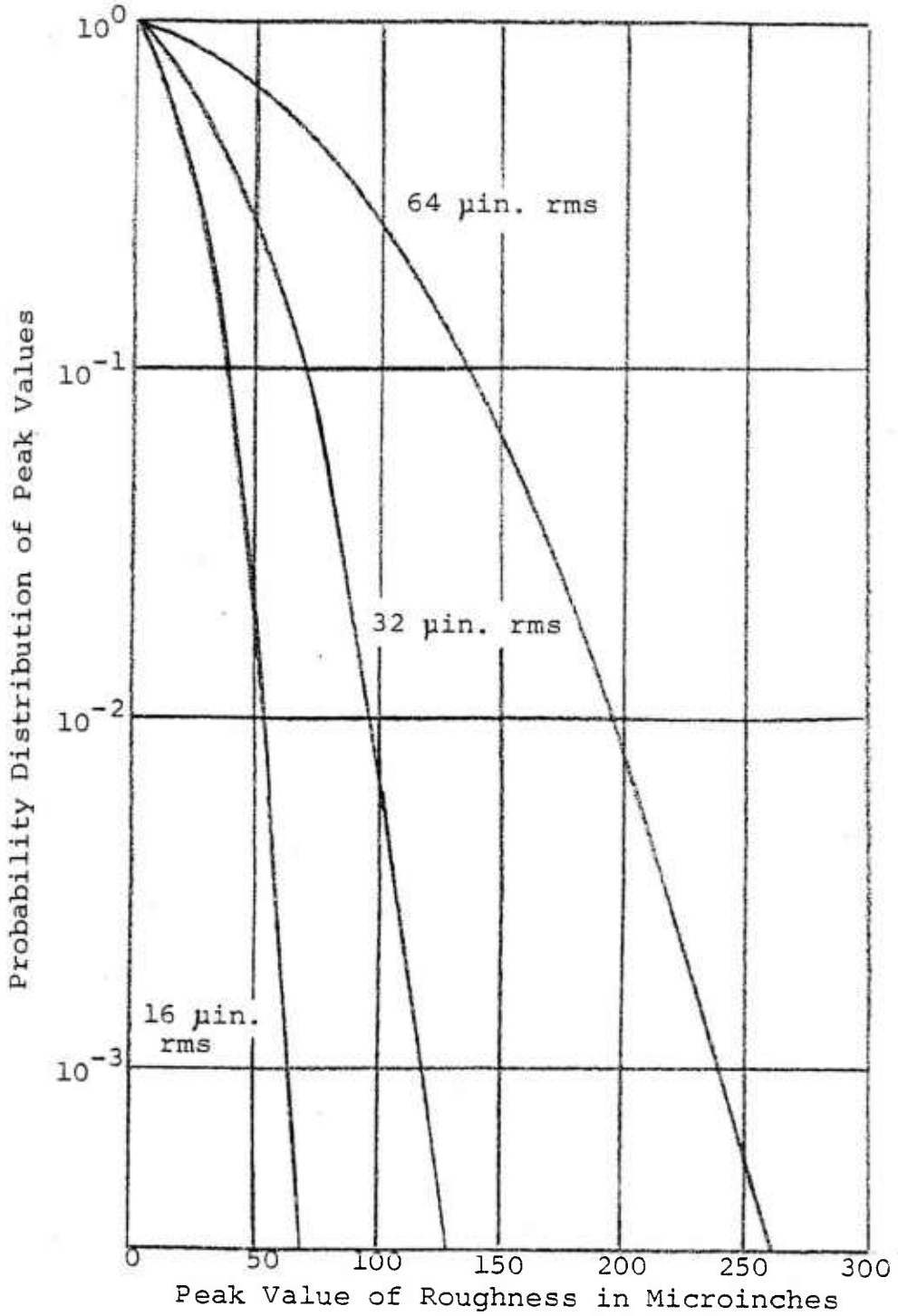

Figure C-1. Probability distribution of surface roughness values.

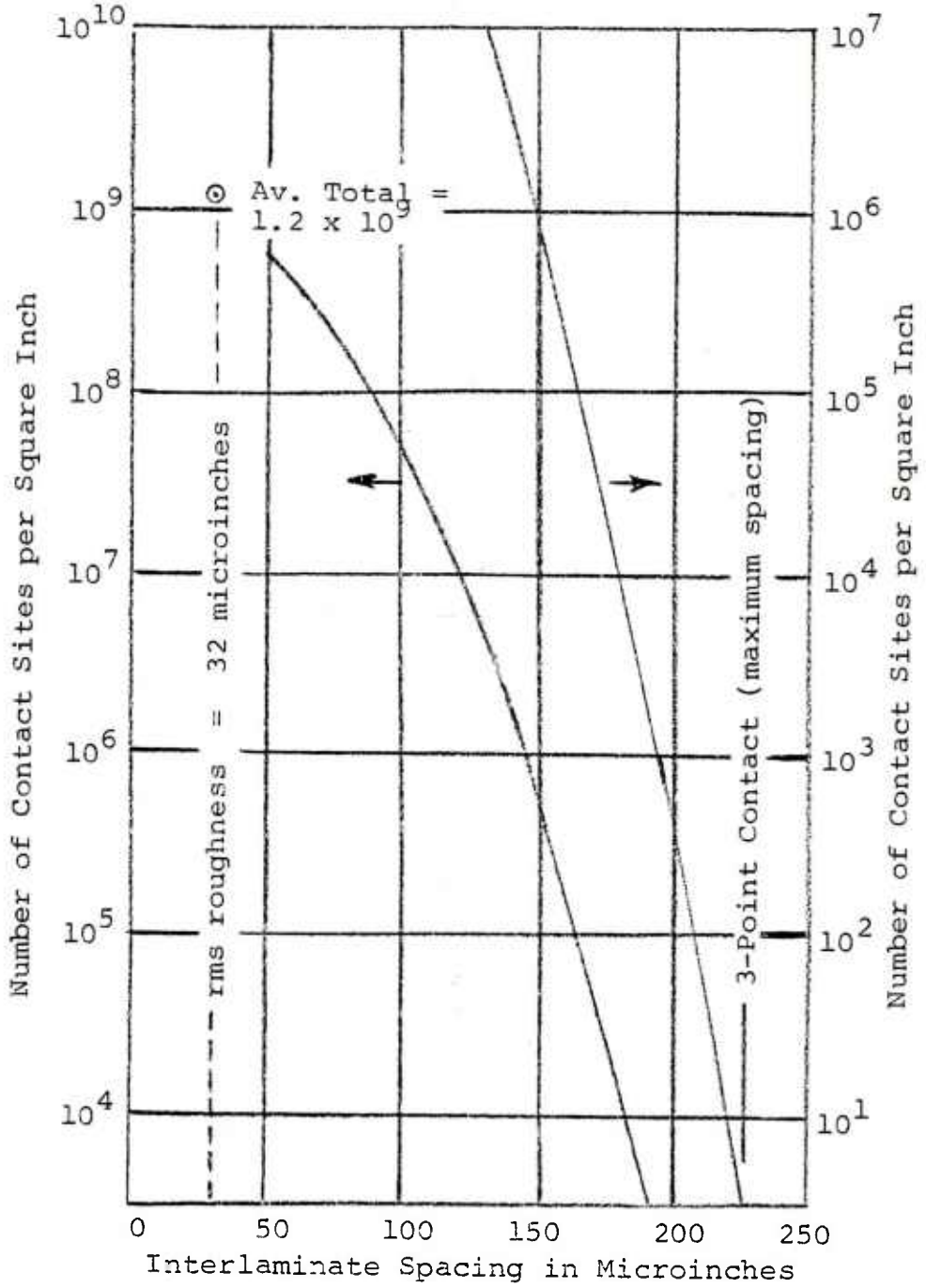

Figure C-2. Contact between two rough surfaces.

APPENDIX D

ELECTRICAL RESISTANCE OF ALUMINUM FLUIDIC STACKS

1. Introduction

An unbonded assembly of aluminum laminates (as used in fluidic devices) behaves electrically as a three-dimensional resistor matrix consisting of both series and parallel elements. The series elements include:

a. The ohmic resistance (R_o) of the aluminum alloy in the thickness direction.

b. The surface film resistance (R_F) of the laminate.

c. The constriction resistance (R_c) of the current path through the contact points.

d. The composite layer resistance (R_L) of the aluminum-aluminum oxide binary composite.

e. The electrode resistance (R_e) of the area contacts made to measure the stack resistance.

For N laminates, the total stack resistance (R_T) is the series circuit summation given by:

$$R_T = N(R_o + 2R_F) + (N - 1)(2R_c + R_L) + R_e.$$

With ultrasonically activated diffusion bonding, the film resistance (R_F) approaches zero and the constriction resistance (R_c) approaches a finite value determined by the laminate pattern geometry as bonding approaches completion. Hence, by monitoring stack resistance, in situ, during ultrasonic activation, the progress of diffusion bonding can be evaluated.

2. Ohmic Resistance

The electrical resistivity of high-purity aluminum is listed in various handbooks as shown in Table D-1.

Handbook data for compositions like the foil 1145 alloy gave a room temperature resistivity value of 2.87 microhms per cubic centimeter (or microhm-cm). For an 18-layer stack of 3-mil-thick laminates and a nominal overlap region 1/2 by 1/2 inches, the calculated ohmic resistance was found to be:

$$R_o = N \frac{t}{A} \rho$$

$$R_o = \frac{18(0.003 \times 2.54)\ \text{cm}}{0.211\ (6.45)\ \text{cm}^2} \times 2.87 \times 10^{-6}\ \Omega\text{-cm}$$

R_o (18 layers, 1/2 x 1/2 in.) = 0.3 microhms

R_o (18 layers, 1 x 1 in.) = 0.06 microhms/sq in.

Obviously the ohmic resistance component of the series equivalent circuit is negligibly small even for the thickest stack with the smallest cross-sectional area.

3. Film Resistance

Whereas most metallic conductors develop surface oxide layers or films which are imperfect insulators or semiconductors, aluminum typically oxidizes to an Al_2O_3 surface which is a good insulator.

The bulk resistivity of Al_2O_3 is typically greater than 10^{11} ohm-cm in the form of a polycrystalline ceramic. The aluminum oxide layer which rapidly develops on any exposed aluminum surface has a thickness in the order of 15 to 50 angstroms. Using these values and a 1/2 by 1/2 inch overlap region, the calculated film resistance becomes:

$$R_F = 2N \frac{t}{A} \rho_F$$

TABLE D-1. RESISTIVITY OF HIGH-PURITY ALUMINUM

Alloy	Composition (wt % others)	Temperature (°C)	Resistivity (ρ) (microhm-cm)	Temperature Coefficient	Reference
1199	<0.01	20	2.652	--	(19)
99.95 Al	--	0	2.655	--	
		20	2.67	0.0042/°C	
1100	1(Si + Fe) + .02 Cu	20	(-0) 2.92	--	
			(H-18) 3.00	--	
1145	0.5(Si + Fe)	20	2.87	0.0038/°C	(19)
		100	--	0.0030/°C	(19)
Al Conductors	0.29 Si + 0.14 Fe	20	2.828	0.0039/°C	(6) NBS Standard
Pure Al	--	0	2.63	--	Handbook Chemistry & Physics
		100	3.86	0.0040/°C	
		400	8.0	--	
		500	--	0.0050/°C	
Pure Cu	--	20	1.7241	--	(6) NBS Standard

$$R_F = 2 \times 6 \left(\frac{15 \times 10^{-8}}{0.211 \times 6.45} \right) 10^{11} = 1 \times 10^5 \text{ ohms.}$$

For stack resistances under one ohm, the aluminum oxide film must be disrupted in one or more contact sites. Thus, the film resistance acts primarily to constrict the current flow to the points of metallic contact.

4. Tarnish Films

Dixon and Holm (6) note that very thin and invisible molecular or atomic films of gases or lubricants, which often cover contacts, conduct by means of the tunnel effect. These tarnish films have thicknesses in the order of 5×10^{-7} to 5×10^{-5} centimeters. Such films were detected on uncleaned laminates and probably did contribute to the initial high stack resistance (0.03 to 0.5 ohms) found as the bonding system static clamping force was increased from near zero.

Electrical breakdown (fritting) of tarnish films at contact points requires field strengths of about 10^6 volts per centimeter in the film (or 0.5 to 50 volts). Dixon and Holm (6) further note that a voltage of 0.3 volt will cause melting (bridge transfer) in aluminum. Since the microhmeter uses a constant current source of 1 ampere, melting voltages were not attainable during dynamic measurements.

5. Constriction Resistance

Since both the ohmic resistance and the film resistance play negligible roles once significant contact pressure is applied, the series equivalent circuit simplifies to the constriction resistance component. Because the number of contact sites and the contact area increase as the diffusion bonding progresses, the measured stack resistance becomes a direct measure of the percent area bonded.

---

(6) Dixon, H. S. and R. Holm, "Electrical Conductors and Contacts," Engineering Materials Handbook, Section 19, McGraw-Hill Book Co., New York, 1958.

According to F. L. Jones (12), the constriction resistance on one side of a flat disk contact is given by:

$$R_c(1) = \frac{\rho}{4a},$$

where a = contact disk radius,

ρ = bulk resistivity (see Table C-1).

A single disk contact then has a constriction resistance of twice the above value, or $2R_c(1)$. For a disk radius of 10 microinches, the constriction resistance becomes:

$$2R_c(1) = \frac{2\rho}{4a}$$

$$2R_c(1) = \frac{2 \times 2.87 \times 10^{-6}}{4 \times 10 \times 10^{-6} \times 2.54} = 0.057 \text{ ohms.}$$

Stack resistances of a few hundredths of an ohm were obtained under small contact pressures (1 pound for 0.2 square inch or 5 psi) during preliminary testing.

Percent contact area of the above example equals:

$$\text{Area \%} = \frac{\pi a^2}{A} \times 100.$$

$$\text{Area \%} = \frac{\pi (10^{-5})^2}{0.211} \times 100 = 1.5 \times 10^{-7} \text{ \%.}$$

Higher contact pressures lead to larger contact areas and more contact sites.

6. Number of Contact Sites

The constriction resistance decreases with the number of metal contacts where each new contact can be considered a resistance in parallel with all other contacts. The

---

(12) Jones, F. L., The Physics of Electrical Contacts. Oxford Press, London, 1957.

Plastic Yielding: $R_c \propto \frac{1}{\sqrt{P}}$.

When graphs of contact resistance versus normal loading are plotted on log-log graph paper, the above equations become straight lines with slopes of (-1/3) and (-1/2) respectively.

9. Test Fixture Ohmic Resistance

The static test fixture shown in Figure D-1 was calibrated by measuring the copper electrode contact resistance (R_e) under the same loading conditions used in measuring laminate stacks. The calibration data for both increasing and decreasing static loads asymptotically approached a finite lower limit.

A lower limit exists via the ohmic resistance of the sheet copper material. A brief survey of resistance measurements is provided in Table D-2.

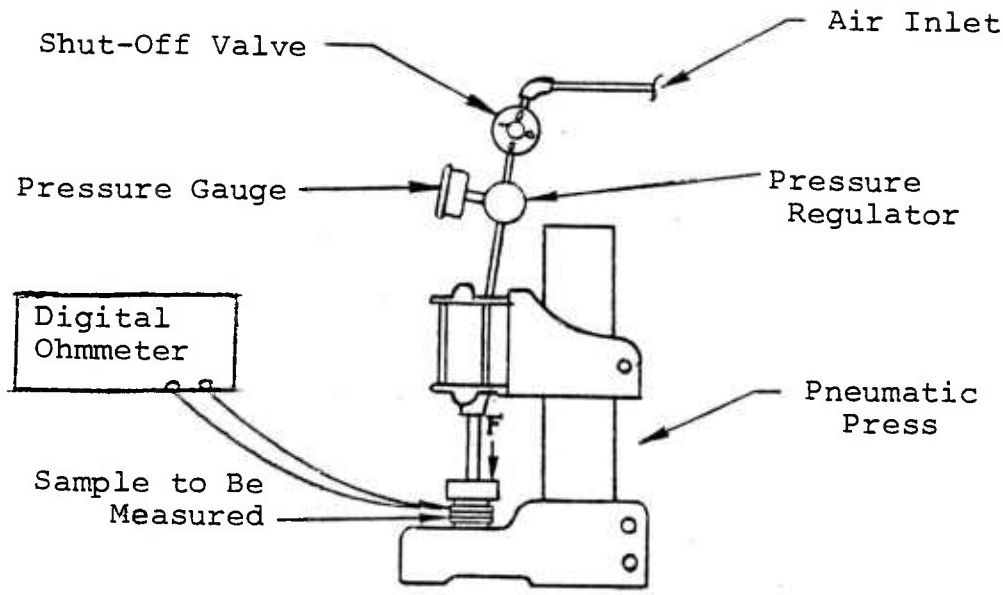

Figure D-1. Pneumatic press arrangement for static resistance measurements.

TABLE D-2. OHMIC RESISTANCE OF COPPER SHEET AS USED FOR ELECTRODES

Copper Electrode			Measured Resistance	
Thickness (in.)	Width (in.)	Length (in.)	Clip Spacing 1" c-c (microhms)	Clip Spacing 1-7/8" c-c (microhms)
0.010	1/2	2	120 (R_o = 118) ($2R_s \approx 4$)	230 (R_o = 236) ($2R_s \approx 4$)
0.010	1	2	90 (R_o = 59) ($2R_s \approx 38$) Calc = 97	160 (R_o = 118) ($2R_o \approx 38$) Calc = 155

$R_o = \frac{\rho L}{t\ w}$.

L = Clip Spacing - Clip Jaw Width (1/8").

ρ(copper) = 1.724 microhm-cm @ 20°C.

R_s = spreading resistance at electrode end.

Note: Calculated (Calc) electrode resistances differ from the measured values by 10 microhms or less for each example.

TABLE D-3. CONSTRICTION RESISTANCE OF MULTIPLE CONTACT SITES
(CALCULATED VALUES)

	Contacts		Site Area	Resistance (microhms) for No. of Laminates:				Inter-face Spacing	Contact Area
	No.	Radius (10^{-5} in.)	(sq in.)	2	6	12	18	(μin.)	(sq in.)
Contact Radius (a) Assumed Constant	1	1	3.14×10^{-10}	57,000				230	3×10^{-10}
	3	1	3.14×10^{-10}	19,000	95,000	209,000	323,000	225	9×10^{-10}
	50	1	3.14×10^{-10}	1,000	5,500	12,000	18,000	210	2×10^{-8}
	1,000	1	3.14×10^{-10}	57	280	620	970	190	3×10^{-7}
	10,000	1	3.14×10^{-10}	6	28	62	97	160	3×10^{-6}
Contact Radius Increases $a \propto \sqrt{N}$	1	1	3.14×10^{-10}	57,000				230	3.2×10^{-10}
	3	1.7	9.4×10^{-10}	5,700	30,000	63,000	100,000		2.8×10^{-9}
	50	7	1.5×10^{-8}	17	86	190	290		7.6×10^{-7}
	1,000	32	3.2×10^{-7}	0.06	0.3	0.6	1		3.2×10^{-4}
	10,000	100	3.2×10^{-6}				0.01		3.2×10^{-2}

APPENDIX E

CHARACTERISTICS OF ALUMINUM AND ALUMINUM FOIL

The aluminum industry has defined foil as thin aluminum sheet ranging in thickness from a commercial minimum of 0.00017 inch to a maximum of 0.0059 inch. "Foil is generally rolled from 99.45 percent minimum purity aluminum and is well adapted for precision rolling to extreme thinness because of its workability." (2). The finished rolled-to-gage foil is in the extra hard -H19 temper. Annealed or full-soft foil is identified as -0 temper.

Because of the surface oxide layer, foil properties differ from bulk aluminum alloy properties and exhibit a thickness-dependent effect. Thickness in the range of 0.002 to 0.005 inch were of prime interest to this study. Data compiled in this Appendix were used for the analytical studies discussed elsewhere in this report.

---

(2) Alcoa Aluminum Foil, Aluminum Company of America, Inc., Pittsburgh, PA, 1960.

TABLE E-1

CHEMICAL COMPOSITION LIMITS OF ALUMINUM PURITY GRADES AND ALLOYS **

ELEMENTS IN PER CENT, BY WEIGHT

Alloy No.	Silicon	Iron	Copper	Manganese	Magnesium	Chromium	Zinc	Titanium	Others Each	Others Total	Aluminum (Minimum)
1199	0.006	0.006	0.006	—	0.006	—	0.006	—	0.002	0.010	99.99
1188	0.06	0.06	0.005	0.01	0.01	—	0.01	0.01	0.01	—	99.88
1180	0.09	0.09	0.01	—	—	—	—	0.02	0.02	—	99.80
1145	0.55	Si+Fe	0.05	0.05	—	—	—	—	0.03	—	99.45
1100	1.0	Si+Fe	0.20	0.05	—	—	0.10	—	0.05	0.15	99.00
3003	0.6	0.7	0.20	1.0-1.5	—	—	0.10	—	0.05	0.15	Remainder
5052	0.45	Si+Fe	0.10	0.10	2.2-2.8	0.15-0.35	0.10	—	0.05	0.15	Remainder

*Values are maximum, unless shown as range.

** Table 1 from Ref. 19: Knight, J. W., Kaiser Aluminum Foil, Kaiser Aluminum Co., Oakland, CA, 1958.

TABLE E-2

TYPICAL PHYSICAL PROPERTIES OF ALUMINUM PURITY GRADES AND ALLOYS **

Alloy No.	Specific Gravity	Density Lb./Cu. In.	Melting Range (Approx.) F	Electrical Conductivity*
1199	2.70	0.098	1215 1225	65
1188	2.70	0.098	1200 1225	—
1180	2.70	0.098	1200 1220	—
1145	2.70	0.098	1200 1220	60
1100	2.71	0.098	1190 1215	59
3003	2.73	0.099	1190 1210	50
5052	2.68	0.097	1100 1200	35

*Per cent of International Annealed Copper Standard at 20 C (68 F).

** Table 2 from Ref. 19: Knight, J.W., Kaiser Aluminum Foil, Kaiser Aluminum Co., Oakland, CA, 1958

TABLE E-3

MECHANICAL PROPERTIES OF ALUMINUM ALLOYS AS MODIFIED BY HIGH AND LOW TEMPERATURES *

Alloy and Temper	Mechanical Properties*	Low Temperature			Room Temp.	Elevated Temperature					
		−320 F	−110 F	−20 F	75 F	212 F	300 F	400 F	500 F	600 F	700 F
1145—O	UTS	25.	15.	14.	13.	11.	8.5	6.0	4.0	2.5	2.0
	YS	6.0	5.0	5.0	5.0	5.0	4.5	3.5	2.0	1.5	1.0
	El	57.	50.	46.	45.	45.	55.	75.	75.	80.	85.
—H14	UTS	30.	20.	19.	18.	16.	13.	9.5	4.0	2.5	2.0
	YS	20.	18.	17.	17.	15.	12.	7.0	2.5	1.5	1.0
	El	42.	23.	20.	20.	20.	22.	25.	75.	80.	85.
—H18	UTS	35.	26.	25.	24.	22.	18.	6.0	4.0	2.5	2.0
	YS	26.	23.	23.	22.	18.	14.	4.0	2.0	1.5	1.0
	El	35.	17.	15.	15.	15.	20.	65.	80.	80.	85.

KEY: UTS—Ultimate tensile strength in thousands of pounds per square inch.
YS —Yield Strength (0.2 per cent offset) in thousands of pounds per share inch.
El —Elongation in two inches, or four diameters, in per cent.

* Table 5 from Ref. 19: Knight, J. W., Kaiser Aluminum Foil, Kaiser Aluminum Co., Oakland, CA, 1958.

TABLE E-4. DYNAMIC ELASTIC PROPERTIES NEAR ROOM TEMPERATURE

Material (Alloy)	Spec. Grav. ρ	Young's Modulus Y	Shear Modulus G	Bulk Modulus K	Pois. Ratio ν	Wave Velocity Long. C_o	Wave Velocity Dilat. C_D	Wave Velocity Shear C_S	Acoustic Impedance Z_O	Acoustic Impedance Z_S	Ref.
		10^6 psi	10^6 psi	10^6 psi		10^5cm/s	10^5cm/s	10^5cm/s	$10^5\Omega$	$10^5\Omega$	
1100-0	2.71	10.0				5.04			13.7		10
1100-1/2H	2.71	10.0				5.04			13.7		10
1100-Hard	2.71	10.0				5.04			13.7		10
Al	2.711	10.24	3.80	10.9	0.345	5.102	6.374	3.111	13.83	8.43	4
Duralumin	2.70	10.27	3.81	10.9	0.345	5.120	6.398	3.122	13.83	8.43	4
Al Rolled	2.695	9.8-10.3	3.5-3.8		0.355	5.00	6.42	3.04	13.5	8.19	23
Dural 17S	2.79	10.4	3.87		0.335	5.15	6.32	3.13	14.3	8.73	23
Al	2.7	10.2	3.77	10.6	0.34	5.09	6.32	3.10	13.7	8.73	20
α-Al_2O_3	3.986	58.4	23.7	36.4	0.233						

TABLE E-5. ACTIVATION ENERGIES

Pure Aluminum	Activation Energy (kilocalories per mole)	Ref.
Vacancy Formation	17.5	38
Self Diffusion	15.0	38
Jog Diffusion		See 14

TABLE E-6. OPTICAL PROPERTIES

Reflectivity for white light (tungsten filament lamp)	85 to 88%
Reflectivity for radiant heat (source at 100°F)	95%
Infrared emissivity @ 100°F (Ref. 2)	5%

TABLE E-7. CRYSTALLOGRAPHIC DATA

99.998% Al	Face-centered cubic crystal
	Lattice dimension: a = 4.04960 Å
	X-ray density: 2.69790 g/cm^3
	(Ref. 34, p. 254)
α-Al_2O_3	Trigonal (sapphire)
	Lattice parameters: a = 4.758 Å
	c = 12.925 Å
	(Ref. 34, p. 222)
	X-ray density: 3.986 g/cm^3

TABLE E-8. TEMPERATURE COEFFICIENTS OF ELASTICITY

Apparent temperature coefficients of elasticity for aluminum (Ref. 4):

$$\frac{d \ln Y_a}{d T} = -0.048\%$$

$$\frac{d \ln G_a}{d T} = -0.052\%$$

where: $\frac{1}{Y}\frac{dY}{dT} = \frac{d \ln Y}{d T} = \frac{d \ln Y_a}{d T} - \alpha$

α = temperature coefficient of linear expansion